A Role for β_{cyto}- and γ_{cyto}-Actin at the Sarco/endoplasmic Reticulum-Mitochondrial Interface

A Dissertation
SUBMITTED TO THE FACULTY OF
UNIVERSITY OF MINNESOTA
BY

Allison Rose O'Rourke

IN PARTIAL FULFILLMENT OF THE REQUIREMENTS
FOR THE DEGREE OF
DOCTOR OF PHILOSOPHY

Advisor: James M. Ervasti Ph. D.

May 2017

Acknowledgements

I would like to thank my thesis advisor Jim Ervasti for all the guidance and direction he has provided me on my journey to become a better scientist. I would also like to thank Jim for creating and fostering a laboratory environment that is a pleasure to work in.

I would like to thank my parents Mike and Rose O'Rourke for always seeing the value in education and instilling that value in me. Also, for the support and encouragement they have provided on this long journey. I would like to thank my siblings Megan, Ryan, and Adam for all of their support, conversation, and the happy distractions they have provided along the way.

I would like to thank my grandparents Tom and Rita Willmus for their support, especially in providing me a wonderful place to live.

I would like to thank my committee: Tom Hayes, Dawn Lowe, Melissa Gardner, and Marry Porter for taking the time and energy to provide advice and mentorship at all of the steps along the way.

I would like to thank my labmates, former and current, for the conversation both scientific and not.

I would like to thank my MCSB classmates for their motivation and encouragement.

I would like to thank Courtney and Brandon Coombes, Jami Erickson, Luke Manlove, Beth Morgan, Cassie Pickerign, Lydia Schrupp and my SMC friends, your friendship has meant more than you could know. I also want to thank everyone else I was fortunate enough to spend time with while in graduate school.

I would like to thank and acknowledge Sue Knoblauch, without whom I would have forgotten to take care of much the logistical requirements of graduate school.

I would like to acknowledge the MCSB program for the Graduate Excellence Fellowship.

Dedication

This dissertation is dedicated to my family.

Abstract

Skeletal muscle accounts for 40% of mass in adult humans. The primary function of skeletal muscle is to produce movement via contraction of the sarcomere. The sarcomere is the basic functional until of skeletal muscle and two of the key components in sarcomeric contraction are myosin and actin. Actin, though often referred to as a single entity, separates into two functional groups muscle (α_{sk}-actin, α_{ca}-actin, α_{sm}- and γ_{sm}-actin) and cytoplasmic (β_{cyto}- or γ_{cyto}-actin) actins. Though α_{sk}-actin is the predominate isoform in adult skeletal muscle, specifically in the sarcomere, the ubiquitously expressed β_{cyto}- and γ_{cyto}-actin cytoplasmic actin isoforms are also present.

As may be predicted by their ubiquitous expression patterns, β_{cyto}- and γ_{cyto}-actin, are enmeshed in a wide array of cellular functions including, migration, cell shape, cell division, vesicle trafficking, and organelle anchoring among others. Though collectively involved in many processes the unique and redundant role of both β_{cyto}- and γ_{cyto}-actin are not fully delineated. β_{cyto}- and γ_{cyto}-actin are highly conserved, with 99% homology of the coding sequence. The evolutionary pressure which has maintained both sequences suggests that they are both are necessary. The importance of having both β_{cyto}- and γ_{cyto}-actin was demonstrated through whole body knockouts. Whole body ablation of either β_{cyto}- or γ_{cyto}-actin proved lethal to the majority of animals during embryogenesis or within 24 hours after birth.

The severity of the whole body phenotype while one cytoplasmic actin is still present illustrates the vital role each isoform has.

The lethal nature of whole body knockouts of either cytoplasmic actin isoform made studies into tissue specific phenotypes difficult. One tissue of interest was skeletal muscle, because of the role cytoplasmic actins have in linking the sarcomere to the extracellular matrix. Previously, insight was gained into the functional significance of β_{cyto}- and γ_{cyto}-actin in skeletal muscle via muscle specific knockouts. Each knockout revealed the presence of a mild myopathy associated with muscle death and regeneration which worsened overtime. The focus of my thesis is to better understand how muscle specific ablation of either β_{cyto}- or γ_{cyto}-actin resulted in a progressive mild myopathy. Since, the link between either β_{cyto}- and γ_{cyto}-actin and the observed myopathy wasn't readily apparent I investigated the known interactions of cytoplasmic actins in skeletal muscle. It was previously reported that cytoplasmic actin colocalizes with a host of structures in skeletal muscle including two which could affect cell viability: mitochondria and peri-z-disk region where the sarcoplasmic reticulum also localizes.

My thesis advances understanding for how ablation of cytoplasmic actin isoforms leads to a mild myopathy. Firstly, I showed that both β_{cyto}- and γ_{cyto}-actin isoforms were present at the interface between mitochondria and sarcoplasmic reticulum. Secondly, I showed that β_{cyto}- and γ_{cyto}-actin knockout skeletal muscle had perturbations in sarcoplasmic reticulum and mitochondria morphology. Additionally, I showed that both cytoplasmic actin isoforms contribute to

mitochondrial fission. Finally, I demonstrated that in skeletal muscle lacking β_{cyto}- and γ_{cyto}-actin, changes indicative of decreased sarcoplasmic reticulum function preceded the observed morphological changes.

Though cytoplasmic actin isoforms have been localized to an array of structures in skeletal muscle, we chose to focus on two organelles which can affect cell viability. Further investigation into the source of the observed progressive myopathy revealed morphological aberrations in both the mitochondria and sarcoplasmic reticulum. The stable nature of skeletal muscle structure hindered further examination of the observed mitochondrial morphological phenotype so, we utilized a mouse embryonic fibroblast model. In mouse embryonic fibroblasts lacking either or both cytoplasmic actin isoforms, mitochondria are elongated and display a decrease in fission events.

As mitochondria are a central regulator of cell health and because of the effect we observed β_{cyto}- and γ_{cyto}-actin have on mitochondrial dynamics, we initially hypothesized that mitochondria would be mildly functionally impaired. However, upon investigation of function it was not mitochondrial function which was impaired, but that an indicator of sarcoplasmic reticulum function was decreased. In sarcoplasmic reticulum a functional phenotype preceded the development of morphological changes supporting a potential role for sarcoplasmic reticulum dysfunction to act as a possible stressor linked to the observed mild progressive myopathy.

Table of Contents

List of Tables

List of Figures

Chapter 1 : Introduction

Skeletal Muscle

There are three types of muscle tissue: cardiac, smooth, and skeletal. All types utilize the same basic mechanism to generate force via the conversion of chemical energy, ATP, into mechanical energy, in the form of contractile force (Fontes-Oliveira et al., 2013). All types of muscle tissue employ this same process to produce contraction, however each has been specialized to support unique physiological processes. Smooth muscle lines blood vessels and the digestive system and contracts in a wave pattern called peristalsis to move substances through those vessels. Cardiac muscle cells do not fatigue as they must contract to pump blood continuously for the entire life of the organism. Skeletal muscle is by far the most abundant of the three muscle tissues, accounting for nearly 40% of adult body weight in humans. It is vital for organismal movement, regulation of core body temperature, and for contributing to metabolic rate as the bodies primary consumer of oxygen and metabolites during exercise (Frontera and Ochala, 2015). The organization of skeletal muscle consists of a series of hierarchal ordered bundles (Figure 1-1). The muscle cell or myofiber (Figure 1-1B) contains bundles called myofibrils which consist of sarcomeres arranged in series (Figure 1-1C). The sarcomere is the basic functional until of contraction. Two of the most prevalent proteins found at the sarcomere are actin thin filaments and myosin thick filaments. For muscle to contract, a specific series of events have to take place which result in shortening of the sarcomere and muscle contraction.

Actin Isoforms

Actin is a fundamental component of all cells, functioning in a wide array of cellular processes. While canonically referred to as a single entity, actin, it is actually six different isoforms encoded by 6 separate genes. All actin isoforms share a high degree of sequence homology, but the small sequence changes between isoforms are conserved in birds and mammals (Rubenstein, 1990). The functional significance of six well conserved actin isoforms is not fully understood.

The actin isoforms can be segregated into two functional groups: muscle and cytoplasmic actin isoforms (Figure 1-2). Four are muscle actins: α_{sm}-actin, γ_{sm}-actin, α_{ca}-actin, and α_{sk}-actin (Figure 1-2). Smooth muscle tensile structures consist of α_{sm}-actin and γ_{sm}-actin (Rubenstein, 1990). Two of the muscle actin isoforms are essential constituents of sarcomeric thin filaments in adult muscle (Crawford et al., 2002; Kumar et al., 1997). Cardiac and skeletal muscle express the actin isoforms, α_{ca}-actin and α_{sk}-actin respectively (Rubenstein, 1990). Muscle actin isoforms have conserved differences in sequence but can functionally compensate for one another in certain cases. Loss of α_{sk}-actin from skeletal muscle is fatal during embryogenesis, but when α_{ca}-actin is expressed in a skeletal muscle specific manner it rescues the phenotype (Crawford et al., 2002; Nowak et al., 2009a). Ablation of α_{ca}-actin is fatal, but exogenous expression of γ_{sm}-actin can partially rescue the phenotype (Kumar et al., 1997). This partial functional

redundancy among muscle actin isoforms indicates a compensatory relationship while highlighting their unique roles.

Two ubiquitously expressed cytoplasmic actin isoforms, β_{cyto}- and γ_{cyto}-actin, are encoded by the genes *Actb* and *Actg1,* respectively. β_{cyto}- and γ_{cyto}-actin have a high degree of sequence homology, differing by only four biochemically similar amino acids at the N-terminus of the protein (Figure 1-2). This slight variation in sequence has been maintained through evolution but the functional significance is unclear. Collectively, cytoplasmic actin isoforms are known to be critical to numerous cellular processes.

All actin isoforms encode a globular 43 kDa protein referred to as G-actin. In the presence of millimolar concentrations of monovalent or divalent ions, G-actin reversibly polymerizes to form filamentous or F-actin. Dynamic transitions between G- and F-actin are critical for many of actins functions. The speed at which actin polymerization/depolymerization occurs varies depending on the actin isoform, the end of the actin filament at which they are occurring, ATP/ADP availability, the concentration of ions such as Ca^{2+} or Mg^{2+}, and the presence of actin binding proteins (Carlier and Pantaloni, 1997; Pollard et al., 2000). Ablation of β_{cyto}-actin in primary mouse embryonic fibroblasts (MEFs) has been shown to alter the G:F actin ratio in favor of F-actin (Bunnell and Ervasti, 2010; Bunnell et al., 2011). In vitro a high γ_{cyto}/ β_{cyto}-actin ratio led to more stable F-actin (Bergeron et al., 2010). G- and F-actin have unique functions. G-actin is involved in transcriptional control (Miralles et al., 2003). F-actin is required for a wide range of cellular functions

attributed to all actin isoforms. Muscle actin isoforms, in the F-actin state, form thin filaments along which myosin motors bind and produce contractile force. β_{cyto}- and γ_{cyto}-F-actin forms a track in cells upon which myosin motor proteins can traffic vesicles (Pollard and Cooper, 2009). F-actin also assembles to form filopodial and lamellipodial membrane protrusions required for migration (Pollard and Cooper, 2009).

Cytoplasmic Actin Isoforms in Non-Muscle Cells

The ubiquitous expression of both β_{cyto}- and γ_{cyto} -actin underlies the vital role they have in a wide array of cellular functions. Functionally, β_{cyto}-actin and γ_{cyto}-actin are important for many processes attributed to actin including the contractile ring during cell division, a track for vesicle movement, transcriptional regulation, and cell shape (Pollard and Cooper, 2009). Cytoplasmic actin isoforms also play a vital role in cell migration (Bunnell et al., 2011), providing the force behind lamellipodial and filopodial membrane protrusion (Tondeleir et al., 2012). While cytoplasmic actin isoforms as a whole are implicit in these processes, the conserved sequence differences between the N-termini of β_{cyto}- and γ_{cyto}-actins has elicited questions about their unique contributions.

The specific importance of each cytoplasmic actin isoform was initially demonstrated through the use of animals with severely hypomorphic alleles (Shawlot et al., 1998; Shmerling et al., 2005b) and animals with Actb (Bunnell et al., 2011) or Actg1 (Belyantseva et al., 2009) null alleles. Mice with whole body ablation of β_{cyto}- or γ_{cyto}-actin revealed that, while γ_{cyto}-actin is important, β_{cyto}-actin is essential for survival (Belyantseva et al., 2009; Bunnell and Ervasti, 2010; Bunnell et al., 2011). Loss of β_{cyto}-actin was fatal by E7.5 (Figure 1-3A) in null mice and after E9.5 in hypomorphic animals. Primary mouse embryonic fibroblasts (MEFs) lacking β_{cyto}-actin display decreased migration (Figure 1-4A), are growth impaired, have elevated apoptosis (Figure 1-4C), and a decreased G/F actin ratio

(Bunnell et al., 2011). While loss of γ_{cyto}-actin was less severe, it still resulted in only one-ninth of animals having normal lifespan, with most animals dying in the first 24 hours due to respiratory distress (Figure 1-3 B; Bunnell and Ervasti, 2010). However, primary MEFs lacking γ_{cyto}-actin displayed no defect in cell migration (Figure 1-4B), only a slight decrease in cell viability, and a minimal increase in apoptosis (Figure 1-4D; Bunnell and Ervasti, 2010). In each knockout model alternate actin isoforms were up regulated, presumably to compensate for the loss of one isoform from the actin pool. However, the manifestation of phenotypes indicates that functional compensation was incomplete. Several studies investigating the specific contributions of β_{cyto}- and γ_{cyto}-actin to migration have yielded strikingly different results (Belyantseva et al., 2009; Bergeron et al., 2010; Bunnell and Ervasti, 2010; Karakozova et al., 2006; Lechuga et al., 2014; Tondeleir et al., 2012). The necessity of β_{cyto}-actin over γ_{cyto}-actin, as demonstrated in the Actb and Actg1 whole body knockout animal model, indicates that γ_{cyto}-actin cannot fully functionally compensate for the loss of β_{cyto}-actin.

While β_{cyto}- and γ_{cyto}-actin both function in universal cellular processes, they are also integral to cell type specific functions. In the ear, stereocilia are critical for hearing and loss of either β_{cyto}-actin or γ_{cyto}-actin leads to unique morphological defects and patterns of hearing loss (Belyantseva et al., 2009; Perrin et al., 2010). In neurons, cytoplasmic actin isoforms are involved in regulating Ca^{2+} signaling (Rosenmund and Westbrook, 1993; Wang et al., 2002). Both isoforms are present in neuronal dendritic spines but only γ_{cyto}-actin has been implicated in hippocampal

synaptic plasticity (Johnson and Byerly, 1993; Rosenmund and Westbrook, 1993; Schreiber et al., 2015). Tissue and isoform specific functions reinforce the hypothesis that β_{cyto}- and γ_{cyto}-actin have unique functions despite the high degree of sequence homology.

Cytoplasmic Actin Isoforms in Skeletal Muscle

Cytoplasmic actin isoforms are not incorporated into the sarcomere of adult muscle but predominate during myogenesis (Duan and Gallagher, 2009; Lloyd et al., 1992; Nowak et al., 2009b; Peckham, 2008). The switch in actin isoforms occurs during myoblast fusion when α_{sk}-actin expression is dramatically upregulated (Schwartz and Rothblum, 1981). Following myogenesis, β_{cyto}- and γ_{cyto}-actin expression is downregulated, but very low levels remain in adult skeletal muscle. While α_{sk}-actin is one of the most abundant proteins in skeletal muscle, β_{cyto}-actin and γ_{cyto}-actin account for only 1/4000 of the total actin present (Hanft et al., 2006). In skeletal muscle β_{cyto}-actin and γ_{cyto}-actin colocalize with the dystrophin-glycoprotein complex to the extrasarcomeric membrane cytoskeleton at the costamere and are thought to play a role linking the extracellular domain to the sarcromere (Craig and Pardo, 1983; Otey et al., 1988; Prins et al., 2011; Rybakova et al., 2000). β_{cyto}-actin and γ_{cyto}-actin have also been shown to localized with other structures in skeletal muscle including the myotendonus junction (Papponen et al., 2008), the neuromuscular junction (Hall et al., 1981), and to peri-Z disk regions where mitochondria and sarcoplasmic reticulum (SR) also localize (Craig and Pardo, 1983; Gokhin et al., 2010; Kee et al., 2004).

Muscle-specific Actb and Actg1 knockout mice were generated through human skeletal actin (HSA) promoter driven CRE expression which acted on loxp sites flanking exon 2 and 3 of either β_{cyto}-actin or γ_{cyto}-actin leading to

recombination and functional gene knockout (Figure 1-5A; Perrin et al., 2010; Prins et al., 2011; Sonnemann et al., 2006). Ablation of either β_{cyto}-actin or γ_{cyto}-actin resulted in a mild progressive myopathy delineated by the increase in centrally nucleated fibers, a hallmark of degeneration and regeneration of that portion of the muscle fiber (Figure 1-5B-E; Prins et al., 2011; Sonnemann et al., 2006). While some slight physiological responses were altered including susceptibility to exhaustion, eccentric contraction induced fatigue, and hind limb contractures, it was unclear how loss of either cytoplasmic actin could result in progressive fiber death.

Several studies have observed a similar but more rapid myopathy when ablating proteins with which actin is known to colocalize or bind. Clathrin heavy chain ablation leads to γ_{cyto}-actin displacement from the costameres and loss of contractile force, likely as a result of uncoupling the sarcomeres from the extracellular matrix at costameres (Vassilopoulos et al., 2014). γ_{cyto}-actin has also been isolated with the four-and-a-half LIM domain protein 1 protein complex (Wang et al., 2013). Loss of four-and-a-half LIM domain protein 1 results in disruption of normal mitochondrial and SR morphology (Domenighetti et al., 2014; Wang et al., 2013). Multiple groups have demonstrated that γ_{cyto}-actin colocalizes with certain isoforms of tropomyosin and tropomodulin which when knocked out altered z-disk proteins linked to defects in excitation-contraction coupling (Almenar-Queralt and Lee, 1999; Gokhin et al., 2010; Kee et al., 2004). One isoform of tropomodulin colocalizes with γ_{cyto}-actin at the SR (Gokhin and Fowler, 2011; Gokhin et al.,

2010), when that colocalization is disrupted a defect in SR ultrastructure becomes apparent, but only after 6 months of age (Gokhin and Fowler, 2011; Gokhin et al., 2010). All of these changes are indicative that cytoplasmic actin isoforms may be affecting the function of numerous organelles in skeletal muscle. Since more rapid phenotypes have been observed with the ablation of cytoplasmic actin interacting proteins, here we hypothesized that the high degree of sequence homology between β_{cyto}- and γ_{cyto}-actin may allow for partial functional compensation, delaying the onset of observable phenotypes. Additionally, we hypothesized that the mild progressive myopathy observed in the absence of either β_{cyto}-actin and γ_{cyto}-actin could be due to dysfunction of the structures with which they normally colocalize such as the mitochondria or SR.

Mitochondria-Sarco/Endoplasmic Reticulum Interface and Actin

Actin is known to interact with the SR membrane through actin binding proteins like inverted formin 2 and tropomodulin 3 (Gokhin and Fowler, 2011; Korobova et al., 2013). The SR is a primary center of protein synthesis, but also critical for the cell stress response and lipid metabolism (Basseri and Austin, 2012; Chevet et al., 2001). The SR is also vital as an intracellular store of Ca^{2+}, which can impact many cellular processes like energy metabolism and cell stress. In skeletal muscle, Ca^{2+} release and reuptake by the SR contributes to sarcomeric contraction-relaxation cycling (Clapham, 2007).

The primary function of mitochondria is to produce energy. Most ATP is generated as a result of coupled oxidative phosphorylation at the electron transport chain in the inner mitochondrial membrane (Hüttemann et al., 2008). This chain of five complexes has multiple inputs and can be regulated to increase or decrease cellular energy output (Wallace, 1999). Alterations in oxidative phosphorylation can greatly affect cell function and viability, especially in a highly metabolic tissue like skeletal muscle. Damage to electron transport chain proteins impacts energy output. Maintenance of a fully functional electron transport chain and a healthy population of mitochondria is achieved through mitochondrial dynamics (Chen and Chan, 2009).

Mitochondria are dynamic organelles, undergoing the opposing processes of fission and fusion. Proper balance between the processes is critical and loss of

mitochondrial fusion proteins mitofusin-1 or -2, or fission protein mitochondrial fission factor, is fatal in mice (Chen et al., 2000; Chen et al., 2015). Alterations in mitochondrial metabolism can affect mitochondrial dynamics. Drug Inhibition of oxidative phosphorylation leads to increased fission resulting in punctate mitochondria (Mishra and Chan, 2016). The opposite is also true, changes in mitochondrial dynamics can impact mitochondrial respiration (Mishra and Chan, 2016). Though the processes of fission and fusion have been well characterized, multiple recent studies have established a functional role for the endoplasmic reticulum and actin polymerization in mitochondrial dynamics (Korobova et al., 2013; Manor et al., 2015). In the canonical fission pathway, dynamin related protein 1 assembles to form a ring encircling and contracting the mitochondria leading to fission. More recently a role for the endoplasmic reticulum was described, when it was identified that the dimeter of the dynamin related protein 1 ring was too narrow to fit around the circumference of the mitochondria. To achieve the initial constriction of mitochondria, endoplasmic reticulum wraps around the mitochondrion and stimulates actin polymerization via inverted formin 2 as the driving force of constriction (Korobova et al., 2013). Which actin isoforms were involved in this process however, was unknown. The actin is anchored both to the endoplasmic reticulum via inverted formin 2 and to the mitochondrial outer membrane via Spire1C (Figure 1-6A; Korobova et al., 2013; Manor et al., 2015). Actin-mediated mitochondrial fission can be inhibited with drugs that alter actin

dynamics at the mitochondrial/endoplasmic reticulum interface (Korobova et al., 2013).

Mitochondria and the SR both play a vital role in cell survival. The mitochondria/endoplasmic reticulum interface (mitochondria-associated membrane) is a hotspot of cellular communication (Figure 1-6B). Energy demand in skeletal muscle is very high and communication at the mitochondria-associated membrane can stimulate increased ATP production if required (Eisner et al., 2013). The 10μm separation between the outer mitochondrial membrane and the endoplasmic reticulum membrane allows for regulation of mitochondrial respiration or cell death signaling (Csordás and Hajnóczky, 2009; Rizzuto et al., 1998). Ca^{2+} in low concentrations can stimulate increased energy production at the electron transport chain, in accordance with tissue demand. Alternatively, when Ca^{2+} concentrations at the mitochondria-associated membrane become too high, they can trigger the mitochondria to initiate cell death pathways (Csordás and Hajnóczky, 2009; Patergnani et al., 2011; Rizzuto et al., 1998). Actin isoforms function at the mitochondria-associated membrane, outside of mitochondrial fission is unclear, as is the identity of the isoforms present. As both the mitochondria and SR are perturbed when various actin binding proteins are ablated (Domenighetti et al., 2014; Gokhin and Fowler, 2011; Gokhin et al., 2010; Wang et al., 2013) they pose likely locations for cytoplasmic actin isoforms to be affecting cell viability overtime potentially contributing to the mild progressive myopathy found in γ_{cyto}- and β_{cyto}-actin skeletal muscle knockout mice.

Figures

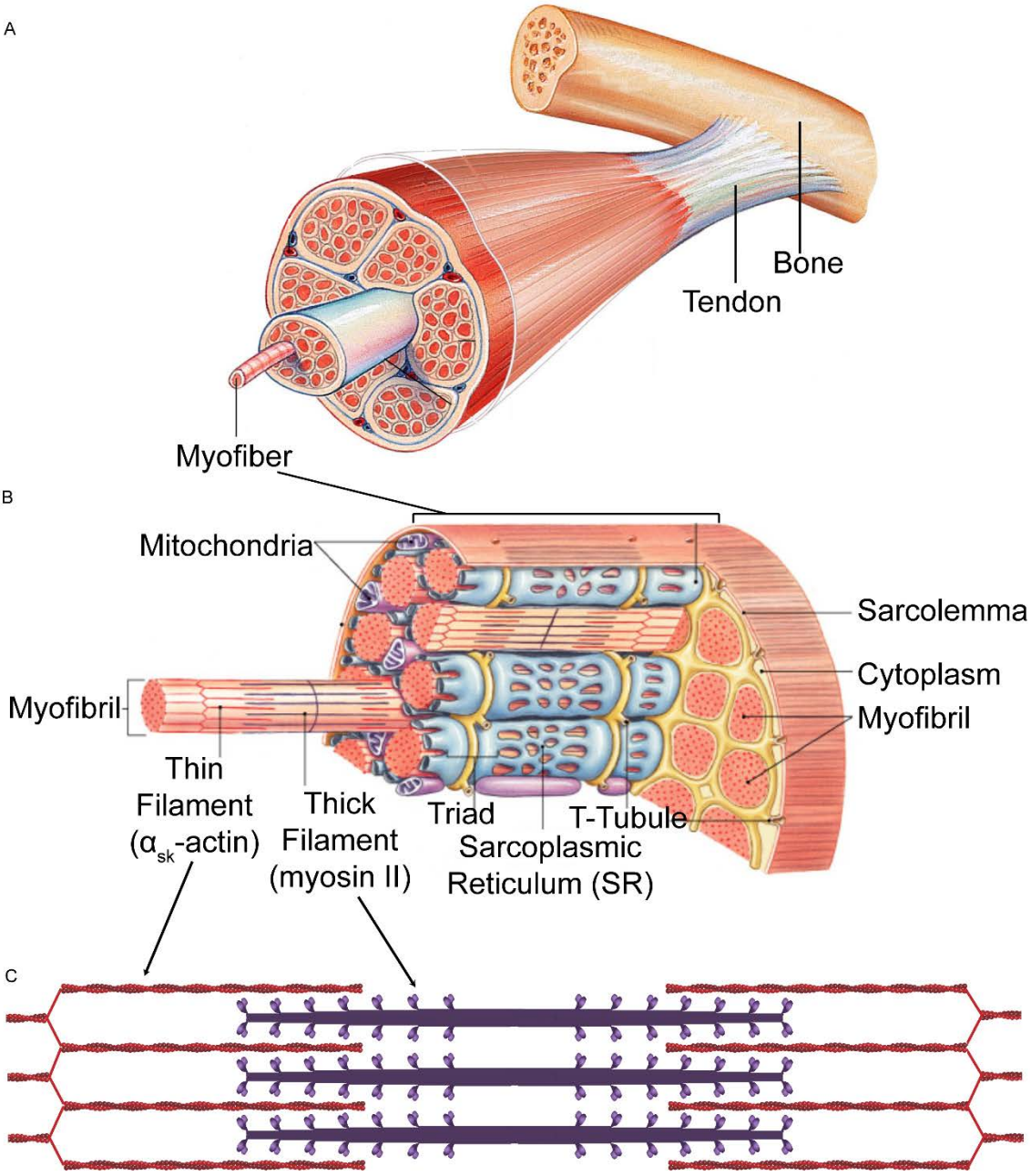

Figure 1-1 Cartoon of Skeletal Muscle Hierarchal Bundling Organization.

(A) Skeletal muscle organization. (B) Myofiber organization. (C) Thin and Thick filaments at the sarcomere. (A Modified from 2009 Pearson Education; B Modified from 2011 Pearson Education).

α-Cardiac Muscle Actin	Ac-D-D-E-E-T-T-A-L-V-C-D-N-G-S-G-L-V-K-
α-Skeletal Muscle Actin	Ac-D-E-D-E-T-T-A-L-V-C-D-N-G-S-G-L-V-K-
α-Smooth Muscle Actin	Ac-E-E-E-D-S-T-A-L-V-C-D-N-G-S-G-L-C-K-
γ-Smooth Muscle Actin	Ac---E-E-E-T-T-A-L-V-C-D-N-G-S-G-L-C-K-
β-Cytoplasmic actin	Ac---D-D-D-I-A-A-L-V-V-D-N-G-S-G-M-C-K-
γ-Cytoplasmic actin	Ac---E-E-E-I-A-A-L-V-I-D-N-G-S-G-M-C-K-

Figure 1-2 Actin Isoforms Amino Acid Sequence.

N-Terminal Domains of the Six Actin Isoforms.

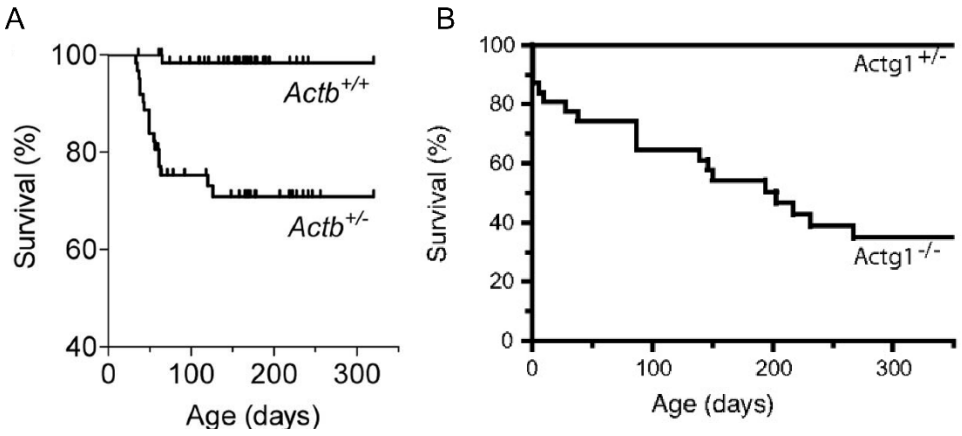

Figure 1-3 Decreased Survival β_{cyto}-actin Heterozygotes and γ_{cyto}-actin Null Mice.

Kaplan Meier survival curve of Actb+/- (A) and Actg1-/- (B) compared to controls. (A modified from Bunnell et al., 2011; B modified from Belyantseva et al., 2009).

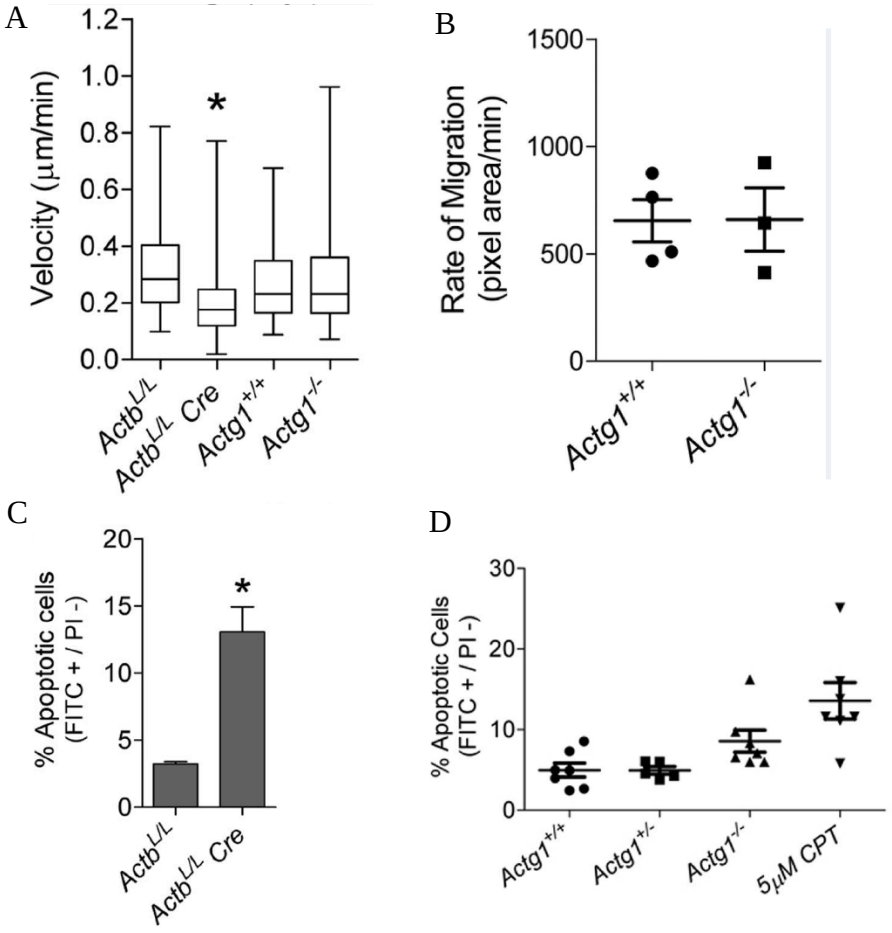

Figure 1-4 Decreased Migration and Elevated Apoptosis in Actb-Knockout MEFs but not Actg1-Knockout MEFs.

Migration of Actb-KO (A) and Actg1-KO (B) MEFs. Percent of Actb-KO (C) and Actg1-KO (D) MEFs undergoing apoptosis (A and C modified from Bunnell et al., 2011; B and D modified from Bunnell and Ervasti, 2010).

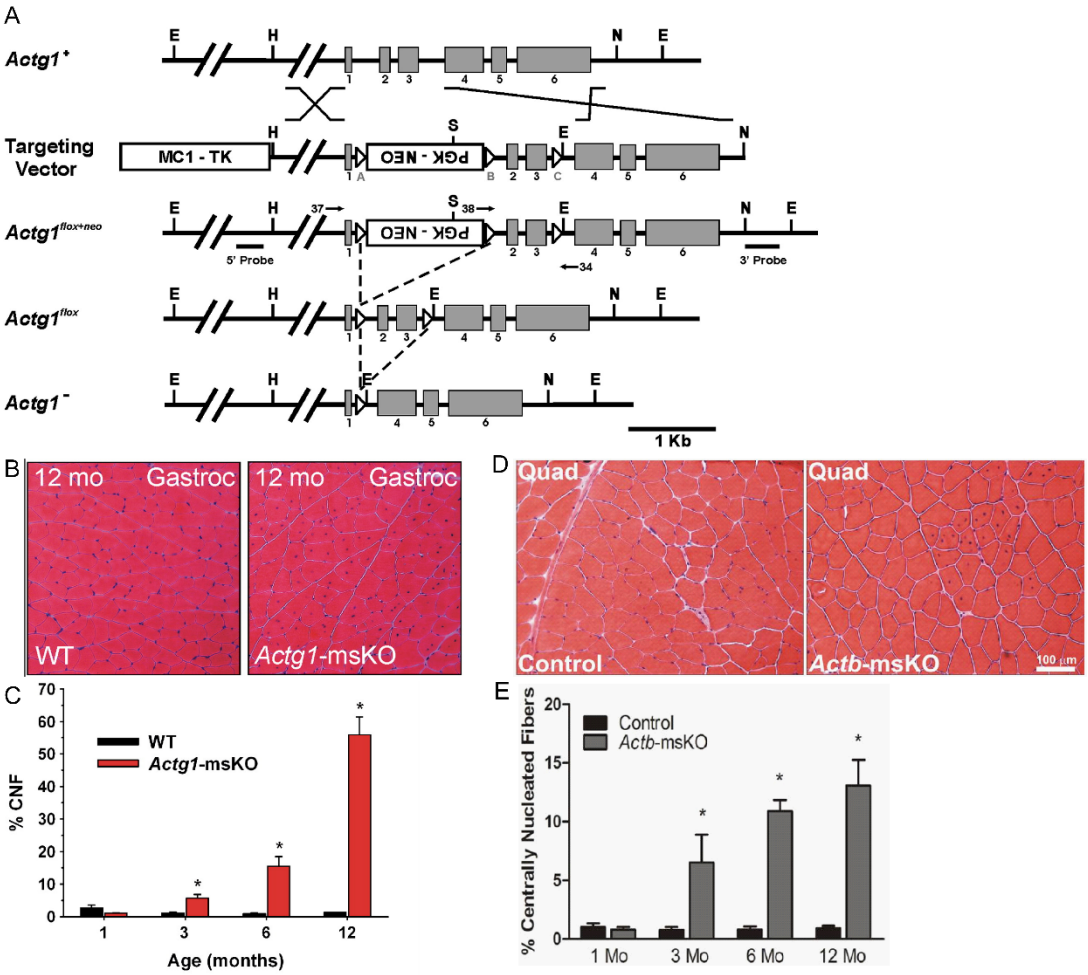

Figure 1-5 Mild Progressive Myopathy in Actb and Actg1 Muscle Specific Knockout Mice.

(A) Gene targeting scheme to flox Actg1 gene in mice. Similar scheme was used to flox Actb gene in mice. H&E staining of 12 moth old mouse muscle from Actg1-msKO Gastroc (B) and Actb-msKO Quad (D). Quantification of centrally nucleated fibers (CNFs) in Actg1-msKO muscle (C) and Actb-msKO muscle (E). (A-C modified from Sonnemann et al., 2006; D-E modified from Prins et al., 2011).

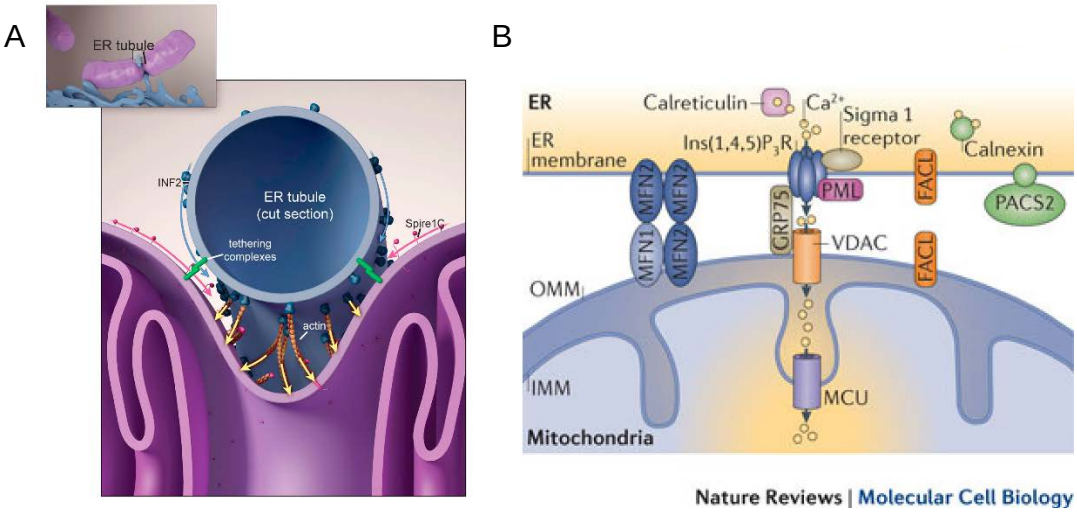

Figure 1-6 Cartoons of Mitochondrial-Sarco/endoplasmic Reticulum Interface.

(A) Mitochondrial fission via endoplasmic reticulum and actin constriction. (B) Mitochondrial-associated membrane with key pathways shown. (A Modified from Manor et al., 2015; B from Rizzuto et al., 2012)

Chapter 2 : Relative importance of βcyto- and γcyto-actin in primary mouse embryonic fibroblasts.

Allison O'Rourke harvested the mouse embryonic fibroblasts used, performed the experiments for Figure 2-1 A-B, Figure 2-3, and Figure 2-8, and participated in the writing of the paper. All other experiments were performed by Xiaobai Patrinostro.

Patrinostro, X., O'Rourke, A. R., Chamberlain, C. M., Moriarity, B. S., Perrin, B. J. and Ervasti, J. M. (2017). Relative importance of βcyto- and γ cyto-actin in primary mouse embryonic fibroblasts. *Mol. Biol. Cell*.

Chapter Summary

The highly homologous beta (β_{cyto}) and gamma (γ_{cyto}) cytoplasmic actins are hypothesized to carry out both redundant and unique essential functions, but studies using targeted gene knockout and siRNA mediated transcript knockdown to examine β_{cyto}- and γ_{cyto}-isoform specific functions in various cell types have yielded conflicting data. Here, we quantitatively characterized actin transcript and protein levels as well as cellular phenotypes in both gene- and transcript-targeted primary mouse embryonic fibroblasts. We found that the smooth muscle α_{sm}-actin isoform was the dominantly expressed actin isoform in WT primary fibroblasts, and was also the most dramatically upregulated in primary β_{cyto}-, or β/γ_{cyto}-actin double knockout fibroblasts. Gene targeting of β_{cyto}-actin, but not γ_{cyto}-actin, led to greatly decreased cell proliferation, decreased levels of cellular ATP, and increased serum response factor signaling in primary fibroblasts while immortalization induced by SV40 largeT antigen supported fibroblast proliferation in the absence of β_{cyto}-actin. Consistent with *in vivo* gene targeting studies in mice, both gene and transcript targeting approaches demonstrate that the loss of β_{cyto}-actin protein is more disruptive to primary fibroblast function than is the loss of γ_{cyto}-actin.

Introduction

Vertebrate actin isoforms, which are encoded by six different genes, share a very high degree of sequence homology and are completely conserved from birds to mammals (Rubenstein, 1990). Four of the actin isoforms are predominately expressed in smooth (α_{sm}- and γ_{sm}-actin), cardiac (α_{ca}-actin) and skeletal muscles (α_{sk}-actin). The two cytoplasmic actins (β_{cyto}- and γ_{cyto}-actin) are ubiquitously expressed in all cell types and differ at only 4 out of 375 amino acids. Despite the remarkable conservation between the β_{cyto}- and γ_{cyto}-actin sequences, purified recombinant β_{cyto}- and γ_{cyto}-actin proteins display marked differences in dynamics *in vitro* (Bergeron et al., 2010). Furthermore, numerous studies of transcript/protein localization, protein overexpression and disease-causing mutations have established a strong argument for unique functions supported by β_{cyto}- or γ_{cyto}-actin (Khaitlina, 2001, Condeelis and Singer, 2005, and Rubenstein and Wen, 2014). More recently, gene targeting studies have been employed to test for non-overlapping functions of actin isoforms (Perrin and Ervasti, 2010). With regard to closely related β_{cyto}- and γ_{cyto}-actins, the embryonic lethality of mice homozygous for severely hypomorphic (Shawlot et al., 1998; Shmerling et al., 2005a), or null alleles of *Actb* (Bunnell and Ervasti, 2011) demonstrated that β_{cyto}-actin is an essential gene. In contrast, γ_{cyto}-actin null animals survive to term but display significant perinatal lethality, stunted growth, and decreased survival into adulthood (Belyantseva et al., 2009; Bunnell and Ervasti, 2010). The distinct

auditory hair cell and deafness phenotypes in mice in which floxed *Actb* and *Actg1* alleles were selectively ablated also support unique roles for β_{cyto}- and γ_{cyto}-actin in some tissues (Perrin et al., 2010; Perrin et al., 2013). On the other hand, mice with skeletal muscle-specific knockouts of either β_{cyto}-, or γ_{cyto}-actin each develop a similar myopathy with progressive myofiber degeneration/regeneration and muscle weakness (Prins et al., 2011; Sonnemann et al., 2006) supporting that some functions of β_{cyto}- and γ_{cyto}-actins are redundant in some tissues.

We previously investigated the isoform-specific functions of β_{cyto}- and γ_{cyto}-actin in primary mouse embryonic fibroblasts (MEFs) from *Actg1*$^{-/-}$ animals (Bunnell and Ervasti, 2010; Bunnell et al., 2011) and from mice with floxed *Actb* alleles conditionally ablated by tamoxifen-inducible Cre recombinase (Bunnell et al., 2011). γ_{cyto}-Actin null MEFs showed mild growth impairment and a small decrease in cell viability, but were otherwise comparable to control cells in all other parameters tested (Bunnell and Ervasti, 2010; Bunnell et al., 2011). In contrast, β_{cyto}-actin knockout MEFs exhibited a wide range of more severe phenotypes (Bunnell et al., 2011). Ablation of β_{cyto}-actin resulted in severe growth impairment and an increase in the percentage of multinucleate cells, suggesting a specific role for β_{cyto}-actin in cell growth and division (Bunnell et al., 2011) as previously supported by localization of β_{cyto}-actin to the cleavage furrow and contractile ring during cell division (Dugina et al., 2009). Furthermore, β_{cyto}-actin knockout cells exhibited significant migration defects that were not observed in γ_{cyto}-actin null cells. The altered expression of genes that regulate the cell cycle and cell migration

observed in β_{cyto}-actin, but not γ_{cyto}-actin knockout MEFs, provided a potential explanation for the more severe phenotypes in β_{cyto}-actin knockout cells and early lethality in β_{cyto}-actin knockout embryos (Bunnell et al., 2011). Also interesting, β_{cyto}-actin knockout MEFs exhibited some characteristics reminiscent of myofibroblasts, such as an increase in stress fibers and greatly elevated expression of α_{sm}-actin (Bunnell et al., 2011).

In contrast to our results, four studies have reached different conclusions that warrant further investigation. One study of immortalized β_{cyto}-actin knockout MEF lines transformed by SV40 largeT antigen (Tondeleir et al., 2012) reported altered morphology, impaired migration and upregulation of α_{sm}-actin similar to what we observed in primary *Actb* null MEFs (Bunnell et al., 2011), but with no impairment of cell growth. Two studies using small interfering RNA (siRNA) methodologies reported that knock down of γ_{cyto}-actin more dramatically impaired motility in human subcutaneous fibroblasts, spontaneously immortalized keratinocytes, and neuroblastoma SH-EP cells than did knock down of β_{cyto}-actin (Dugina et al., 2009; Shum et al., 2011). Most notably, the fourth study demonstrated specific upregulation of myofibroblast-associated gene products (including α_{sm}-actin) after siRNA knock down of γ_{cyto}-actin, but not β_{cyto}-actin, in several epithelial cell lines (Lechuga et al., 2014). While differences in methodologies and cell types studied are obvious explanations for the different outcomes, Lechuga and colleagues further speculated that the different results

could depend on whether the ablated actin isoform was also the most abundant in the cell type under investigation (Lechuga et al., 2014).

To address the bases for differences between ours (Bunnell and Ervasti, 2010; Bunnell et al., 2011) and others (Dugina et al., 2009; Lechuga et al., 2014; Shum et al., 2011; Tondeleir et al., 2012) studies, we quantitatively profiled actin isoforms at both the transcript and protein level. Because MEFs display extensive developmental and phenotypic heterogeneity (Singhal et al., 2016), we employed adenovirus-5 mediated expression of Cre recombinase (Ad5-Cre) to ablate *Actb* and/or *Actg1* in both primary and Large T antigen immortalized MEFs controlled against the same MEFs infected with Ad5-GFP. α_{sm}-Actin and β_{cyto}-actin transcripts predominated in primary MEFs, while α_{sm}-actin was most abundant at the protein level, with equivalent levels of β_{cyto}- and γ_{cyto}-actin protein expressed despite their marked differences in transcript levels. We also found that immortalization by transformation with SV40 largeT antigen appears to negate the essentiality of *Actb* observed in primary MEFs. Finally, siRNA-mediated transcript knockdown of *Actb* and *Actg1* in the same cells used for gene targeting studies yielded similar results as those observed after gene targeting. We conclude that the genetic reprogramming associated with immortalization by transformation with SV40 largeT antigen can markedly influence the cellular response to β_{cyto}- and γ_{cyto}-actin protein ablation.

Results

Adenoviral Cre mediated knock-out of Actb and Actg1.

Because primary MEFs display extensive developmental and phenotypic heterogeneity (Singhal et al., 2016), each of our biological replicates consisted of E13.5 primary MEFs obtained from a single mouse embryo carrying floxed alleles of either Actb ($Actb^{L/L}$, Bunnell and Ervasti, 2011; Perrin et al., 2010), Actg1 ($Actg1^{L/L}$,Sonnemann et al., 2006), or both Actb and Actg1 ($Actb^{L/L}$ $Actg1^{L/L}$). MEFs from each animal were split into two pools that were treated with Ad5-GFP (Figure 1A) as a negative control, or with Ad5-Cre (Figure 1B) to conditionally knock out Actb (β_{cyto}-actin KO), Actg1 (γ_{cyto}-actin KO), or both Actb and Actg1 (dKO). Quantitative reverse transcription polymerase chain reaction (qRT-PCR) analysis showed that Actb and Actg1 transcripts were reduced 95% by 3dpi in β_{cyto}-actin KO, γ_{cyto}-actin KO and dKO MEFs compared to controls (Figure 1C-F). Western blot analysis revealed that β_{cyto}- and γ_{cyto}-actin were each undetectable at 5dpi in single β_{cyto}-actin KO or γ_{cyto}-actin KO cells, respectively (Figure1G, H). In contrast, complete loss of β_{cyto}- and γ_{cyto}-actin in dKO cells was observed at 9dpi (Figure 1I). Thus, Ad5-Cre was an efficient and robust method to eliminate both β_{cyto}-and γ_{cyto}-actin transcripts and proteins in primary MEFs.

β-Actin KO MEFs are growth impaired with reduced ATP levels.

We previously showed that tamoxifen-induced, cre-mediated ablation of β_{cyto}-actin caused significant growth impairment in primary MEFs while only a modest decrease in cell growth was observed in *Actg1-/-* MEFs (Bunnell and Ervasti, 2010; Bunnell et al., 2011). However, our previous experiments involved different methods of gene ablation for Actb and Actg1 and compared knockout MEFs with controls derived from different embryos (Bunnell and Ervasti, 2010; Bunnell et al., 2011). Therefore, we more directly compared the effects of β_{cyto}-versus γ_{cyto}-actin gene ablation on cell growth using β_{cyto}-actin KO and γ_{cyto}-actin KO MEFs. Under these more controlled conditions, γ_{cyto}-actin KO MEFs exhibited a normal growth rate, while both β_{cyto}-actin KO and dKO MEFs displayed growth impairment by 3dpi that became significantly different from controls at 7dpi (Figure 2). Because growth deficiency was not previously observed in MEFs ablated for β_{cyto}-actin expression after transformation by SV40 largeT antigen (Tondeleir et al., 2012), we immortalized $Actb^{L/L}$, $Actg1^{L/L}$ and double $Actb^{L/L}$ $Actg1^{L/L}$ MEFs by transformation with SV40 largeT antigen and measured cell growth after infection with either Ad5-Cre or Ad5-GFP. Both SV40 largeT antigen immortalized β_{cyto}-actin KO and γ_{cyto}-actin KO MEFs exhibited growth rates not different from controls (Supplemental figure 1A-B), suggesting that β_{cyto}-actin is important for cell growth in primary MEFs, but not in MEFs transformed by SV40 largeT antigen. In contrast, SV40 largeT antigen immortalized dKO MEFs displayed growth impairment that was significantly different from control at 8-10dpi (Supplemental figure 1C), but less severe than in primary MEFs, suggesting that MEFs immortalized by SV40

largeT antigen transformation are able to circumvent the essential function supported by β_{cyto}-actin in primary cells and during embryonic development.

To assess whether growth deficiencies seen in β_{cyto}-actin KO and dKO MEFs could potentially be due to decreases in energy availability, we utilized a luciferase-based assay to measure the relative levels of cellular ATP in β_{cyto}-actin KO, γ_{cyto}-actin KO and dKO MEFs. Correlating with the deficiencies seen in growth, ATP levels were significantly decreased in β_{cyto}-actin KO and dKO MEFs compared to controls, but not in γ_{cyto}-actin KO MEFs (Figure 3A). However, western blot analysis demonstrated that a number of proteins in the mitochondrial electron transport chain complexes were equivalent across the MEF lines tested (Figure 3B-C), as were basal and maximal oxygen consumption rates measured in β_{cyto}-actin KO and γ_{cyto}-actin KO MEFs using a Seahorse XF24 extracellular flux analyzer (Figure 3D). Therefore, we conclude that the measured decreases in cellular ATP are not due to impaired mitochondrial function in β_{cyto}-actin KO and dKO MEFs.

Quantitation of actin isoform transcript and protein levels in primary MEFs.

qRT-PCR was used to measure transcript levels for all six actin isoforms in control, β_{cyto}-actin KO, γ_{cyto}-actin KO and dKO MEFs after 5dpi. The amount of transcript for each actin isoform in MEFs was calculated from standard curves that were amplified in parallel (Supplemental figure 2-2 A-F). In all control MEFs, α_{sm}- and β_{cyto}-actins were the dominant transcripts (Figure 2-4 A-C), in contrast to

NIH3T3s fibroblasts cultured under the same conditions, where β_{cyto}-and γ_{cyto}-actins were the predominant transcripts (Supplemental figure 2-3 A). α_{sm}-Actin was the only actin transcript significantly upregulated in β_{cyto}-actin KO MEFs (Figure 4A) while both α_{sm}- and β_{cyto}-actins transcripts were upregulated in γ_{cyto}-actin KO MEFs (Figure 2-4 B). Similar to β_{cyto}-actin KO MEFs (Figure 2-4 A), α_{sm}-actin was the only transcript significantly upregulated in dKO MEFs (Figure 2-4 C). The high levels of α_{sm}-actin transcript suggest a myofibroblast-like phenotype in the primary MEFs that was enhanced to a greater extent by ablation of Actb over Actg1.

Since α_{sm}-, β_{cyto}- and γ_{cyto}- were the most abundant actin transcripts in primary MEFs, we measured α_{sm}-, β_{cyto}- and γ_{cyto}-actin protein levels in both control and KO MEFs via quantitative Western blot analysis at 5dpi in each single KO and at 9dpi in the dKO using purified α_{sm}-, β_{cyto}- and γ_{cyto}-actin proteins as standards. α_{sm}-Actin was the most abundant actin isoform protein expressed, while β_{cyto}- and γ_{cyto}-actin proteins were expressed to similar levels in all control MEFs (Figure 2-5 B-D). Consistent with transcript analysis (Supplemental figure 2-3 A), β_{cyto}- and γ_{cyto}-actin were the dominant actin proteins expressed in NIH3T3 fibroblasts cultured under the same conditions (Supplemental figure 2-3 B). In β_{cyto}-actin KO MEFs, α_{sm}-actin protein was dramatically increased by 6 fold over controls, but γ_{cyto}-actin protein was not significantly increased (Figure 2-5 A-B). In γ_{cyto}-actin KO MEFs, α_{sm}-actin protein was upregulated by 1.7 fold while β_{cyto}-actin protein was not significantly increased (Figure 2-5 A, C). α_{sm}-Actin protein was also significantly upregulated by 7 fold in dKO MEFs (Figure 2-5 A, D). Thus, α_{sm}-actin was

prominently expressed in all control primary MEFs and more dramatically upregulated upon ablation of Actb compared to Actg1, suggesting that primary MEFs may be predisposed to a myofibroblast-like phenotype that can be most enhanced by selective perturbation of Actb. Also interesting, β_{cyto}-actin transcript was expressed six-fold higher than γ_{cyto}-actin transcript in all control MEFs, yet the ratio of β_{cyto}-actin protein to γ_{cyto}-actin protein was 1:1 (Figure 2-6 A-C). The unequal transcript-to-protein ratio supports other studies concluding that Actb and Actg1 gene expression are differentially regulated post-transcriptionally (Hüttelmaier et al., 2005; Zhang et al., 2010).

siRNA mediated knockdown of Actb andActg1.

Since other studies reporting results different from ours used siRNA approaches to knock down (KD) Actb and Actg1 transcripts and proteins (Dugina et al., 2009; Lechuga et al., 2014; Shum et al., 2011), we assessed how siRNA-mediated KD of β_{cyto}- and/or γ_{cyto}-actin in $Actb^{L/L}$ (β_{cyto}-actin KD), $Actg1^{L/L}$ (γ_{cyto}-actin KD), and $Actb^{L/L}$ $Actg1^{L/L}$ (β/γ_{cyto}-actin dKD) primary MEFs impacted cell phenotype. On average, we were able to specifically KD β_{cyto}-actin protein by 70% and γ_{cyto}-actin protein by 55% when compared to controls. In dKD MEFs, β_{cyto}-actin protein was reduced by 65% and γ_{cyto}-actin protein was reduced by 55% (Figure 2-7 A). Quantitative Western blot analysis showed that α_{sm}-actin protein was dramatically increased 9-fold in β_{cyto}-actin KD cells, over controls, but γ_{cyto}-actin protein was not significantly increased (Figure 2-7 A-B). In γ_{cyto}-actin KD cells,

neither α_{sm}-actin protein nor β_{cyto}-actin protein was significantly increased (Figure 2-7 A, C). α_{sm}-Actin protein was also significantly upregulated 4-fold in β/γ_{cyto}-actin dKD cells (Figure 2-7 A, D). Thus, both siRNA mediated transcript KD and cre mediated gene KO gave similar results in primary MEFs.

Actb gene ablation enhances some myofibroblast-like phenotypes of primary MEFs.

In response to a variety of perturbations (Davis and Molkentin, 2013; Small, 2012), fibroblasts often differentiate into smooth muscle-like cells called myofibroblasts via a process called the fibroblast to myofibroblast transition (FMT). In addition to increased α_{sm}-actin expression, another hallmark of myofibroblasts is increased stress fiber formation (Davis and Molkentin, 2013; Small, 2012), which we observed in β_{cyto}-actin KO, γ_{cyto}-actin KO and dKO MEFs, compared to controls (Figure 2-8 A-F). To quantify the change in the stress fibers of KO MEFs, line scans across the cell width were made (Figure 2-8 G). Peak-to-valley ratios were taken as an average measure of the fluorescence intensity of the stress fibers (Figure 8H). All KO cell types displayed significant elevation in the average peak-to-valley ratios, indicating increased stress fiber formation (Figure 2-8 A-F). Because caldesmon, calponin and transgelin proteins have been shown to be upregulated during epithelial to myofibroblast transition (Lechuga et al., 2014), we measured their protein levels in addition to myosin light chain 2 and phosphorylated myosin light chain 2 protein levels in control and knock out MEFs. Caldesmon expresses

a higher molecular weight isoform in smooth muscle cells ($Cald1_{sm}$) than in non-smooth muscle cells (Frid et al., 1992; Ueki et al., 1987). In agreement with our previously published data (Bunnell et al., 2011), $Cald1_{sm}$ was upregulated in β_{cyto}-actin KO, γ_{cyto}-actin KO and dKO primary MEFs, though more so in β_{cyto}-actin KO MEFs than γ_{cyto}-actin KO MEFs (Figure 2-9 A-D). In contrast, none of the other myofibroblast marker proteins interrogated were significantly upregulated (Figure 9A-D). siRNA-treated primary MEFs showed similar upregulation of $Cald_{sm}$ in KD MEFs (Supplemental figure 2-4 A-D). Thus, increased stress fiber formation and expression of $Cald1_{sm}$ suggests that ablation of *Actb* enhances a partial myofibroblast-like phenotype in primary MEFs.

Finally, actin dynamics are known to play a role in myofibroblast differentiation via the serum response factor (SRF)/myocardin-related transcription factor (MRTF) gene regulatory pathway (Small, 2012). Therefore, we investigated whether either SRF or MRTF-A protein expression, and SRF activity, was perturbed when cytoplasmic actins were ablated. In all knockout MEFs, SRF protein levels were not significantly altered compared to controls (Figure 2-10 A, C). MRTF-A protein level was downregulated in all gene knockout MEFs, which was significant in dKO MEFs (Figure 2-10 A-B). Similar results were observed in siRNA KD MEFs (Supplemental figure 2-5 A-B). Although no drastic changes in protein expression were observed, SRF activity was significantly increased by 6-fold in both β_{cyto}-actin KO and dKO MEFs compared to controls. SRF activity increased by 2-fold in γ_{cyto}-actin KO MEFs, although this increase was not

significantly different from controls. Our data suggest that Actb knockout more significantly and specifically impacts the SRF/MRTF gene regulatory pathway than does the loss of Actg1.

Discussion

β_{cyto}-actin is thought to be an essential protein based on the early embryonic lethality observed in Actb gene-targeted mice (Bunnell et al., 2011; Shawlot et al., 1998; Shmerling et al., 2005b). In addition, many cell biological studies provide further compelling support to the essentiality of β_{cyto}-actin in a wide array of cellular processes (Hofmann et al., 2004; Hu et al., 2004; Karakozova et al., 2006; Leung et al., 2006; Yao et al., 2006; Zhao et al., 1998). While γ_{cyto}-actin is clearly important *in vivo*, it is not essential given that Actg1 null mice can survive up to 2 years (Belyantseva et al., 2009). Here we attempted to resolve the different results reported across a group of cell-based studies all seeking to elucidate the respective roles of β_{cyto}- and γ_{cyto}-actin through ablation of protein expression using different targeting approaches in different cell types. Most vexing, β_{cyto}-actin gene knockout in two studies caused essentially the same effects on cell motility and α_{sm}-actin expression (Bunnell et al., 2011; Tondeleir et al., 2012) as those caused by γ_{cyto}-actin knockdown in three other studies (Dugina et al., 2009; Lechuga et al., 2014; Shum et al., 2011). Because gene and transcript targeting have been shown to cause strikingly different *in vivo* phenotypes for a number of loci (Rossi et al., 2015), we anticipated that actin gene knockout and transcript knockdown experiments carried out in the same cells would explain the discrepant results. Instead, we observed the same experimental outcomes whether siRNA-mediated transcript knockdown or Cre-

mediated gene knockout were employed. As an alternative explanation for the discrepant results across studies (Bunnell et al., 2011; Dugina et al., 2009; Lechuga et al., 2014; Shum et al., 2011; Tondeleir et al., 2012), Lechuga and colleagues hypothesized that loss of the most abundantly expressed actin isoform may dictate a given cell type's response to actin gene ablation (Lechuga et al., 2014). However, our quantitative western blot analysis demonstrated that β_{cyto}- and γ_{cyto}-actin proteins were present in equal abundance in the primary MEFs studied here. We conclude that neither differences in actin isoform targeting method or endogenous protein levels can explain the dramatically different and often opposite results reported in the six studies from five different groups.

Here (Figure 2-2) and previously (Bunnell et al., 2011), we measured dramatic cell proliferation defects with ablation of β_{cyto}-actin in primary MEFs that could account for the embryonic lethality associated with Actb gene deletion (Bunnell et al., 2011; Shawlot et al., 1998; Shmerling et al., 2005b). We measured significantly decreased levels of cellular ATP associated with knockout of β_{cyto}-actin in the presence of apparently unaffected mitochondrial function (Figure 2-3). While the basis for decreased ATP levels in β_{cyto}-actin knockout MEFs remains an interesting question for future studies, it will be challenging to answer given that ablation of functionally disparate genes in MEFs has been shown to impact cellular ATP levels independent of corresponding defects in mitochondrial respiration (Gautier et al., 2008; Giaime et al., 2012). We also found that immortalization

induced by transformation with SV40 largeT antigen rendered Actb nonessential for proliferation (Supplemental Figure 2-1). Although Tondeleir et al., 2012 previously noted that cell survival was not impaired in their Actb null MEFs immortalized by transformation with SV40 largeT antigen, a more recent study reported a general delay in cell cycle progression, impaired colony growth and reduced proliferation rate in the same cell line (Almuzzaini et al., 2016). While we cannot exclude other effects of transformation with SV40 largeT antigen, cell immortalization has been associated with substantial changes in gene expression (Gordon et al., 2014; Kuo et al., 2012). A recent comparison of primary and spontaneously immortalized MEFs reported almost 2,000 transcripts that were up- or down-regulated by 3-fold (Kuo et al., 2012). Other studies have demonstrated that immortalization can significantly impact cell behavior both in the absence (Vasioukhin et al., 2000), or presence of subsequent perturbations (Wade et al., 2002), and even after reversal (Wang et al., 2014). In one highly cited study, primary epithelial cells form prominent “adhesion zippers” that become challenging to detect after immortalization (Vasioukhin et al., 2000). Moreover, the essential role for p27 in mediating the growth-inhibitory effects of vitamin D in mouse knockout models and primary MEFs was not recapitulated in immortalized MEFs (Wade et al., 2002). Given the unpredictable effects of immortalization and transformation on cell biological function, we suggest that primary MEFs more appropriately model the embryonic lethality associated with Actb gene ablation in mice.

We measured striking differences between the ratios of β_{cyto} to γ_{cyto}-actin transcript versus protein in primary MEFs: β_{cyto}-actin transcript was 6-fold greater than γ_{cyto}-actin transcript, yet β_{cyto}- and γ_{cyto}-actin protein levels were equivalent (Figure 6). β_{cyto}-actin translation is more rapid than γ_{cyto}-actin (Zhang et al., 2010) and also tightly regulated via an RNA regulatory sequence in its 3'UTR named the "zipcode" (Hüttelmaier et al., 2005; Kislauskis et al., 1993; Ross et al., 1997). Because β_{cyto}-actin protein is the more dynamic of the two cytoplasmic actin isoforms (Bergeron et al., 2010), it is tempting to speculate that the greater abundance of the β_{cyto}-actin transcript is maintained for rapid translation and dynamic cytoskeletal rearrangement. However, the similar levels of β_{cyto}- and γ_{cyto}-actin protein (Figure 2-6) and similar rates of decay after gene ablation in primary MEFs (Figure 2-1) suggest that β_{cyto}-actin transcript may play some additional function in cells independent of its role as a template for translation. As one possibility, the large pool of Actb transcript may serve to buffer miRNAs important in regulating the expression of other genes important for cell proliferation, motility, and/or differentiation. Of the more than 20 different miRNA binding sites collectively predicted by TargetScan, microRNA.Org, and PicTar to be present in the 3' UTR of the Actb transcript but absent from Actg1 (Supplemental table 2-1), only mir-205 was identified by all three programs while mir-1 and mir206 were identified by two of three algorithms. Interestingly, mir-1, mir-205 and mir-206 have all been previously hypothesized to function as tumor suppressors based on experiments demonstrating a correlation between growth inhibition with miRNA

overexpression (Hudson *et al.*, 2012; Jalali *et al.*, 2012; Liu *et al.*, 2012; Koshizuka *et al.*, 2016), or increased proliferation after miRNA inhibition (Jalali et al., 2012). Of further relevance to our study, overexpression of mir-1, mir-205 and mir-206 also was associated with significantly decreased cell motility, increased expression of α_{sm}-actin and calponin, and perturbations in actin cytoskeletal dynamics (Hudson et al., 2012; Jalali et al., 2012; Liu et al., 2012). We speculate that ablation of Actb transcript could indirectly drive similar phenotypic changes by freeing up normally sequestered miRNAs. Finally, differential miRNA binding may not be required to explain different phenotypic outcomes for Actb versus Actg1 transcript ablation. The miRNA mir-145 is predicted to bind both Actb and Actg1 and is important in smooth muscle cell proliferation and differentiation (Cordes et al., 2009) so it is possible that more abundant Actb transcript could play the dominant role in sequestering mir-145 during development.

Finally, the differentiation status and/or tissue origin of cells utilized may also account for some of the differences between studies (Bunnell et al., 2011; Dugina et al., 2009; Lechuga et al., 2014; Shum et al., 2011; Tondeleir et al., 2012). While Actb and/or β_{cyto}-actin are essential during relatively early stages of embryonic development (Bunnell et al., 2011; Shawlot et al., 1998; Shmerling et al., 2005b), neither is specifically required for later stage development of more differentiated auditory hair cells (Perrin et al., 2010), neurons of the peripheral (Cheever et al., 2011) or central (Cheever et al., 2012) nervous systems, or skeletal muscle (Prins et al., 2011; Sonnemann et al., 2006). These data suggest

that cells transition from an Actb-essential state to an Actb-important state as development and differentiation progress *in vivo*. Clearly, the challenge remains to define the *in vivo* biological process modeled by any particular cell in culture.

Materials and Methods

Cell Culture

Primary MEFs were cultured from E13.5 Actb $^{L/L}$, Actg1$^{L/L}$ and double Actb$^{L/L}$/Actg1$^{L/L}$ mouse embryos as described previously (Bunnell and Ervasti, 2010). Cells were grown to 80% confluency on 10-cm plates and frozen down at passage 1 at 1x10^{6} cells/mL in MEF freezing media (DMEM supplemented with 10% FBS, 1% Pen/Strep, 0.5ug/mL Fungizone and 5% dimethyl sulfoxide). Primary MEFs were immortalized by transformation with SV40 largeT antigen expression, which was incorporated into the genome via the piggyBac transposase system. MEFs from individual embryos were thawed, cultured in MEF media (DMEM supplemented with 10% FBS, 1% Pen/Strep, 0.5ug/mL Fungizone), grown to 80% confluency, split into two culture dishes and treated with either Ad5-GFP control virus (Ad5CMV-hrGFP) or Ad5-Cre (Ad5CMV-Cre-eGFP) virus purchased from The University of Iowa Viral Vector Core following their Adenovirus Adfection Protocol (http://www.medicine.uiowa.edu/vectorcore).

SiRNA transfection

MEFs from individual embryos were thawed, grown to 80% confluency, split into two culture dishes and treated with either control or β_{cyto}- and/or γ_{cyto}-actin ONTARGET*plus* siRNAs purchased from Dharmacon following their protocol.

(http://dharmacon.gelifesciences.com/uploadedFiles/Resources/basic-dharmafect-protocol.pdf) See supplemental methods for siRNA sequences.

SRF Luciferase Activity Assay

Actb$^{L/L}$, Actg1$^{L/L}$ and double Actb$^{L/L}$Actg1$^{L/L}$ MEFs from individual embryos were treated with either Ad5-GFP or Ad5-Cre. sKO at 3dpi and dKO at 7dpi were nucleofected (Amaxa® Nucleofector® II) with PGL3-Basic-luc (control) or PGL3-FHL2_145-luc (Four and a half LIM domain protein-2) promoter (SRF reporter) constructs (Schmidt et al., 2012), generously provided by Dr. Hannelore V. Heemers. Two days post nucleofection, at 5dpi for sKO and 9dpi for dKO, cells were lifted and hand counted using a hematocytometer. Equal numbers of cells between Ad5-GFP and Ad5-Cre treated MEFs were washed with PBS and processed based on manufacture protocols (Dual-Luciferase® Reporter Assay, Promega). Aliquots (20µL) of cleared processed lysates were used to determine SRF luciferase activity (BioTek Synergy 4 spectrometer with Gen5 2.07 software).

Quantitative Reverse Transcription Polymerase Chain Reaction (qRT-PCR)

Mouse actin isoform cDNAs were amplified from WT MEFs by PCR using the primers listed in the supplemental methods and cloned into pENTR™/D-TOPO vector (Life Technologies) to generate a control construct for each actin isoform. Each actin isoform qRT-PCR primer set, listed in the supplemental methods, was tested for amplification of all control constructs to assess primer specificity. Total

RNA was extracted from Actb $^{L/L}$, Actg1$^{L/L}$ and double Actb$^{L/L}$/Actg1$^{L/L}$ MEF samples using the Biorad-Aurum ™ Total RNA Mini Kit following the manufacturer's instructions. RNA concentration and purity (260/280 ratio) were determined using a NanoDrop spectrophotometer (Wilmington, DE). First-strand cDNA was synthesized with a Biorad-iScript Advanced cDNA Synthesis Kit for qRT-PCR using the same initial RNA amount (1ug) for all samples. Individual control constructs, were used in a 10-fold dilution to generate a standard curve, and MEF samples were amplified in parallel with each specific qRT-PCR primer set using Biorad -SsoAdvanced Universal SYBR polymerase on the Biorad-CFX96 Real Time System C1000 Touch Thermal Cycler to profile each actin isoform transcript amount (pmol).

Actin Isoforms

Platelet non-muscle actin (β_{cyto}- and γ_{cyto}-actin) was purchased from Cytoskeleton, Inc. (Denver, CO). Recombinant γ_{cyto}- and α_{sm}-actin were expressed in the Bacto-Bac insect cell-expression system and purified as previously described (Perrin *et al.*, 2013). Protein concentrations were determined using a NanoDrop spectrophotometer (Wilmington, DE). Contamination of recombinant γ_{cyto}- and α_{sm}-actins by insect cell actin was measured by ESI mass spectrometry acquired using a QSTAR Pulsar i (Applied Biosystems, Inc., Foster City, CA) quadrupole-TOF (time-of-flight) mass spectrometer equipped with a turbo-ESI source. Protein samples were loaded directly in 50% Acetonitrile and 0.1% formic

acid. The ion spray voltage was 1000 V, the TOF region acceleration voltage was 4 kV, and the injection pulse repetition rate was 7.0 kHz. External calibration was performed using renin

(monoisotopic mass [MH3+] 586.9830 and [MH2+] 879.9705; Sigma-Aldrich, St. Louis, MO). Mass spectra were summed and averaged over the injection peak. Deconvolution of the charge envelope was performed with the Bioanalyst, AnalystQS software package (ABI).

Western Blotting

For western blot quantitation of actin isoforms against a standard curve, Total MEF protein was extracted with 1%SDS buffer in 1xPBS and a cocktail of protease inhibitors (Aprotinin 100uM, Benzamide 0.79mg/mL, E-64 10nM, Leupeptin 10uM, Pepstatin 0.1mg/mL, PMSF 1mM), sonicated (Model 150V/T Ultrasonic homogenizer, BioLogics, Inc.), boiled and centrifuged to remove the insoluble fraction. An increasing amount (25-300ng) of purified actin protein and all MEF samples were run on the same blot to ensure consistency. LiCor fluorescent signal verses purified actin protein amount (ng) was used to generate a standard curve, in order to calculate specific actin isoform concentration (Supplemental Figure 2-6; ng protein/µL of total lysate). All samples were western blotted with β-actin (AC-15; Sigma-Aldrich), γ-actin (mAb 117; and α_{sm}-actin (A14; Sigma-Aldrich). For comparisons of relative immunoreactivities, equal amounts of cleared total MEF lysate protein (25µg) were blotted with antibodies to

Caldesmon1 (Cat #2980, Cell signaling), SM22 (ab14106; Abcam), Calponin (ab46794; Abcam), SRF (G-20; Santa Cruz), MRTF-A (H-140; Santa Cruz), MTOC1 (ab14705; Abcam), SDHA (ab14715; Abcam), UQCR (ab110252; Abcam), ATP5A (ab14748; Abcam), MLC2 (ab48003; abcam), MLC2 (phosphor S20) (ab2480; abcam), and GAPDH (G9545 or G8795; Sigma-Aldrich) was used as loading control.

Cell Fixation and Staining

MEFs cultured for 6 to 8 days post infection (DPI) with either Ad5-GFP or Ad5-CRE were plated on [5ug/ml] fibronectin-coated coverslips at a density of $1x10^4$ cells per coverslip and incubated in MEF culturing media. The following day, cells were fixed with fresh 4% paraformaldehyde in PBS for 15min at room temperature. To stain actin filaments, fixed cells were treated with a 0.2% Triton X-100 and 16.5nM Phalloidin (Life Technologies A22285) in PBS for 30 minutes at room temperature. Coverslips were mounted in Prolong (Life Technologies P36931) mounting media.

Cell Imaging and Quantification

Samples were imaged using a Delta Vision PersonalDV microscope under a 60x1.42 NA objective (GE Technologies). All cells were imaged with the same laser intensity and exposure time. The intensity of the stress fibers was quantified

from line scans across the widest part of the cell using ImageJ. The peaks and corresponding valleys were then determined (excluding the first peak which represents the edge of the cell).

The average peak to valley ratio per cell was then plotted using GraphPad Prism.

ATP Quantification

At 7 or 9 DPI, cells were lifted and counted. Equal number of CT and KO MEFs were lysed using boiling water (Yang *et al.*, 2002). The lysate was spun at 12,000x*g* for 5 min at 4°C and the supernatant was collected. Following the luciferase based ATP Determination Kit (A22066) protocol, the reaction solution (reaction buffer, DTT, D-luciferin, and firefly luciferase) was added to the cell lysate supernatant. After a 15 min incubation, ATP levels were determined using a BioTek Synergy 4 spectrometer with Gen5 2.07 software and quantified using an ATP standard ranging from 0nm-1µM.

Analysis of cell growth

$5x10^5$ of MEFs/well were treated with either Ad5-GFP or Ad5-Cre. Samples were counted every other day beginning 1dpi, in duplicate, using a hematocytometer to generate growth curves.

Oxygen Consumption

Cells were plated in triplicate on fibronectin [5ug/ul] coated XF24 cell culture microplates (Seahorse Bioscience) at $5x10^4$ cells per well 24 hours prior to the experiment. Mitochondrial function was examined using the Seahorse XF24 extracellular flux analyzer and the cell mitochondrial stress assay (Seahorse Bioscience). Oligomycin [2ug/ml Final], FCCP (Carbonyl cyanide-p-trifluoromethoxyphenylhydrazone) [0.5µM Final], and Antimycin A [4µM Final] were injected at time points throughout the experiment according to the company protocol (all compounds from Seahorse Bioscience). Oxygen consumption was measured at multiple points in between each injection and normalized to background controls.

Statistics

For quantitative RT-PCR and quantitative Western blots; two-way ANOVA with a Bonferoni post-test was used on calculated amount of transcript (pmol) and protein (ng/uL of lysate) to determine statistics. For all relative Western blots; immuno-reactivity levels for all samples were normalized to GAPDH and relative to the paired embryo control, which was set at 1, and a One sample t-test was performed to evaluate statistics.

Figures

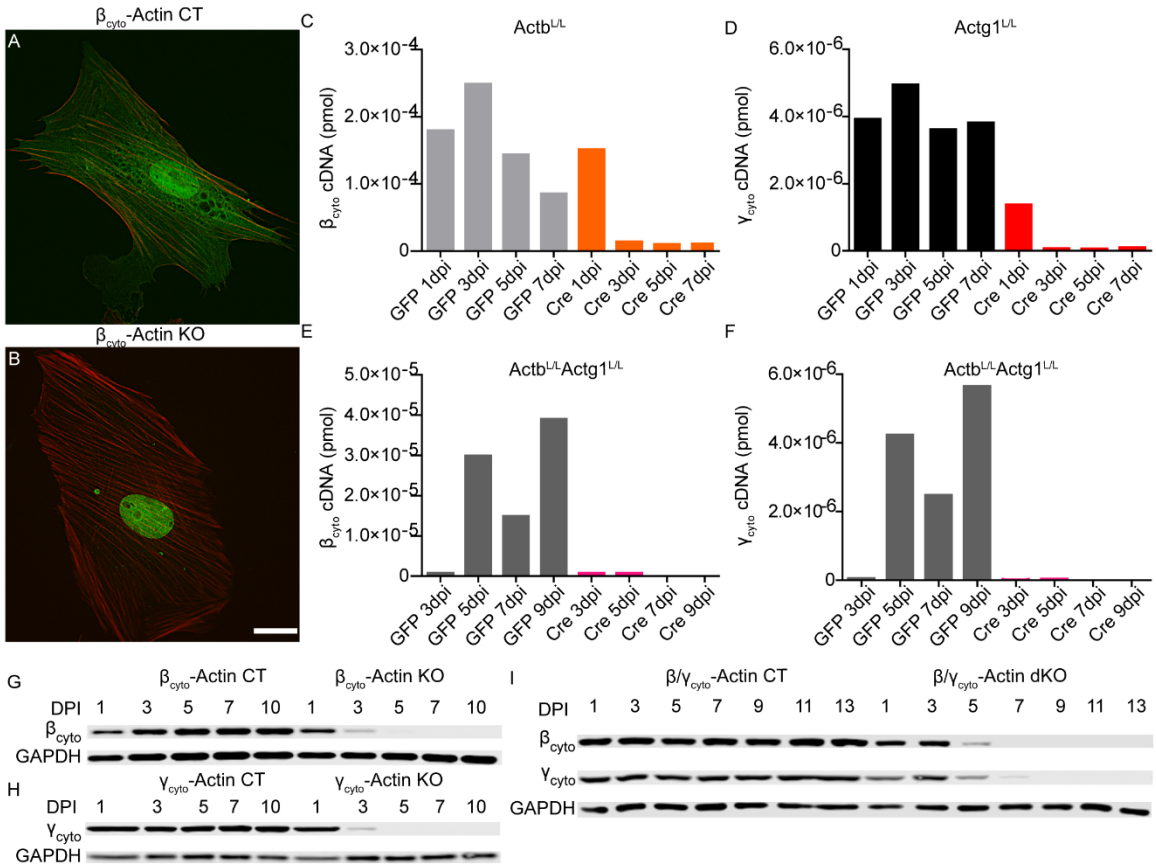

Figure 2-1 Adenoviral Cre efficiently ablated β_{cyto}- and γ_{cyto}-actin in primary mouse embryonic fibroblasts.

(A, B) Representative images of β_{cyto}-actin CT and β_{cyto}-actin KO cells at 7dpi. Scale bar is 20 µm. (C-F) Representative qRT-PCR analysis of β_{cyto}- and γ_{cyto}-actin transcript amount (in pmol) in $Actb^{L/L}$, $Actg1^{L/L}$ and $Actb^{L/L}$ $Actg1^{L/L}$ MEFs. (G-I) Representative relative Western blot analysis of MEF lysates probed with β_{cyto}-actin and γ_{cyto}-actin antibodies; GAPDH served as loading control. Experiments for panels C-I performed by Xiaobai Patrinostro.

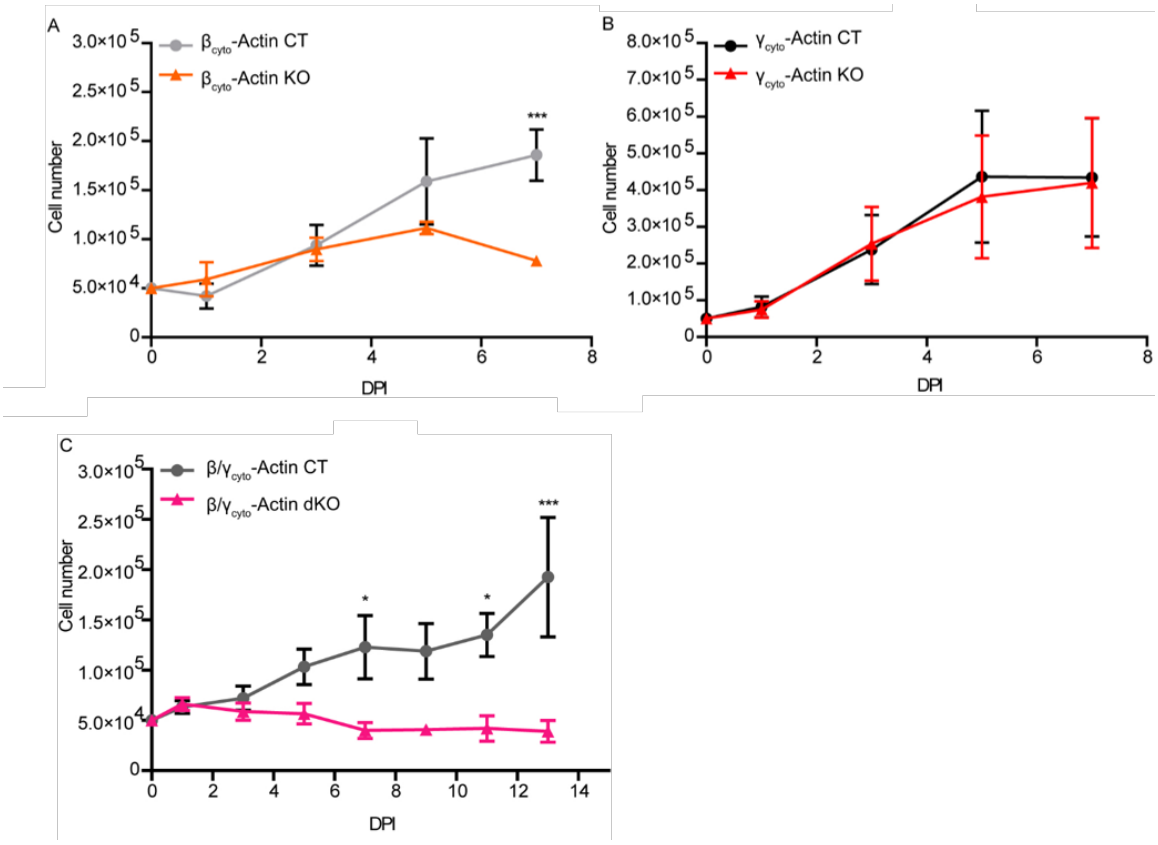

Figure 2-2 β_{cyto}-actin deficient MEFs were growth impaired.

(A-C) Growth curve analysis of $Actb^{L/L}$, $Actg1^{L/L}$ and $Actb^{L/L}Actg1^{L/L}$ MEFs treated with either Ad5-GFP or Ad5-Cre (n=3, hand counted in duplicate). (B). Asterisks denote *P<0.05, *** P<0.001. (Two-way ANOVA with Bonferoni post-test, error bars are s.e.m.). Experiments performed by Xiaobai Patrinostro.

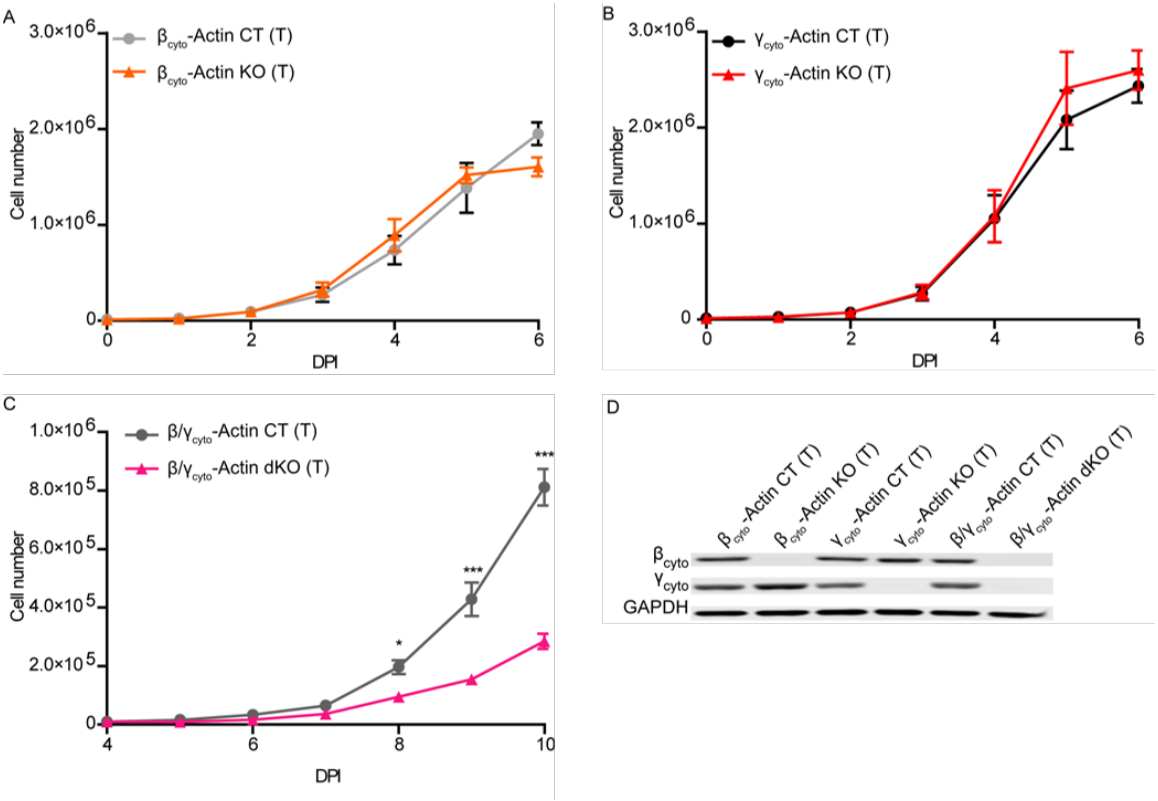

Supplementary Figure 2-1 β_{cyto}-actin sKO SV40 LargeT antigen immortalized MEFs were not growth impaired.

(A) Representative Western blot of SV40 LargeT antigen transformed (T) CT and KO MEF lysates blotted with α_{sm}-actin, β_{cyto}-actin and γ_{cyto}-actin antibodies; GAPDH served as loading control. (B-D) Growth curve analysis of SV40 LargeT antigen transformed (T) CT and KO MEFs (n=3, hand counted in duplicate). Asterisks denote *P<0.05, *** P<0.001. (Two-way ANOVA with Bonferoni post-test, error bars are s.e.m.). Experiments performed by Xiaobai Patrinostro.

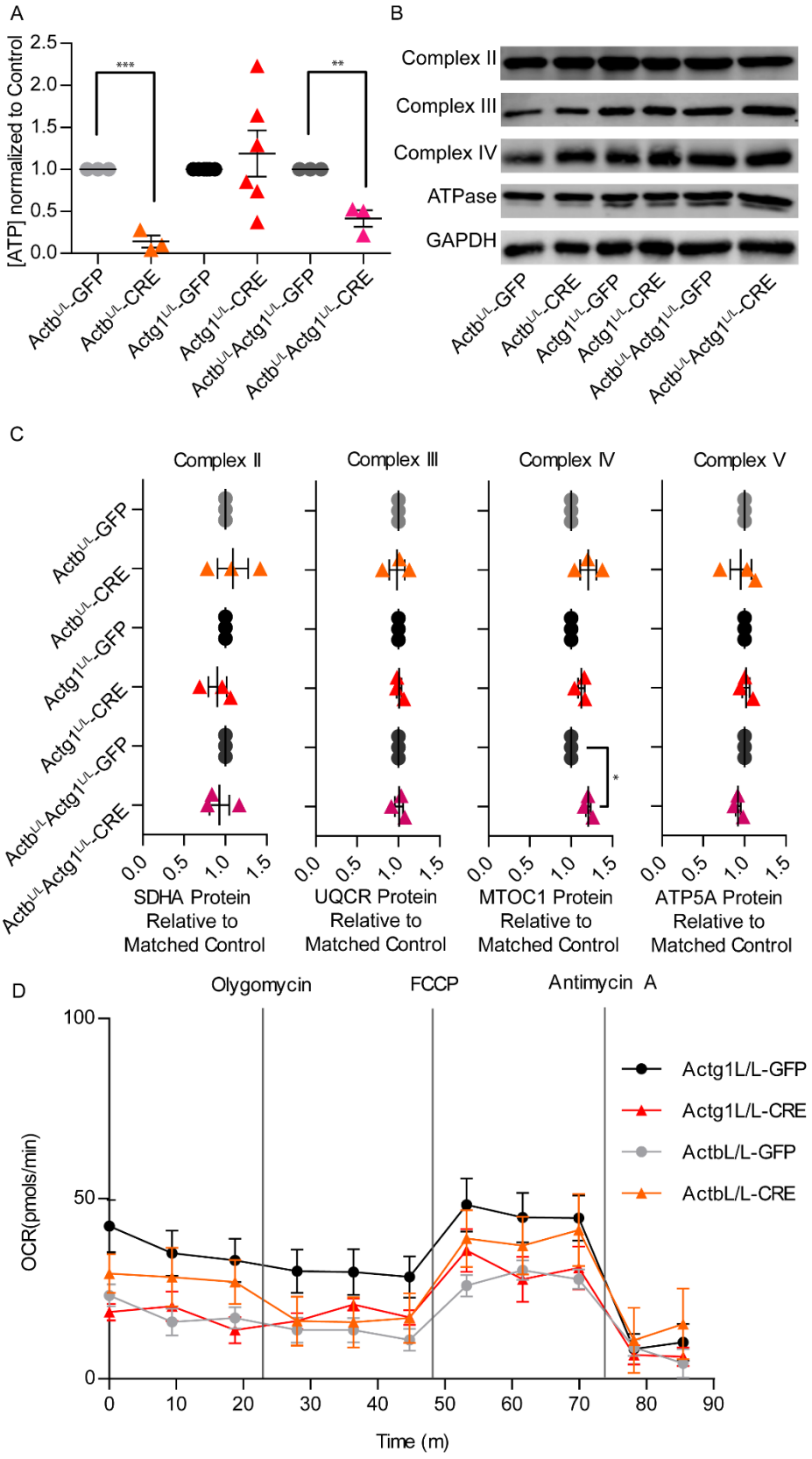
A
[ATP] normalized to Control
2.5
2.0
1.5
1.0
0.5
0.0
***
**
Actb L/L-GFP
Actb L/L-CRE
Actg1 L/L-GFP
Actg1 L/L-CRE
Actb L/L Actg1 L/L-GFP
Actb L/L Actg1 L/L-CRE
B
Complex II
Complex III
Complex IV
ATPase
GAPDH
C
Complex II
Complex III
Complex IV
Complex V
SDHA Protein Relative to Matched Control
UQCR Protein Relative to Matched Control
MTOC1 Protein Relative to Matched Control
ATP5A Protein Relative to Matched Control
D
Olygomycin
FCCP
Antimycin A
OCR(pmols/min)
Time (m)
Actg1L/L-GFP
Actg1L/L-CRE
ActbL/L-GFP
ActbL/L-CRE

Figure 2-3 β_{cyto}-actin deficient MEFs displayed lower ATP levels but maintained ETC protein abundance.

(A) ATP levels for CT and KO MEFs determined through a luciferase assay at 7dpi. Results were normalized to cell number and relative to the paired embryo control ($6 \geq n \geq 3$). (B-C) Western blot and relative quantification of protein levels of Succinate Dehydrogenase Complex, Subunit A, Flavoprotein (SDHA) for Complex II; Ubiquinol-Cytochrome C Reductase Core Protein I (UQCR) for Complex III; Mitochondrially Encoded Cytochrome C Oxidase I (MTCO1) for Complex IV; and ATP5a ATP synthase, H+ transporting, mitochondrial F1 complex, alpha subunit (ATP5A) for the F1/F0 ATPase; GAPDH served as loading control. Levels were normalized to GAPDH and relative to the paired embryo control which was set at 1 (n=3). (D) Oxygen consumption data for control and KO MEFs following treatment with various drugs. Asterisks denote **P<0.01, *** P<0.001. (One sample T-test, error bars are s.e.m.).

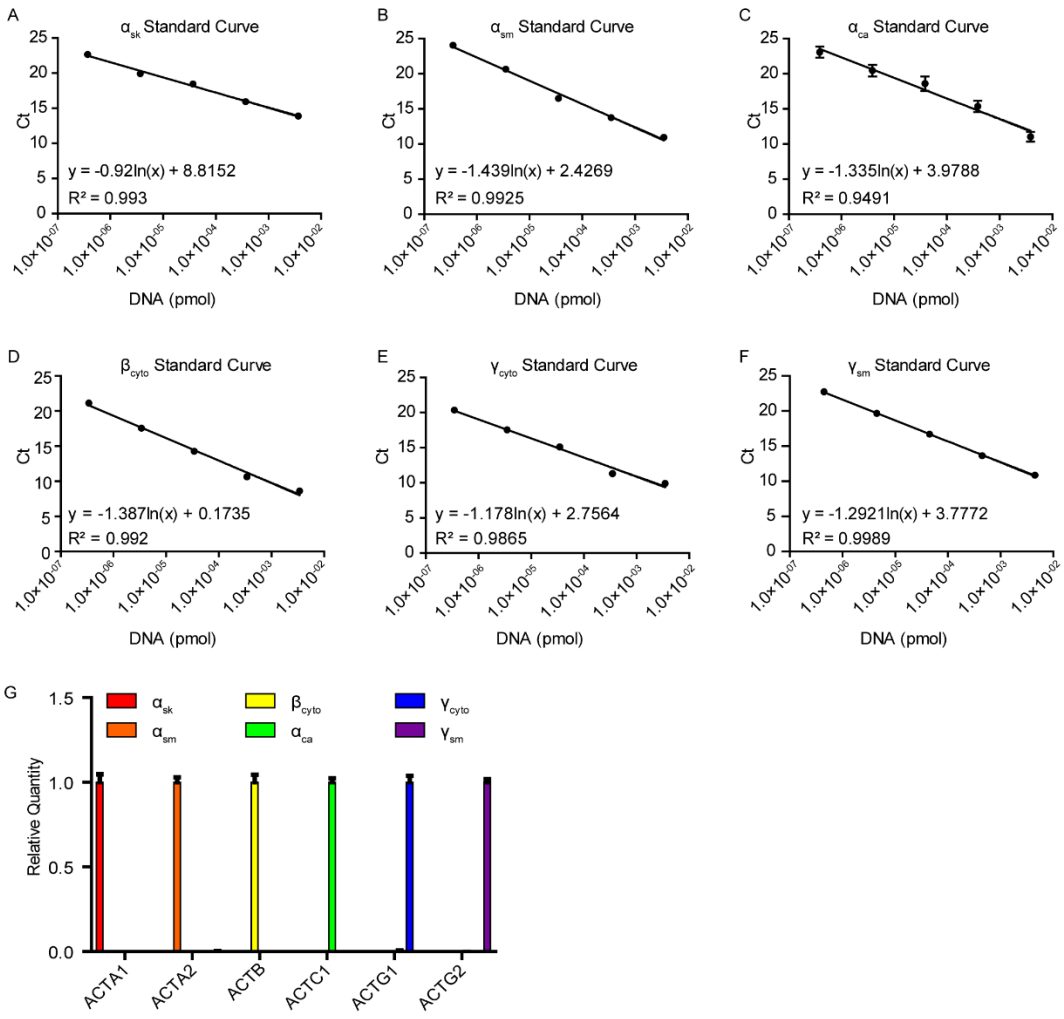

Supplementary Figure 2-2 Mouse actin isoform standard curves and primer specificity analysis.

(A-F) Representative standard curves generated using specific actin isoform primers with the corresponding control actin construct in a ten-fold dilution. (G) Representative graph of qRTPCR primer specificity. Each primer set was used to amplify all actin isoform control constructs to calculate relative quantity. Color bars represent individual actin isoform, y-axis denotes relative quantity, x-axis denotes primer set. Experiments performed by Xiaobai Patrinostro.

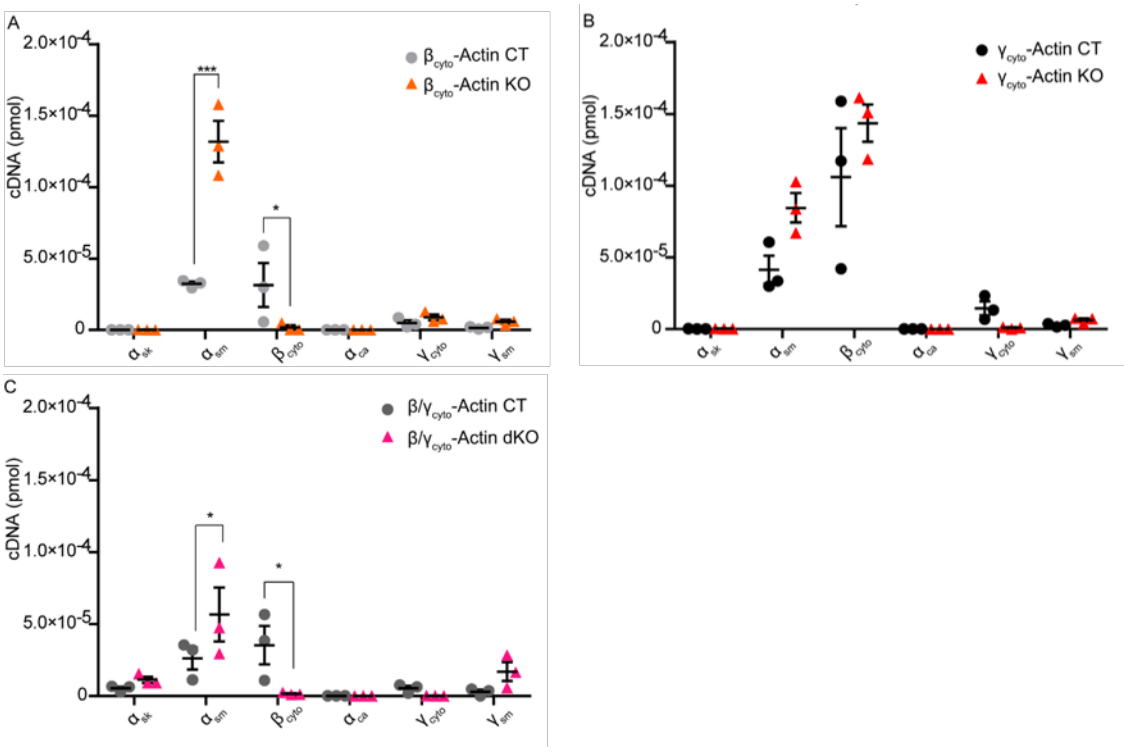

Figure 2-4 α_{sm}-actin transcript was upregulated in β_{cyto}-actin ablated MEFs.

(A-C) qRT-PCR analysis of six mouse actin isoforms in CT and KO MEFs at 5dpi (n=3, in triplicate). Calculated transcript amount (pmol) were calculated based on the standard curve, amplified in parallel. Asterisks denote *P<0.05, *** P<0.001 (Two-way ANOVA with Bonferoni post-test, error bars are s.e.m). Experiments performed by Xiaobai Patrinostro.

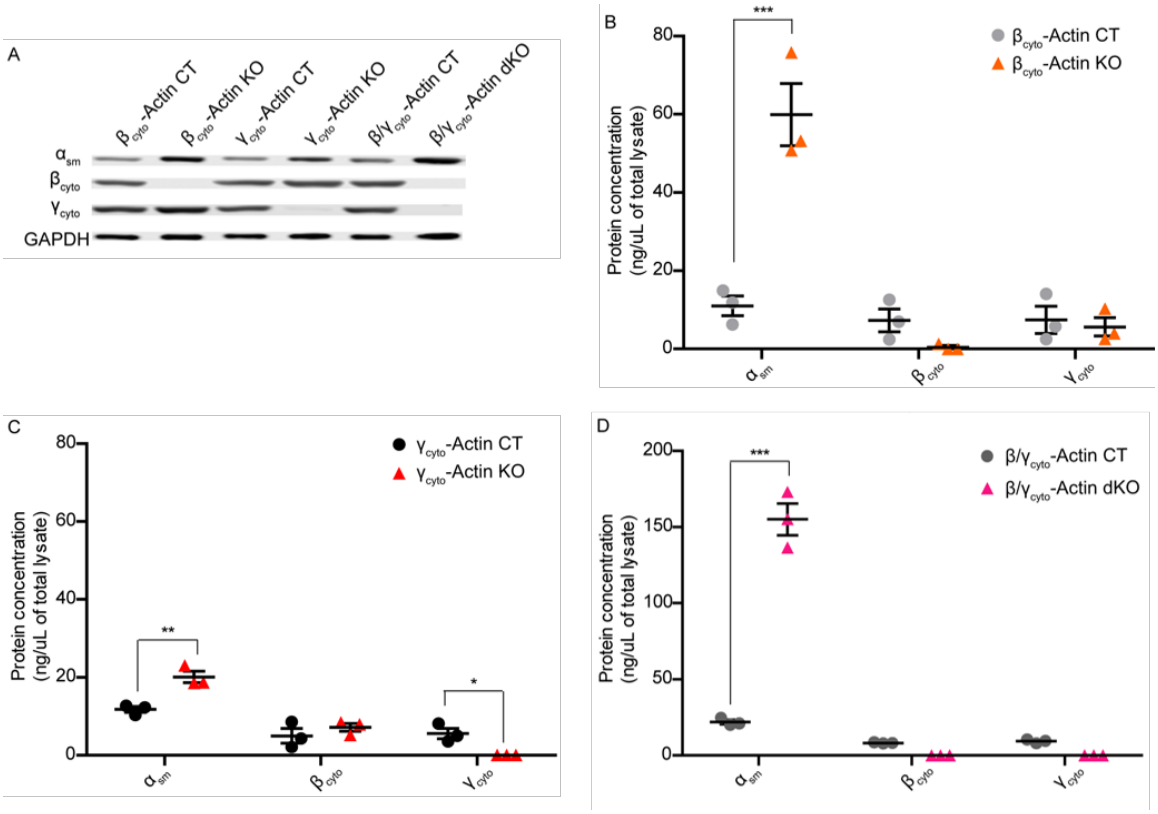

Figure 2-5 α_{sm}-actin protein was upregulated in cytoplasmic ablated MEFs.

(A) Representative Western blot of CT and KO MEF lysates blotted with α_{sm}-actin, β_{cyto}-actin and γ_{cyto}-actin antibodies; GAPDH served as loading control. (B-D) qWB analysis of CT and KO MEF lysates (n=3). Calculated protein concentrations (ng/µL of lysate) were determined based on the standard curve blotted in parallel. Asterisks denote *P<0.05, **P<0.01, and *** P<0.001. (Two-way ANOVA with Bonferoni post-test, error bars are s.e.m.). Experiments performed by Xiaobai Patrinostro.

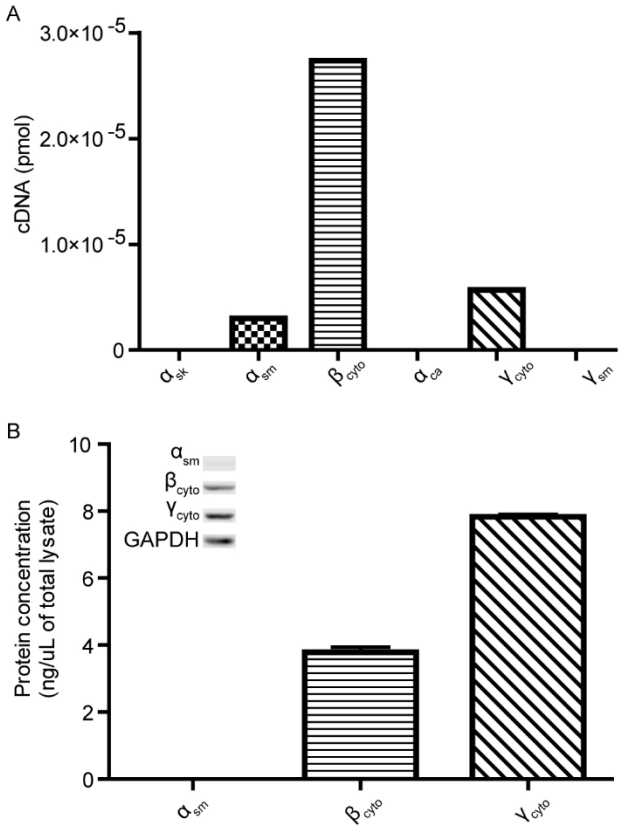

Supplementary Figure 2-3 β_{cyto}- and γ_{cyto}-actin are the dominant actin isoforms in NIH3T3 fibroblast.

(A) Actin isoform transcript profiling in NIH3T3 fibroblasts. Calculated transcript amount (pmol) were calculated based on the standard curve, amplified in parallel (n=1, in triplicate). (B) Representative Western blot of NIH3T3 fibroblast lysates blotted with α_{sm}-actin, β_{cyto}-actin and γ_{cyto}-actin antibodies; GAPDH served as loading control. Calculated protein concentrations (ng/µL of lysate) were determined based on the standard curve, blotted in parallel (n=1, in duplicate). Experiments performed by Xiaobai Patrinostro.

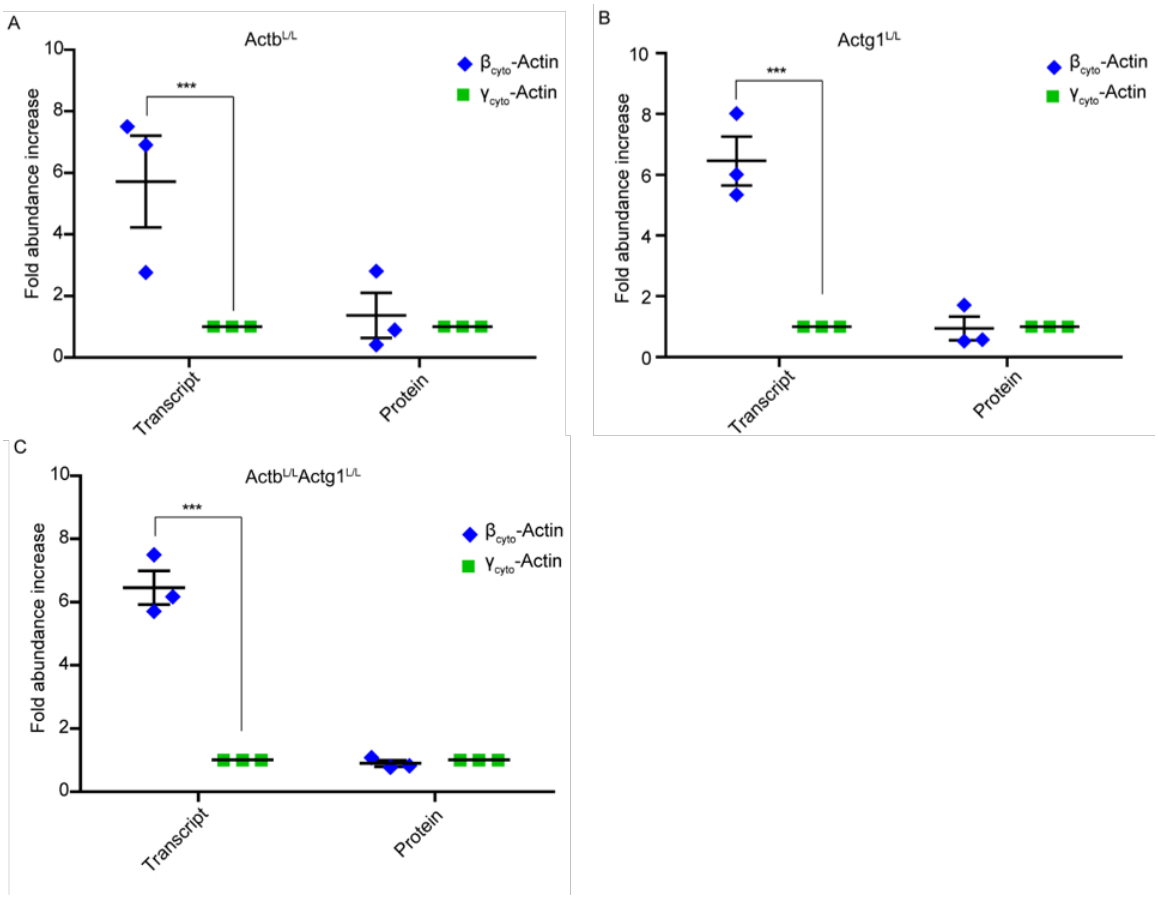

Figure 2-6 Unequal Actb/Actg1 transcript and protein ratios in primary MEFs.

Calculated transcript and protein ratios between β_{cyto}- and γ_{cyto}-actin in CT MEFs (n=3). Calculations were based on the qRT-PCR and qWB data; γ_{cyto}-actin was set at 1. Asterisks denote *** P<0.001 (One sample T-test, error bars are s.e.m.). Experiments performed by Xiaobai Patrinostro.

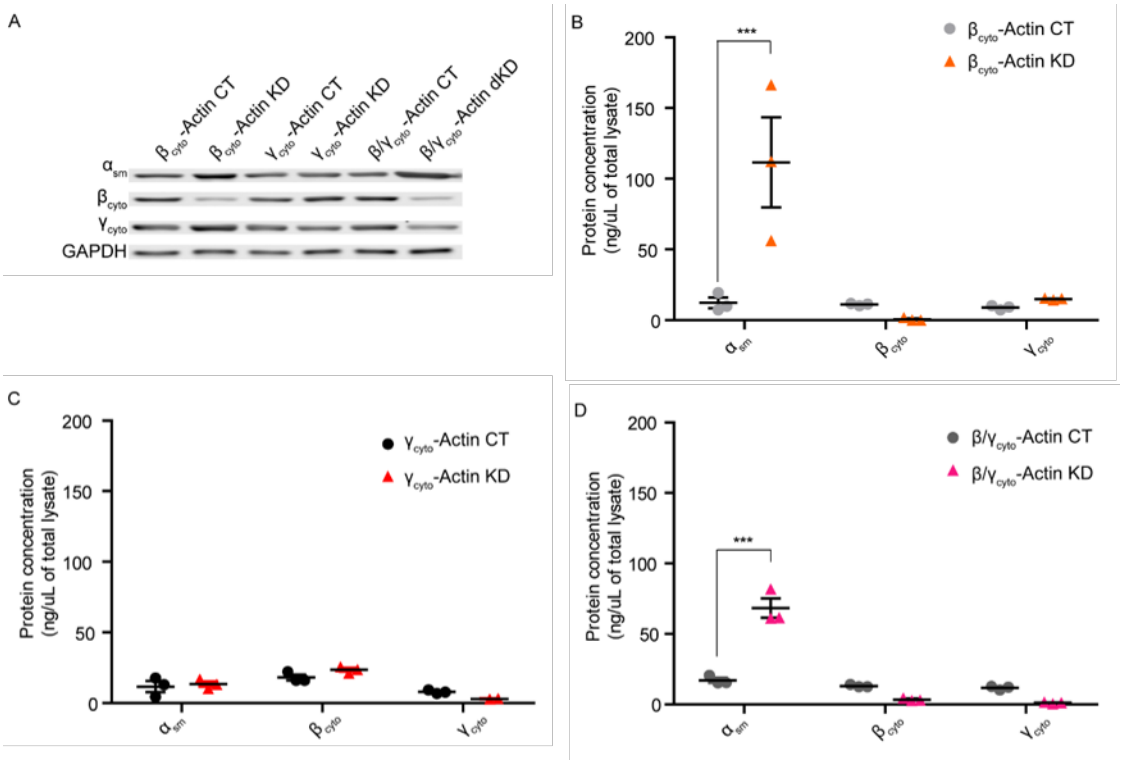

Figure 2-7 α_{sm}-actin protein was upregulated in siRNA mediated βcyto-actin knocked-down MEFs.

(A) Representative Western blot of CT and β_{cyto}- and/or γ_{cyto}-actin KD MEF lysates 3dpi for sKD and 4dpi for dKD blotted with α_{sm}-actin, β_{cyto}-actin and γ_{cyto}-actin antibodies; GAPDH served as loading control. (B-D) qWB analysis of control and KD MEF lysates (n=3). Calculated protein concentrations (ng/µL of lysate) were determined based on the standard curve, blotted in parallel. Triple asterisks denote P<0.001 (Two-way ANOVA with Bonferoni post-test, error bars are s.e.m). Experiments performed by Xiaobai Patrinostro.

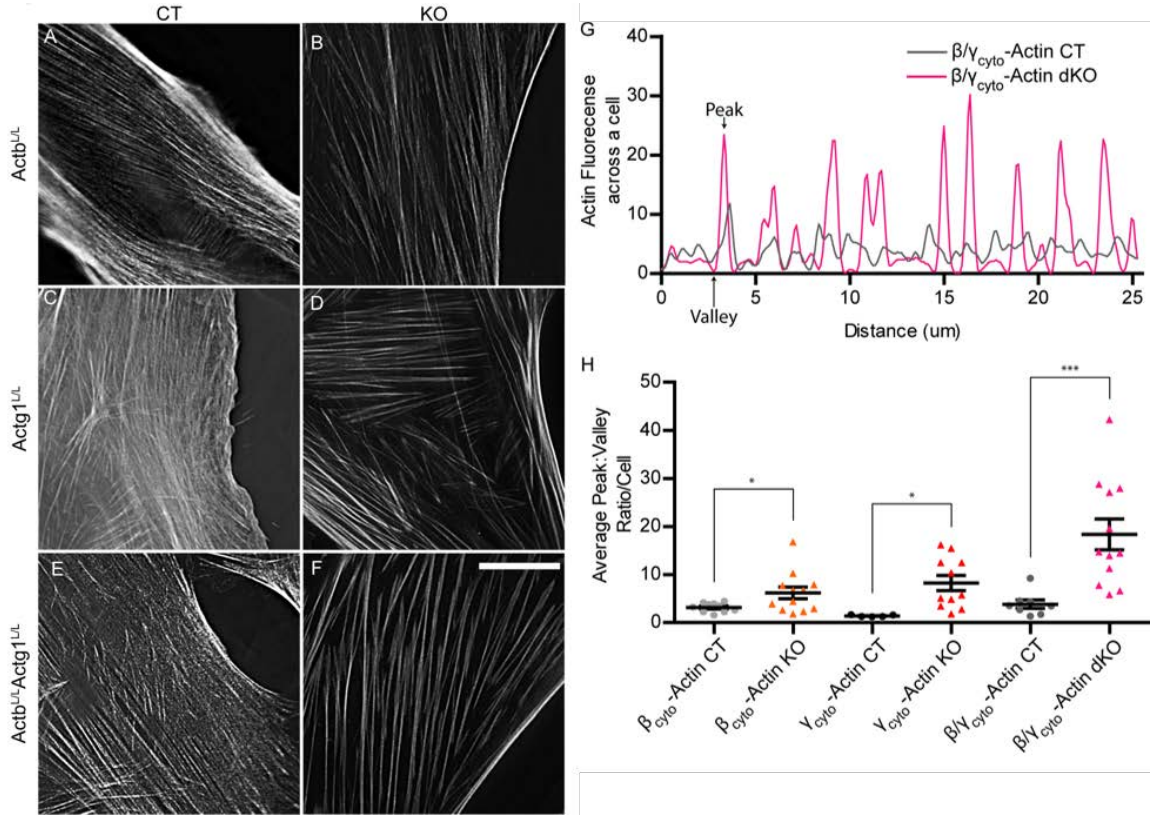

Figure 2-8 β_{cyto}- and/or γ_{cyto}-actin ablated MEFs displayed increased stress fiber thickness.

(A-F) Representative images of phalloidin stained actin filaments in Ad5-GFP or Ad5-Cre treated primary Actb $^{L/L}$, Actg1 $^{L/L}$, and Actb$^{L/L}$Actg1$^{L/L}$ MEFs imaged at 7, 7, and 9 DPI respectively. Scale bar is 20 µm. (G) Representative line scans of actin fluorescence across the dKO cells shown in E and F. Arrows denote sample valley and peak. (H) Quantification of differences between valley:peak ratios for all genotypes (n≥8). Asterisks denote *P<0.05, ***P<0.001 (Two-way ANOVA, error bars are s.e.m.).

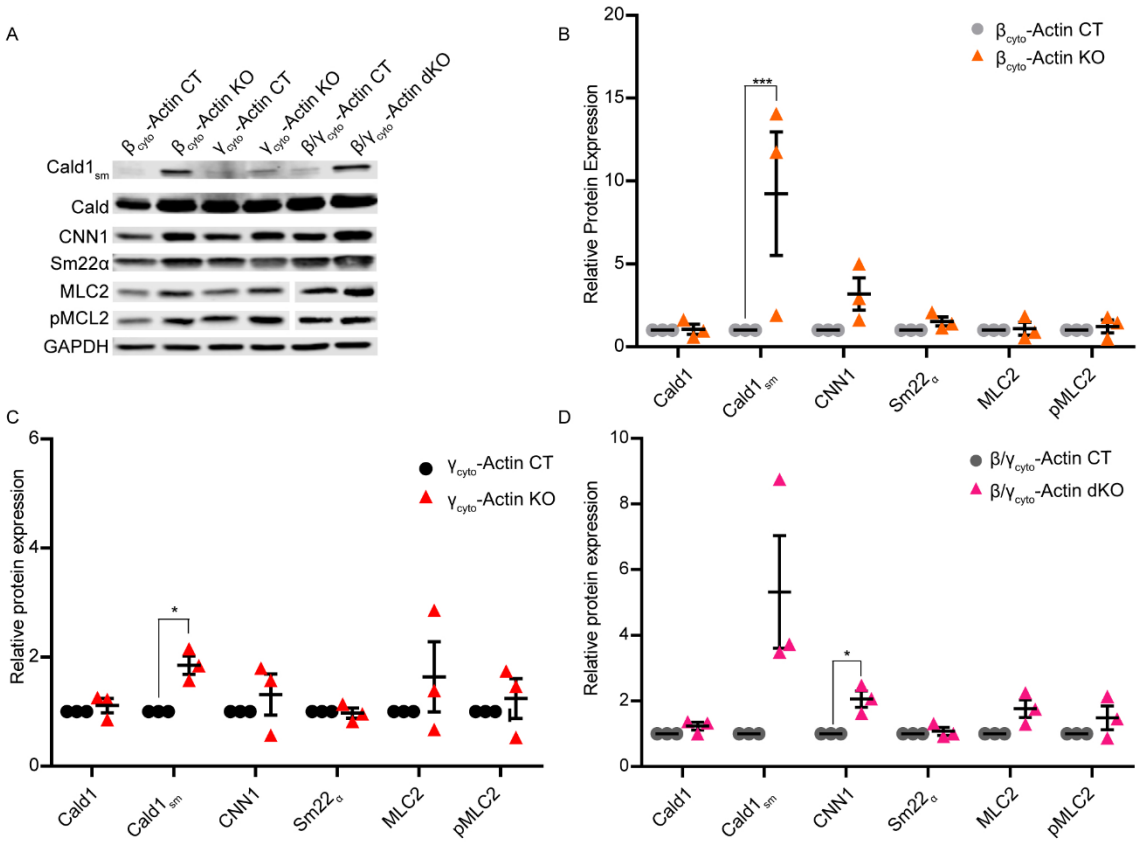

Figure 2-9 Caldesmon smooth muscle isoform protein expression was upregulated in β_{cyto}-actin deficient MEFs.

(A) Representative Western blot analysis of CT and KO MEFs blotted with Cald, CNN1, and Sm22α, MLC2 and pMLC2; GAPDH served as loading control. (B-D) Relative protein expression were normalized to GAPDH and relative to the paired embryo control. Asterisks denote *P<0.05, *** P<0.001. (One sample T-test, error bars are s.e.m.). Experiments performed by Xiaobai Patrinostro.

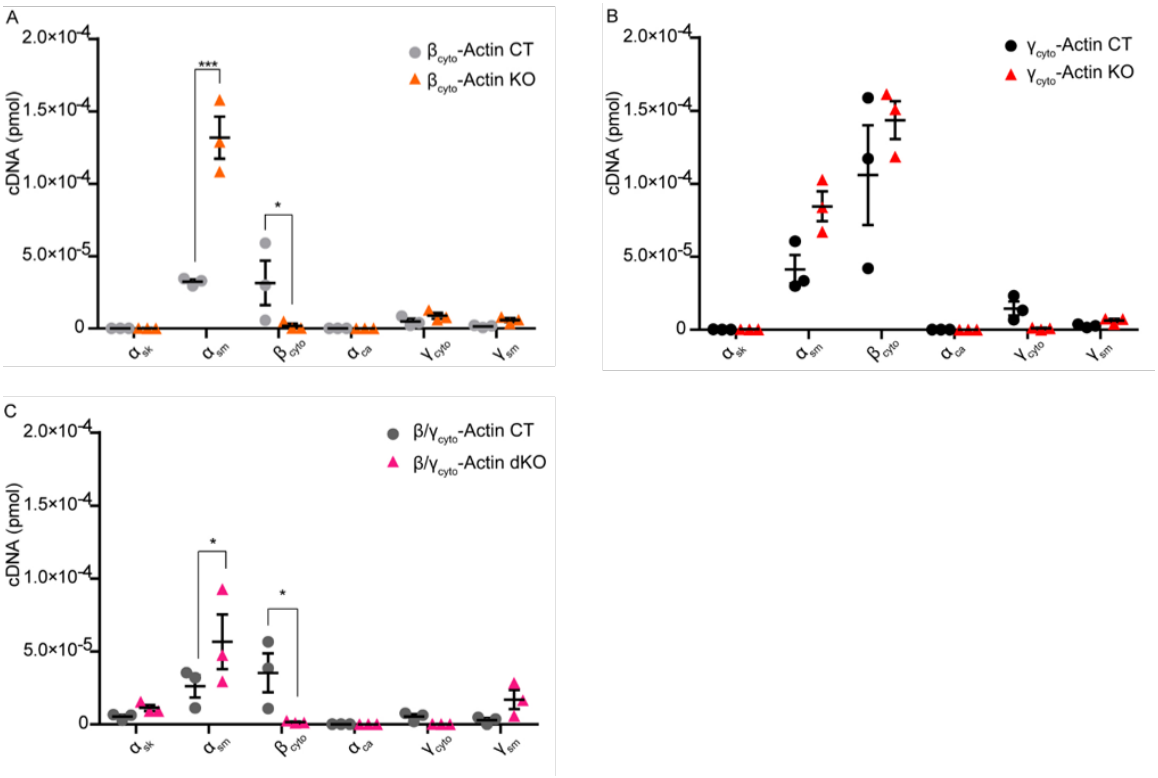

Supplementary Figure 2-4 Cald1 and CNN1 protein expression are upregulated in β_{cyto}-actin siRNA KD MEFs.

(A) Representative Western blot analysis of CT and KD MEFs at 3dpi for sKD and 4dpi for dKD blotted with Cald, CNN1, and Sm22α; GAPDH was used as loading control. (B-D) Relative protein expression were normalized to GAPDH and relative to the paired embryo control (n=3). (One sample T-test, error bars are s.e.m.). Experiments performed by Xiaobai Patrinostro.

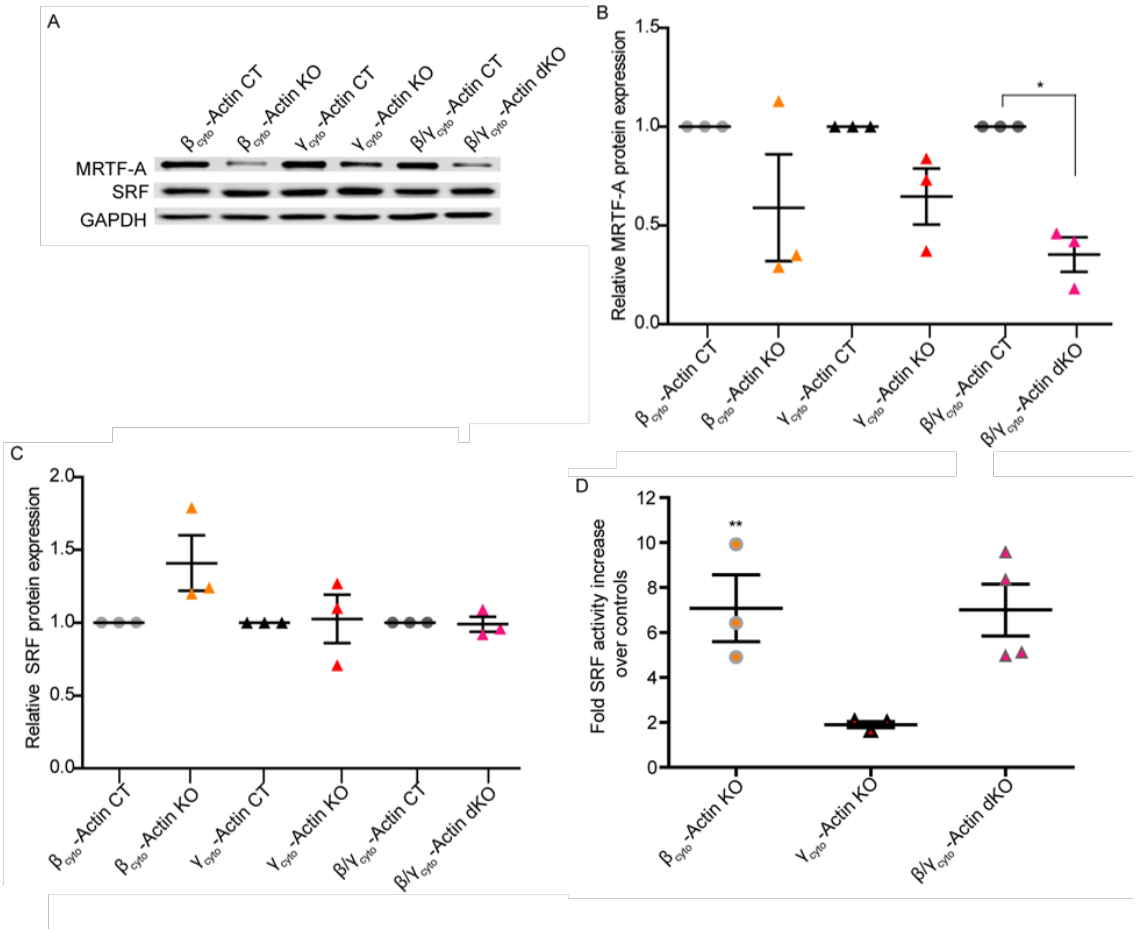

Figure 2-10 SRF activity but not protein was upregulated in β_{cyto}-actin ablated MEFs.

(A) Representative Western blot analysis of CT and KO MEFs blotted with MRTF-A and SRF; GAPDH served as loading control. (B-C) Relative protein expression was normalized to GAPDH and relative to the paired embryo control (n=3). (D) Calculated fold increase in SRF activity, via luciferase assay, in KO over CT MEFs (n=3). Asterisks denote *P<0.05, **P<0.01 (One sample T-test, error bars are s.e.m.). Experiments performed by Xiaobai Patrinostro.

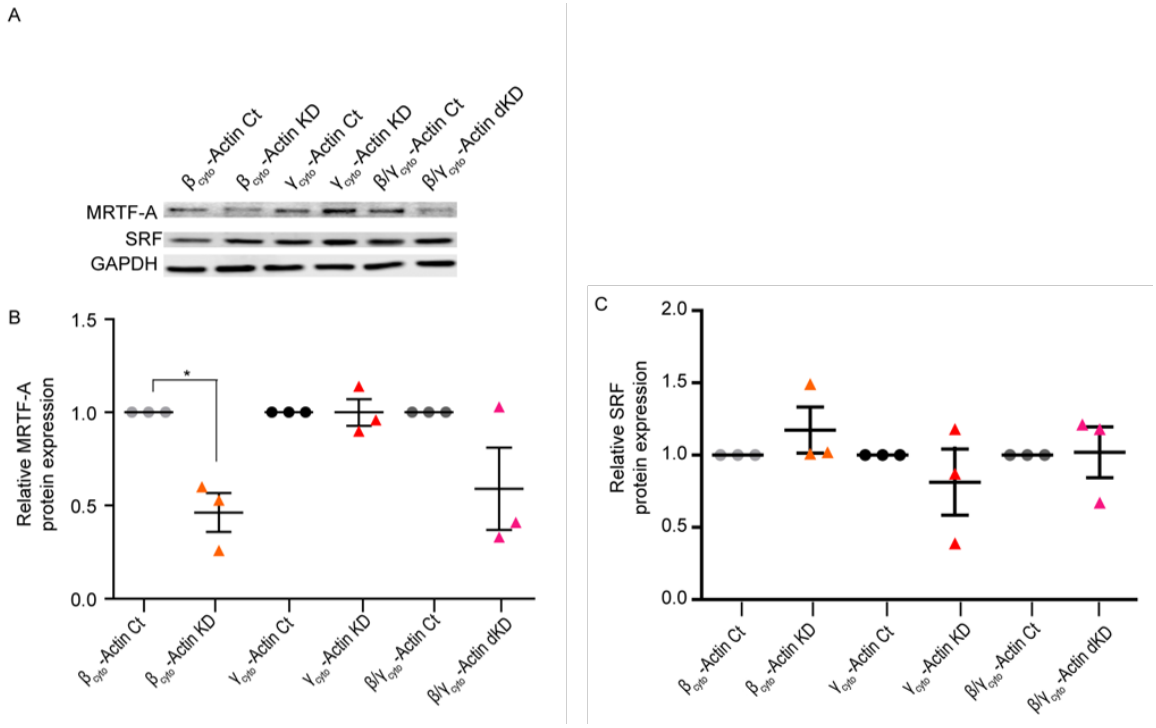

Supplementary Figure 2-5 MRTF-A protein expression is down regulated ion β_{cyto}-actin KD MEFs.

(A) Representative Western blot analysis of CT and KD MEFs at 3dpi for sKD and 4dpi for dKD blotted with MRTF-A and SRF; GAPDH served as loading control. (B) Calculated relative protein expression were normalized to GAPDH and relative to the paired embryo control (n=3). Asterisk denotes *P<0.05 (One sample T-test, error bars are s.e.m.). Experiments performed by Xiaobai Patrinostro.

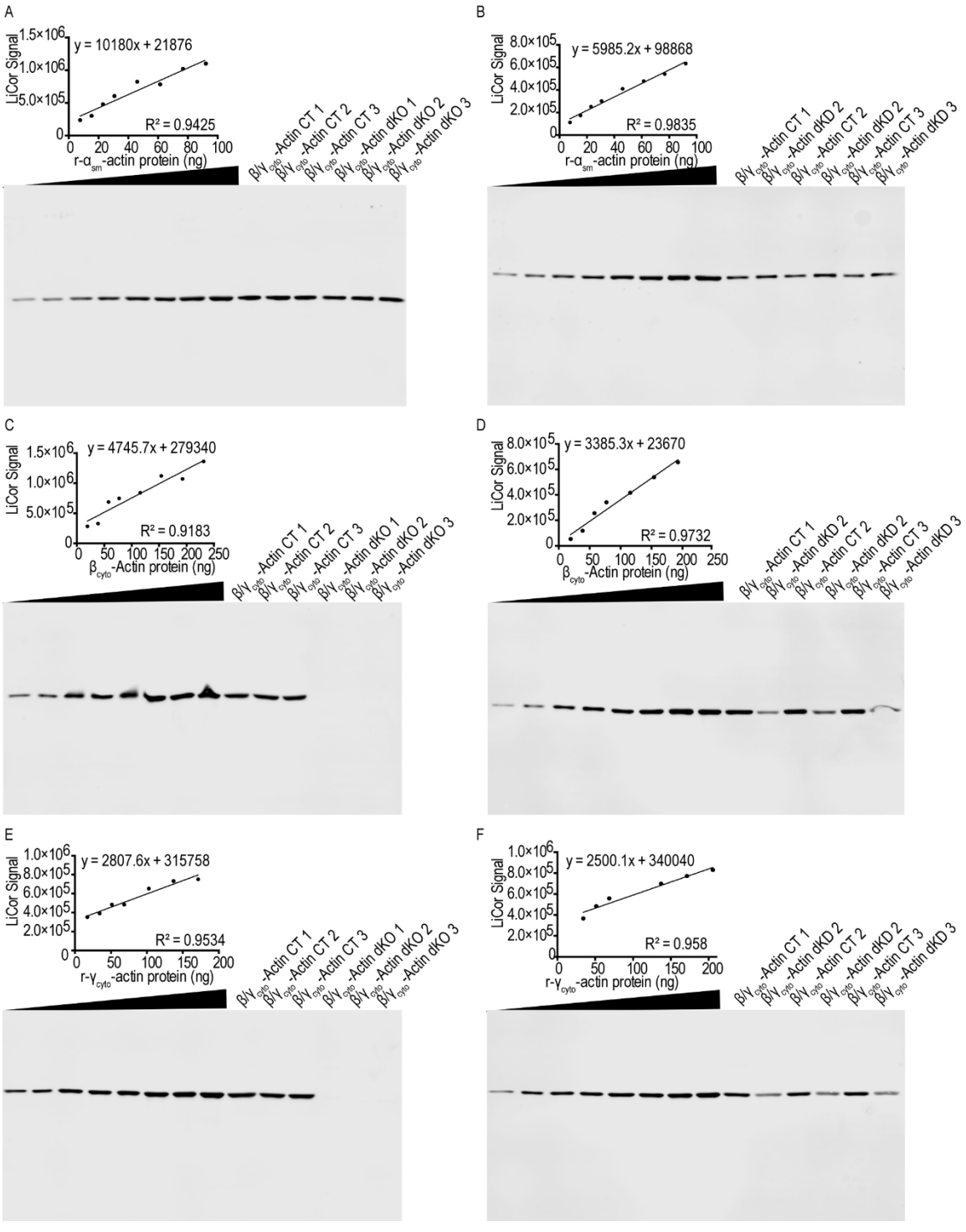
A
LiCor Signal
y = 10180x + 21876
R² = 0.9425
r-α_sm-actin protein (ng)
B
y = 5985.2x + 98868
R² = 0.9835
C
y = 4745.7x + 279340
R² = 0.9183
β_cyto-Actin protein (ng)
D
y = 3385.3x + 23670
R² = 0.9732
E
y = 2807.6x + 315758
R² = 0.9534
r-γ_cyto-actin protein (ng)
F
y = 2500.1x + 340040
R² = 0.958
β/γ_cyto -Actin CT 1
β/γ_cyto -Actin CT 2
β/γ_cyto -Actin CT 3
β/γ_cyto -Actin dKO 1
β/γ_cyto -Actin dKO 2
β/γ_cyto -Actin dKO 3
β/γ_cyto -Actin dKD 2
β/γ_cyto -Actin dKD 3

Supplementary Figure 2-6 Representative quantitative Western blots.

(A, C, E) β/γ_{cyto}-Actin CT and β/γ_{cyto}-Actin dKO, at 9dpi, from 3 separate embryos are blotted with α_{sm}-, β_{cyto}- and γ_{cyto}-actin antibodies. (B, D, F) β/γ_{cyto}-Actin CT - and β/γ_{cyto}-Actin dKD, at 4dpi, from 3 separate embryos blotted with α_{sm}-, β_{cyto}- and γ_{cyto}-actin antibodies. For α_{sm}-actin Western blots, both KO and KD samples were diluted by at least 5-fold in order for the immune activity intensity to fit within the standard curve. An increasing amount of purified α_{sm}-, β_{cyto}- and γ_{cyto}-actins are blotted in parallel to generate a standard curve and used to calculate the amount of individual actin isoform in lysates. Experiments performed by Xiaobai Patrinostro.

Chapter 3 : Impaired muscle relaxation and mitochondrial fission associated with genetic ablation of cytoplasmic actin isoforms.

Allison O'Rourke performed all experiments except isolated muscle fiber respiration was done by Michael Tarpey and Espen Spangenberg. Whole body respiration experiments were done by the physiology core at the University of Minnesota. In vitro muscle physiology experiments were done with the help of Angus Lindsey.

Chapter Summary

While α-actin isoforms predominate in adult striated muscle, skeletal muscle-specific knockouts of non-sarcomeric cytoplasmic β_{cyto}- or γ_{cyto}-actin each cause a mild, but progressive myopathy effected by an unknown mechanism. Using transmission electron microscopy, we identified morphological abnormalities in both the mitochondria and the sarcoplasmic reticulum (SR) in aged muscle-specific β- and γ-actin knockout mice. We found β- and γ-actin proteins to be enriched in isolated mitochondrial associated membranes, which form signaling and mechanical links between the sarco-endoplasmic reticulum and mitochondria important for mitochondrial dynamics. Corresponding with an important role for actin in mitochondrial dynamics, we measured significantly elongated and interconnected mitochondrial morphologies associated with a significant decrease in mitochondrial fission events in primary mouse embryonic fibroblasts (MEFs) lacking β_{cyto}- and/or γ_{cyto}-actin. Interestingly, mitochondrial respiration in muscle was not detectably affected as oxygen consumption by skeletal muscle fibers from 12 month-old muscle-specific β_{cyto}- and γ_{cyto}-actin knockout mice were similar. Instead, the maximal rate of relaxation after isometric contraction was significantly slowed in muscles of 12 month-old β_{cyto}- and γ_{cyto}-actin muscle-specific knockout mice, which suggests that impaired Ca^{2+} re-uptake may presage development of the observed SR morphological changes in older mice while providing a potential pathological mechanism for the observed myopathy.

Introduction

While abundantly expressed skeletal (α_{sk}-actin) and cardiac (α_{ca}-actin) actins are essential constituents of sarcomeric thin filaments in adult striated muscle (Crawford et al., 2002; Kumar et al., 1997), non-sarcomeric cytoplasmic actins (β_{cyto}- and γ_{cyto}-actin) are the predominant isoforms in myoblasts (McHugh et al., 1991; Schwartz and Rothblum, 1981) and have been implicated in several key steps of myogenesis during development (Duan and Gallagher, 2009; Lloyd et al., 1992; Nowak et al., 2009b; Peckham, 2008). After myogenesis, very low levels of β_{cyto}- and γ_{cyto}-actin remain in adult skeletal muscle and localize to a membrane-associated extrasarcomeric cytoskeleton that includes the subsarcolemmal costamere, (Craig and Pardo, 1983; Otey et al., 1988; Prins et al., 2011; Rybakova et al., 2000) regions of the sarcoplasmic reticulum (SR) flanking the Z-disk, and mitochondria (Craig and Pardo, 1983; Gokhin et al., 2010; Kee et al., 2004).

Several studies have shown that γ_{cyto}-actin colocalizes with isoforms of ankyrin, tropomyosin and tropomodulin at the extrasarcomeric cytoskeleton (Almenar-Queralt and Lee, 1999; Ayalon et al., 2008; Gokhin et al., 2010; Kee et al., 2004). Knockout of the tropomyosin isoform TM5NM1 (Vlahovich et al., 2009), or disruption of tropomodulin 3 (Tmod3) localization as a result of tropomodulin 1 (Tmod1) knockout (Gokhin and Fowler, 2011) both perturb the peri-Z-disk elements with associated defects in triad morphology and excitation-contraction

coupling. Knockdown of clathrin heavy chain was shown to drive γ_{cyto}-actin displacement from the sarcolemma and loss of contractile force presumably due to uncoupling of myofibrils from costameres (Vassilopoulos et al., 2014). A recent proteomic study reported that γ_{cyto}-actin was found in an isolated complex containing four-and-a-half LIM domain protein 1 (FHL1) protein (Wang et al., 2013), while gene knockout of FHL1 causes a progressive skeletal myopathy associated with sarcoplasmic reticulum and mitochondrial disorganization in mice (Domenighetti et al., 2014). Collectively, these studies suggest that non-sarcomeric cytoplasmic actins contribute to the function of several organelles in adult skeletal muscle.

To more directly test the functional importance of non-muscle cytoplasmic actins in skeletal muscle, we previously generated muscle-specific knockout mice lacking either γ_{cyto}-actin (*Actg1*-msKO, Sonnemann *et al.*, 2006), or β_{cyto}-actin (*Actb*-msKO, Prins *et al.*, 2011). These two single knockouts developed qualitatively similar phenotypes characterized by a progressive myopathy with significant myofiber degeneration/regeneration and muscle weakness, but without any detectable perturbations of the costameric lattice or intracellular organelles in mice 3-6 months old (Prins et al., 2011; Sonnemann et al., 2006). Notably, ultrastructural defects in the sarcoplasmic reticulum of Tmod1 knockout mice were not apparent until 6 months of age (Gokhin and Fowler, 2011; Gokhin et al., 2010). The progressive nature of both *Actg1*-msKO and *Actb*-msKO suggests partial redundancy may be playing a role, preventing the more rapid development of

phenotypes observed (Gokhin and Fowler, 2011; Gokhin et al., 2010). Therefore, we hypothesized that non-muscle β_{cyto}- and γ_{cyto}-actin collaborate to support functional interaction between mitochondria and the sarcoplasmic reticulum in skeletal muscle, but are sufficiently redundant to delay or obscure a measureable phenotype when either isoform is singly ablated.

Here, we report that primary mouse embryonic fibroblasts ablated for β_{cyto}- and/or γ_{cyto}-actin exhibit markedly increased mitochondrial lengths and decreased rates of fission. Examination of muscle ultrastructure as a function of age using transmission electron microscopy (TEM) revealed that skeletal muscles from 22-25 month old *Actg1*-msKO and *Actb*-msKO mice exhibit misshapen mitochondria and dilated and vesiculated sarcoplasmic reticulum compared to age-matched WT, or younger knockout animals. We also demonstrate that both β_{cyto}- and γ_{cyto}-actin co-enrich with biochemically isolated mitochondrial-associated membrane fractions. However, no deficit in mitochondrial respiration or oxygen consumption in isolated *Actg1*-msKO or Actb-msKO skeletal muscle fiber bundles or intact *Actb*-msKO mice was identified. Finally, we measured a small but significant decrease in the maximal rate relaxation in EDL muscles of *Actg1*-msKO and *Actb*-msKO mice. Collectively, our present data are consistent with previous studies (Korobova et al., 2013; Manor et al., 2015; Domenighetti et al., 2014; Gokhin and Fowler, 2011; Vlahovich et al., 2009), and extend them by showing that specific loss of either β_{cyto}- or γ_{cyto}-actin from mouse embryonic fibroblasts causes defects in mitochondrial dynamics while their loss from the extrasarcomeric

cytoskeleton causes a mild skeletal muscle myopathy apparently through impairment of sarcoplasmic calcium regulation.

Results

Altered Sarcoplasmic Reticulum and Mitochondrial Morphologies in Aged Cytoplasmic Actin KO Skeletal Muscle

Several other groups have observed age-dependent morphological defects in sarcoplasmic reticulum and mitochondria after genetic ablation of actin binding proteins associated with the extrasarcomeric actin cytoskeleton (Domenighetti et al., 2014; Gokhin and Fowler, 2011; Gokhin et al., 2010), therefore, we utilized TEM to examine the muscle ultrastructure from Actg1-msKO and Actb-msKO animals at 6, 12, and 22-25 months of age (Figure 3-1). Consistent with our observations in MEFs, TEM examination of skeletal muscle in cross section revealed abnormal mitochondrial morphology in Actg1-msKO and Actb-msKO muscles at 22-25 months of age (Figure 3-1 A-C, M). Actg1-msKO and Actb-msKO muscle exhibited a subset of rounded mitochondria (white arrows, Figure 3-1 B, C) in comparison to the more prevalent elongated mitochondria observed in age-matched WT muscle (white arrow heads, Figure 3-1 A-C). The measured mitochondrial length to width ratios confirmed the qualitative observation (Figure 3-1 M). Analysis of longitudinal sections from 6 month-old animals showed muscle architecture, including Z-disk alignment, was not different from age-matched WT mice (Figure 3-1 D-F, N; Supplemental Figure 3-1). While muscles from most 12 month-old animals were also not different from WT (denoted with a white

arrowhead in Figure 3-1 G, I, N), one Actg1-msKO sample displayed dilation of the sarcoplasmic reticulum (denoted with a white arrow in Figure 3-1 H, N). At 22-25 months of age, all Actg1-msKO and Actb-msKO muscles displayed normal Z-disk alignment, but presented with sarcoplasmic reticulum dilation (Figure 3-1 J-L, N; Supplemental Figure 3-1). Consistent with previous studies (Domenighetti et al., 2014; Gokhin and Fowler, 2011; Gokhin et al., 2010), our TEM data reveal age-dependent structural defects in the sarcoplasmic reticulum and mitochondria of Actg1-msKO and Actb-msKO muscles, which take longer to manifest than previously observed with genetic ablation of Tmod1 or FHL1 (Domenighetti et al., 2014; Gokhin and Fowler, 2011; Gokhin et al., 2010).

Morphological defects in both the sarcoplasmic reticulum and mitochondria of Actg1-msKO and Actb-msKO muscles suggested that β_{cyto}- and γ_{cyto}-actin may interact with both organelles at their site of close apposition. Mitochondrial associated membranes (MAMs) are functionally important in stimulating increased mitochondrial respiration, Ca^{2+} crosstalk between mitochondria and the sarco-/endo-plasmic reticulum, cell death signaling, lipid metabolism, and mitochondrial dynamics (Brito and Scorrano, 2008; Patergnani et al., 2011; Raturi and Simmen, 2013; Rizzuto et al., 1998; Szabadkai et al., 2006). Therefore, we biochemically isolated MAM, mitochondrial, and endoplasmic reticulum fractions from WT mouse liver (Wieckowski et al. 2009) and performed western blot analysis to identify the fractions containing β_{cyto}- and γ_{cyto}-actin immunoreactivity (Figure 3-2). As expected, both γ_{cyto}- and β_{cyto}-actin were present in the cytosolic fraction (identified

by tubulin), weakly present in the crude mitochondrial fraction (identified by cytochrome C), and enriched in the isolated MAM fraction verified by the presence of FACL4, a lipid enzyme localized to the MAM (Krisans and Coleman, 2002; Lewin et al., 2001). Thus, both β_{cyto}- and γ_{cyto}-actin co-enrich with a membrane fraction thought to represent the interface between the organelles which display altered morphologies, the sarcoplasmic reticulum and mitochondria.

Perturbation of Mitochondrial Dynamics but not Respiration when Cytoplasmic Actins are Ablated

We previously observed that ablation of β_{cyto}-, but not γ_{cyto}-actin, led to perturbations in cellular proliferation and ATP content, but didn't alter mitochondrial respiration in primary mouse embryonic fibroblasts (MEFs). Because actin plays a key role in mitochondrial dynamics (De Vos et al., 2005; Korobova et al., 2013; Manor et al., 2015), we imaged mitochondria in primary MEFs homozygous for floxed Actb or Actg1 alleles, which were treated with adenovirus-5 CRE to knockout the target gene or adenovirus-5 GFP as a control (Patrinostro et al., 2017). MEFs ablated for either β_{cyto}-actin, γ_{cyto}-actin, or both actins displayed significantly larger mitochondria compared to control MEFs (Figure 3-3 A-H). Abnormalities in mitochondrial morphology imply a defect in mitochondrial dynamics controlled by the opposing processes of fission and fusion (Reviewed by Westermann 2010). The most likely explanations for the measured increase in

mitochondrial size would be a decrease in the rate of mitochondrial fission, or an increase in mitochondrial fusion. Therefore, mitochondria were live-imaged and the frequencies of fission and fusion events were quantified. While the frequency of fusion events was not different across all MEF pools analyzed (Figure 3-3 I), the frequency of fission events were significantly decreased in Actg1, Actb, and Actb/Actg1 KO MEFs compared to WT MEFs (Figure 3-3 J). Our results are consistent with the important role for actin in mitochondrial fission and extend previous studies by demonstrating that both β_{cyto}- and γ_{cyto}-actin isoforms support mitochondrial fission.

Because perturbations in mitochondrial shape, dynamics, and function are often interlinked (reviewed in Anesti and Scorrano, 2006; Chen and Chan, 2005; Chen et al., 2000), we investigated whether mitochondrial respiration was altered in muscle fiber bundles from the red portion of the gastrocnemius muscle from 12 month-old Actg1-msKO and Actb-msKO mice. No change was detected in the abundance of protein components of electron transport chain complexes I-IV (ETC; Supplementary Figure 3-2), which correspond to no differences in respiratory function. Specifically, no differences were detected in basal or ADP-stimulated Complex I respiration between fiber bundles isolated from age-matched Actg1-msKO, Actb-msKO, or WT animals (Figure 3-4 A-C). Nor were differences detected in Complex II or IV-mediated respiration (Figure 3-4 D-E). Succinate control: the portion of respiration attributed to the Q-junction via complex II (Figure 3-4 G), respiratory control ratio (RCR) and coupling efficiency: an indicators of

mitochondrial coupling (Figure 3-4 H-I), E-Super-C; a measure of the additive effect of Complex I and II at the Q-junction (Figure 3-4 I), and, were also not different among fiber bundles from each group. Taken together these data indicate that the absence of either β_{cyto}-actin or γ_{cyto}-actin does not lead to perturbations in mitochondrial respiration at 12 months.

As defects in mitochondrial morphology were only evident in aged Actg1-msKO and Actb-msKO muscles (Figure 3-1), we also measured whole body energy expenditure in 22-25 month-old WT and Actb-msKO mice (Supplemental Figure 3-2). Consistent with our findings in isolated gastrocnemius muscles (Figure 4) and MEFs (Patrinostro et al., 2017), there was no difference between aged WT and Actb-msKO mice in any measured parameter of whole body respiratory function (Supplemental Figure 3-2). These results indicate that the alterations in mitochondrial morphology and dynamics caused by genetic ablation of Actg1 or Actb (Figure 3-2) are not associated with a measureable impairment in mitochondrial function.

Impaired Relaxation in Cytoplasmic Actin KO Skeletal Muscle

In the absence of a measureable deficit in mitochondrial function (Figure 3-4, Supplemental Figure 3-2) to explain the mild, but progressive myopathy caused by muscle-specific ablation of Actb or Actg1 (Prins et al., 2011; Sonnemann et al., 2006), we measured contractile function of isolated EDL muscles from 12 and 22-

25 month-old WT, Actb-msKO mice and 12 month-old Actg1-msKO animals. Twitch force development time and ½ relaxation time normalized to peak twitch force were not different between WT control and KO muscles (Table 3-1). Analysis of tetanic isometric contractions showed that specific force and maximal contraction rates before and after muscle fatigue was induced were also not different (Table 3-1, Figure 3-5 A-C), indicating that the ability of Actg1-msKO and Actb-msKO muscles to respond to electrical stimuli, release Ca^{2+}, and produce force (Brown and Hasser, 1996; reviewed in Ebashi and Endo, 1968; reviewed in Stephenson et al., 1998) were unaffected. Interestingly, the maximal relaxation rate was significantly slowed in 12 month-old Actg1-msKO and Actb-msKO muscles compared to age matched WT (Table 3-1, Figure 3-5 D). By 22-25 months of age, the maximal rate of relaxation in WT muscles slowed to the point that it was no longer significantly different from Actb-msKO muscles (Table 3-1, Figure 3-5 D). While Ca^{2+} reuptake by the sarco/endoplasmic reticulum Ca^{2+}-ATPase (SERCA) is primarily responsible for muscle relaxation rate (Ebashi and Endo, 1968; Odermatt et al., 1996), western blot analysis revealed similar levels of immunoreactivity in WT, Actg1-msKO and Actb-msKO skeletal muscle lysates against the two primary isoforms of SERCA expressed in skeletal muscle (Figure 3-6 A-C). Dysregulation of Ca^{2+} can result in the activation of the unfolded protein response (UPR) as a result of cellular stress (Liang et al., 2006; Ma and Hendershot, 2001; Niwa and Walter, 2000; Schröder, 2008). However, we observed no change in the abundance of examined UPR proteins in Actg1 and

Actb KO skeletal muscle (Supplemental Figure 3-4). None-the-less, the dilated sarcoplasmic reticulum (Figure 3-1) and slowed relaxation (Table 3-1, Figure 3-5) suggest that sarcoplasmic Ca^{2+} regulation may be impaired in in Actg1-msKO and Actb-msKO skeletal muscles.

Discussion

Though only accounting for a minute fraction of the total actin pool in adult skeletal muscle (Hanft et al., 2006), non-sarcomeric γ_{cyto}- and β_{cyto}- actin isoforms have been shown to localize to a diverse array of cellular structures in skeletal muscle including mitochondria (Craig and Pardo, 1983), the neuromuscular junction (Hall et al., 1981), costameres (Ayalon et al., 2008; Rybakova et al., 2000), the Z-disk (Kee et al., 2004; Nakata et al., 2001; Papponen et al., 2009; Rybakova et al., 2000), and the myotendonous junction (Papponen et al., 2008). Localization of non-sarcomeric actins to a number of these structures is disrupted in the *mdx* mouse model of Duchenne muscular dystrophy (Hanft et al., 2006; Rybakova et al., 2000). However, it is still unclear how knockout of γ_{cyto}- and β_{cyto}-actin in skeletal muscle cause mild, but progressive myopathy (Prins et al., 2011; Sonnemann et al., 2006). Here we show that knockout of γ_{cyto}- or β_{cyto}- actin causes perturbation in both mitochondrial morphology and fission, supporting a link between γ_{cyto}- or β_{cyto}- actin localization at the mitochondria and a functional role in mitochondrial dynamics.

Dynamic mitochondria in skeletal muscle are critical for maintaining bioenergetics (Eisner et al., 2014; Mishra and Chan, 2016). As a consequence of the high energy demand of skeletal muscle, perturbations in multiple aspects of mitochondrial dynamics can be fatal in mice (Chen et al., 2000; Chen et al., 2015). Mitochondria are distributed in skeletal muscle to enable maximal functional

connectivity with surrounding structures (Csordás and Hajnóczky, 2009; Eisner et al., 2013; Rizzuto et al., 1998). Though localized to specific areas within the myofiber, mitochondria are interconnected (Glancy et al., 2015) and regularly undergo fusion (Eisner et al., 2014). In non-muscle cells, both actin and the endoplasmic reticulum have been implicated in the fission process (Korobova et al., 2013; Manor et al., 2015; Spät et al., 2008). Because mitochondrial dynamics are critical in all cell types and occur with higher frequency in non-muscle cells, we utilized a MEF model to study dynamics and found γ_{cyto}-, β_{cyto}-, and double actin KO MEFs all displayed decreased fission, indicating that γ_{cyto}- and β_{cyto}- actin isoforms are each important for mitochondrial fission.

While the measured changes in mitochondrial dynamics were not paired with detectable differences in mitochondrial respiration it is possible that an alteration in redox balance, specifically reactive oxygen species (ROS) emission, could be contributing to the phenotype. Alterations in ROS emitting potential of mitochondria can affect mitochondrial dynamics and thereby alter morphology (Blanchet et al., 2015; Distelmaier et al., 2012; Pletjushkina et al., 2006; Rakovic et al., 2011; Willems et al., 2015). Mild oxidative stress can also impact Ca^{2+} flow from the SR (Andersson et al., 2011; Ermak and Davies, 2002; Gorlach et al., 2006; Roveri et al., 1992). In turn, Ca^{2+} signaling at the mitochondrial-sarco/endoplasmic reticulum interface, can influence mitochondria respiration rates and even initiate cell death (Chami et al., 2008; Eisner et al., 2014; Ermak and Davies, 2002; Rizzuto et al., 1998). Here, we demonstrate enrichment of both

γ_{cyto}- and β_{cyto}- actin with the mitochondria-associated membrane. The mitochondria-associated membrane forms a small microenvironment which is important for a large array of functions in addition to Ca^{2+} signaling including but not limited to: mitochondrial fission, endoplasmic reticulum stress, ROS signaling, and lipogenesis (Burté et al., 2014; Csordás and Hajnóczky, 2009; Gilady et al., 2010; Grimm, 2012; Kornmann et al., 2009; Korobova et al., 2013; Li et al., 2009; Manor et al., 2015; Rusiñol et al., 1994). Dysregulation of the signaling cascades can be caused by structural malformations of the mitochondria-associated membrane (Dayanithi et al., 2010; Kushnareva et al., 2013; Singaravelu et al., 2011). Therefore, loss of γ_{cyto}- or β_{cyto}- actin from the mitochondrial-sarco/endoplasmic reticulum interface may impair inter-organelle signaling.

Ca^{2+} signaling is critical to regulating skeletal muscle contraction. Problems with Ca^{2+} sequestration can occur at a number of points including: leak through the RYR, SERCA, the membrane, or ryanodine receptor (RYR) or SERCA dysfunction. Changes in the activity of SERCA can affect intercellular Ca^{2+} levels and alter relaxation rate (Tupling et al., 2011). Additionally, swelling of the SR, similar to what we observed here, has been seen alongside defective skeletal muscle Ca^{2+} release (Gokhin and Fowler, 2011), supporting a role for Ca^{2+} in the γ_{cyto}- and β_{cyto}- actin skeletal muscle KO relaxation defect. Cellular stressors can induce Ca^{2+} dysregulation (Ermak and Davies, 2002). One such stress is muscle aging, or sarcopenia, which has been linked to alterations in Ca^{2+} flow (Andersson et al., 2011). Oxidation of the RYR with aging leads to SR Ca^{2+} leak, further ROS

elevation and ultimately loss of muscle (Andersson et al., 2011). We measured a decreased relaxation rate in 12 month old γ_{cyto}- and β_{cyto}- actin KO skeletal muscle that preceded a similar decrease in WT skeletal muscle aged to 22-25 months (Figure 3-5 D), suggesting that knockout of either cytoplasmic actin may accelerate aging in skeletal muscle.

The partial redundancy of the cytoplasmic actin isoforms, illustrated by the similar but modest phenotypes displayed when either are knocked-out, indicates that both are important but can likely compensate in some aspects for the other. An explanation for this partial overlap is likely that the sequences of γ_{cyto}- and β_{cyto}- actin are highly conserved and differ only by the 3'UTR sequences and 4 biochemically similar amino acid changes (Lloyd and Gunning, 1993; Rubenstein, 1990). Despite the high degree of sequence identity, γ_{cyto}- and β_{cyto}- actin have differing polymerization dynamics and modifications (Bergeron et al., 2010; Lloyd and Gunning, 1993; Zhang et al., 2010). The presence of the phenotypes observed here suggests that each isoform does play a unique and vital role in the actin cytoskeleton.

Materials and Methods

Mouse Lines

Mice (*Mus musculus*) containing the conditional floxed *Actb* (Perrin et al., 2010) and *Actg1* (Sonnemann et al., 2006) alleles as described previously were each backcrossed on to the C57BL/6 background for a minimum of five generations. To generate knockout mice, each line was crossed to mice expressing cre-recombinase under the skeletal muscle specific human skeletal actin promoter (HSA-Cre mice were provided by Judith Melki, INSERM, Evry, France; Miniou et al., 1999). Knockout animals were homozygous for either the Actb or Actg1 floxed alleles, and hemizygous for HSA-cre, controls were age-matched floxed mice lacking HSA-cre. All mice examined were male. Standard PCR analysis was used to confirm genotype. All animals were cared for according to the University of Minnesota Institutional Animal Care and Use Committee policy.

Cell Culture and Imaging

Primary MEFs were cultured from E13.5 Actb $^{L/L}$, Actg1$^{L/L}$ and double Actb$^{L/L}$/Actg1$^{L/L}$ mouse embryos as described previously (Bunnell and Ervasti, 2010; Patrinostro et al., 2017). Briefly: MEFs from individual embryos were cultured at 37°C in 5.0 % CO_2 in DMEM media (supplemented with 10% FBS, 1% Pen/Strep, 0.5ug/mL Fungizone; Invitrogen Carlsbad, CA, USA), counted, and split into two pools. One pool was treated with the control adenovirus Ad5-GFP (Ad5CMV-hrGFP) the other group was treated with Ad5-Cre (Ad5CMV-Cre-eGFP)

virus purchased from The University of Iowa Viral Vector Core (Iowa City, IA, USA) explicitly following the Core's Adenovirus Adfection protocol (http://www.medicine.uiowa.edu/vectorcore).

On the seventh (Actb $^{L/L}$, Actg1$^{L/L}$ MEFs) or ninth (Actb$^{L/L}$/Actg1$^{L/L}$ MEFs) day post infection cells showed complete knockout of protein by western blot as previously published (Patrinostro et al., 2017). Once knockout was confirmed by western blot, MEFs were stained with 0.01nM MitoTracker CMXRos (ThermoFisher Scientific M7512; Waltham, MA, USA) in Opti-MEM with 10%FBS for 15 min. Media was replaced and cells were imaged using a GE Applied Precision DeltaVision Deconvolution Microscopy system (Little Chalfont, Buckinghamshire, UK) with a 60x numerical aperture 1.42 objective and Photometrics Coolsnap HQ camera (Tucson, AZ, USA). Imaris Imaging software by Bitplane (Belfast, Northern Ireland, UK) was used to determine the surface area of all individual mitochondrion. To quantify fission and fusion events cells were imaged every 10s for 2min. The time-lapse images were then examined frame by frame for any mitochondrial fission or fusion events. MEFs from at least 3 different individual embryos per genotype were examined.

Transmission Electron Microscopy and Quantification

Mice at 6, 12, or 22-25 months were anesthetized using avertin. Once anesthetized the mice underwent intra-peritoneal perfusion with PBS, followed by

perfusion fixation with 4% PFA and 1.5% glutaraldehyde in 0.1 M Na-cacodylate buffer. The lower limb was removed and further fixed in the same solution at 4°C for 2 hours. *Tibialis Anterior* (TA) muscles were dissected and incubated overnight at 4°C in a secondary fix of 2.5% Glutaraldehyde in 0.1M Na-Cacodylate. Muscles were washed in Na-cacodylate buffer, post-fixed in 1% OsO_4 in 0.1 M Na-cacodylate for 1 hour, and rinsed in Na-cacodylate buffer. After dehydration with increasing concentrations of ethanol, muscles were embedded in Epon 812 resin. 65 nm ultrathin sections were stained with uranyl acetate and lead citrate and visualized on the transmission electron microscope (FEI Technai Spirt BioTWIN, Hillsboro, OR, USA) at 120kV. All chemicals were purchased from Electron Microscopy Sciences, Hatfield, PA, USA. Quantification of mitochondria length:width ratio and Z-disk alignment was measured using Fiji (Schindelin et al., 2012).

Mitochondrial Respiration

In these studies, muscle fiber bundles were used to assess mitochondrial respiration as this approach allows for the assessment of mitochondria in their native state (Perry et al., 2013) . The technique for preparing and permeabilizing muscle fiber bundles has previously been described (Lark et al., 2016). 12 month old mice were anesthetized and red portions of the gastrocnemius muscle were dissected and immediately added to ice-cold buffer X ([mM] - 7.23 K_2EGTA, 2.77 CaK_2EGTA, 20 imidazole, 20 taurine, 5.7 ATP, 14.3 phosphocreatine, 6.56

$MgCl_2 \cdot 6H_2O$, 50 MES, pH 7.1, 295 mosmol/kgH_2O). Under a dissecting microscope, connective tissue and fat were removed from the red portions before separating muscle into fiber bundles of ~ 1 mg wet wt. Muscle fiber bundles were then permeabilized in buffer X containing 30 µg/ml saponin for 30 min with continuous rotation at 4°C. Muscle fiber bundles were transferred to ice-cold buffer Z ([mM] – 110 K-MES, 35 KCl, 1 EGTA, $5K_2HPO_4$, 3 $MgCl_2 \cdot 6H_2O$, 5mg/ml BSA, pH 7.4, 295 mosmol/kgH_2O) and washed for 15 min at 4°C with continuous rotation.

Measurements of high-resolution O2 consumption were made using the OROBOROS Oxygraph-2K (Oroboros Instruments, Innsbruck, Austria) at 37°C with a starting oxygen concentration of ~350µM oxygen as previously described (Ryan et al. 2014). Experiments were conducted in buffer Z supplemented with 20mM creatine monohydrate and 25µM blebbistatin. Mitochondrial respiration was assessed by delivery of the substrates in the following order and at a final concentration of pyruvate 4mM, malate 2.5 mM, glutamate 5 mM, ADP 2.5 mM, succinate 5 mM, cytochrome c 5 µM, rotenone 10 µM, antimycin A 5 µM, ascorbic acid 2 mM and TMPD 0.5 mM (N,N,N',N'-Tetramethyl-p-phenylenediamine dihydrochloride). Preservation of mitochondrial membrane integrity was confirmed by excluding muscle bundles that produced a >10% increase in respiration in response to exogenous cytochrome c addition. Following completion of the protocol, muscle bundles were washed in distilled H2O, freeze-dried (Labconco, Kansas City, MO, USA) and weighed (Orion Cahn C-35, Thermo Electron, Beverly,

MA). All chemicals and reagents were purchased from Sigma-Aldrich (St. Louis, MO, USA).

Indirect calorimetry and body composition

22-25 month old male mice were individually housed for metabolic testing and were habituated to the metabolic chamber for 1 day prior to the collection of data over 2.5 days (n = 4-7). Oxygen consumption (VO2) and carbon dioxide production (VCO2), activity, and energy expenditure were measured using metabolic monitoring systems including the Oxymax Comprehensive Lab Animal Monitoring System (Columbus Instruments, Columbus, OH, USA). VO2 (volume O2), VCO2 (volume CO2), and respiratory exchange ratio (RER) were calculated from the gas-exchange data. Activity was measured on the x- and z-axes with the use of infrared beams. Mice were analyzed for total body fat, lean tissue, and body water content using an EchoMRI quantitative magnetic resonance system (Echo Medical Systems, Houston, TX, USA). Energy expenditure was calculated with the formula provided by the manufacturer, expressed as Kcal/h and analyzed with body weight as continuous predictors in an ANCOVA model (Tschöp et al., 2012).

Mitochondria-Associated Membrane Fractionation

Mouse liver from 12 month male animals was fractionated according to the protocol in Wieckowski et al (Wieckowski et al., 2009). Briefly: the mouse was anesthetized using avertin, sacrificed by cervical dislocation. The liver was

immediately removed and successively washed in buffer (225mM mannitol, 75-mM sucrose, 0.5% BSA, 0.5mM EGTA and 30mM Tris-HCL, followed by 225mM mannitol, 75-mM sucrose, 0.5% BSA, and 30mM Tris-HCL, and 225mM mannitol, 75-mM sucrose, and 30mM Tris-HCL). The liver was minced, homogenized using a Teflon and glass mortar and pestle at 4°C, and spun at 740g for 5min, supernatant was collected and respun under the same conditions. The supernatant was collected and spun at 9,000xg for 10min, the pellet contains the crude mitochondria (the supernatant containing the cytoplasm and endoplasmic reticulum were centrifuged at 20,000xg for 30min, the supernatant was spun for 1h at 100,000xg, the resulting supernatant is the cytoplasmic fraction and the pellet is the endoplasmic reticulum fraction). The pellet containing the crude mitochondria was washed and spun at 10,000xg for 10min twice. The washed pellet was gently homogenized in buffer and layered on top of percoll media. The fractionation of the crude mitochondria into pure mitochondria and mitochondria-associated membrane was done by centrifuging the percoll layered suspension at 95,000xg for 30min using a swinging rotor (SW32 Beckman-Coulter, Brea, CA, USA). The resulting upper band (the mitochondria-associated membrane) and lower band (pure mitochondria) were each collected, washed, and centrifuged at 6,300xg for 10 min. The pellet from the pure mitochondrial sample was collected. The mitochondria-associated membrane supernatant was centrifuged at 100,000xg for 1h, the pellet was the mitochondria-associated membrane fraction (rotor 50.2 Beckman-Coulter, Brea, CA, USA). All spins were done at 4°C in a

Beckman JS-HS high-speed centrifuge (20,000xg and under) or Beckman L8-M ultra-high-speed centrifuge (over 20,000xg). All reagents from Sigma-Aldrich, St. Louis, MO, USA.

Western Blotting

12 or 22-25 month old male mice were anesthetized using avertin and sacrificed by cervical dislocation. The whole *quadriceps femoris* muscle was immediately dissected and any fat or connective tissue was removed. Protein was then extracted through mechanical tissue disruption via homogenization in liquid nitrogen and chemical disruption using 1%SDS buffer in 1xPBS with a cocktail of protease inhibitors (Aprotinin 100uM, Benzamide 0.79mg/mL, E-64 10nM, Leupeptin 10uM, Pepstatin 0.1mg/mL, PMSF 1mM; Sigma-Aldrich, St. Louis, MO, USA). Lysate was boiled for 5 min and centrifuged at 20,000xg for 3 min to remove the insoluble fraction. Protein concentration was determined by A280 on a NanoDrop ND-1000 Spectrometer (Thermo Fisher Scientific; Waltham, MA, USA). For comparison of relative immunoreactivities, 40ug of protein lysate was run on a 10% polyacrylamide gel for 1h at 150v. Samples were transferred onto PVDF membrane for 1h at 100v. Antibodies to ATP5A (ab14748; Abcam, Milton, Cambridge, UK), BiP (C50B12; Cell Signaling Technology, Danvers, MA, USA), β_{cyto}-Actin AC-15 (A5441; Sigma-Aldrich, St. Louis, MO, USA), γ_{cyto}-Actin (mAb 2-4; as published in Hanft et al., 2007), Cytochrome C (ab13575; Abcam, Milton, Cambridge, UK), FACL4 (ab155282; Abcam, Milton, Cambridge, UK), GAPDH

(Sigma-Aldrich, St. Louis, MO, USA), IP3R-3 (610312; BD Biosciences), IRE1α (14C10; Cell Signaling Technology, Danvers, MA, USA), PDI (C81H6; Cell Signaling Technology, Danvers, MA, USA), PERK (D11A8; Cell Signaling Technology, Danvers, MA, USA), SDHA (ab14715; Abcam, Milton, Cambridge, UK), SERCA1 (ab2819; Abcam, Milton, Cambridge, UK), SERCA2 (ab2861; Abcam, Milton, Cambridge, UK), Tubulin B512 (T6074; Sigma-Aldrich, St. Louis, MO, USA), and UQCR (ab110252; Abcam, Milton, Cambridge, UK), were used at the recommendation concentrations. Membranes were imaged on a Licor Odyssey (Lincoln, NE, USA).

In Vitro Contraction

Mice were anesthetized with sodium pentobarbital (100 mg/kg BW; Diamondback Drugs, Socttsdale, AZ, USA). *Extensor Digitorium Longus* (EDL) muscles were removed from 12 and 22-25 month old mice and mounted on a dual-mode muscle lever system (300B-LR; Aurora Scientific Inc., Aurora, ON, Canada) with 5-0 suture in a 1.5 mL bath assembly and filled with oxygenated (95 % O_2) Krebs Ringer bicarbonate buffer that was maintained at 25 ˚C. Muscles were adjusted to their anatomic optimal length (L_o) based on resting tension. Muscle length was then measured from myotendonous junction to myotendonous junction using digital calipers. Muscles remained quiescent in the bath for 5 min before beginning a protocol for testing contractile function. Maximal isometric tetanic contractions (P_o) were performed every 2 min until plateaued by stimulating the

muscle for 200ms at 150Hz (Grass S48 stimulator delivered through a SIU5D stimulus isolation unit; Grass Telefactor, Warwick, RI, USA). Peak twitch force was measured by stimulating the muscle with a 0.5-ms pulse at 150 V. A second twitch was elicited 30s later followed 30s later by an isometric tetanic contraction. Every two minutes, isometric tetanic contractions were performed until the muscle reached a plateau of force (three contractions within 0.1 g). Maximal rates of contraction (+dP/dt) and relaxation (-dP/dt) were derived from the slopes of the force-time traces. Two minutes of rest were followed by a fatigue protocol of submaximal (60Hz) isometric contractions every 7.5s for 200ms over 5min. Fatigue recovery was monitored by isometric tetanic contractions (200ms at 150 Hz) every 5min for 30min.

Statistical Analysis

1-way ANOVAs with Tukey's post hoc test were performed to determine significance. * is $0.01<p<0.05$, *** is $p<0.001$. Error bars are S.E.M.

Figures

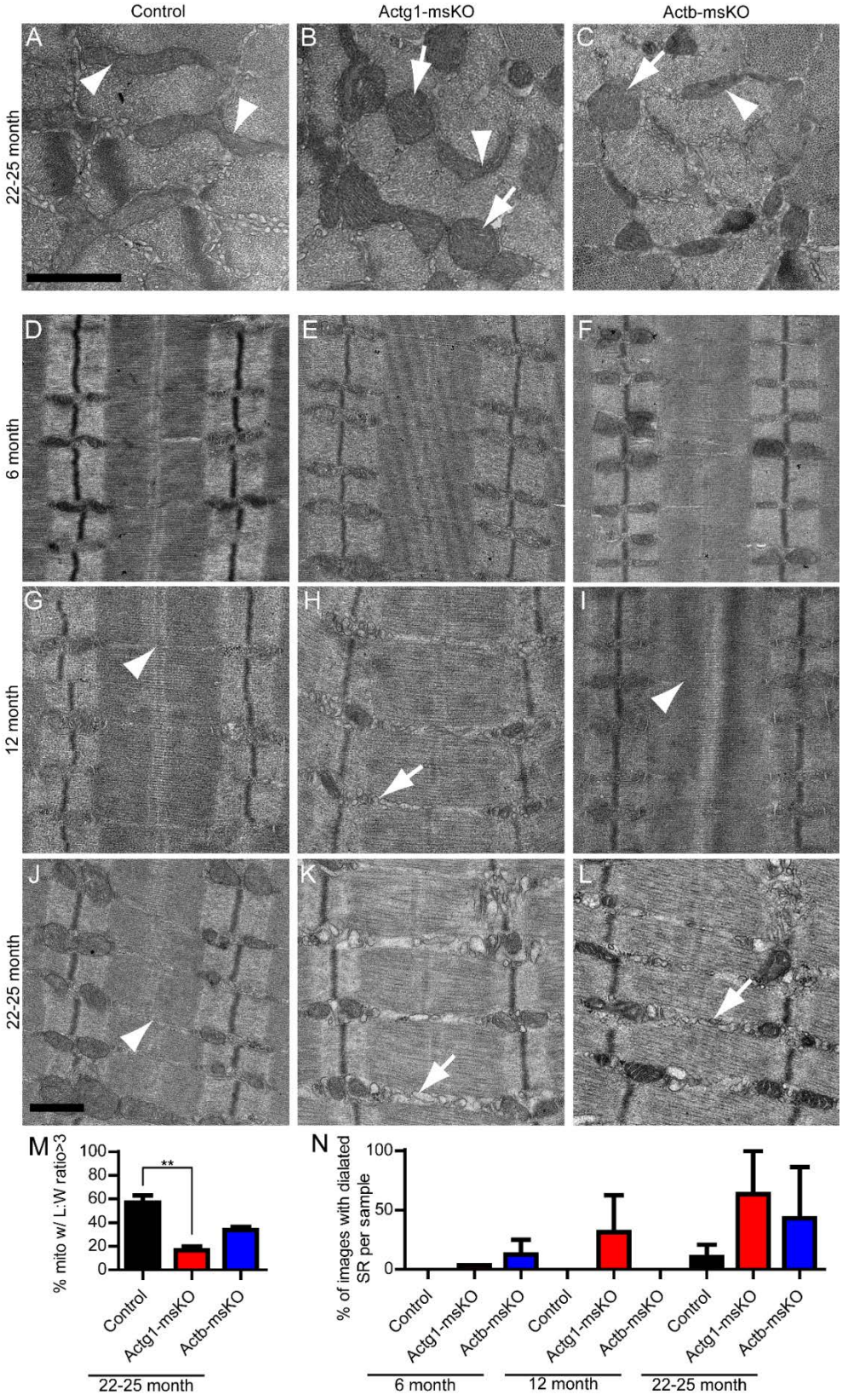
Control
Actg1-msKO
Actb-msKO
A
B
C
22-25 month
D
E
F
6 month
G
H
I
12 month
J
K
L
22-25 month
M
% mito w/ L:W ratio>3
100
80
60
40
20
0
**
Control
Actg1-msKO
Actb-msKO
22-25 month
N
% of images with dialated SR per sample
100
50
0
Control
Actg1-msKO
Actb-msKO
Control
Actg1-msKO
Actb-msKO
Control
Actg1-msKO
Actb-msKO
6 month
12 month
22-25 month

Figure 3-1 Altered sarcoplasmic reticulum and mitochondrial morphology in aged Actg1 and Actb KO skeletal muscle.

(A-C) Transverse sections of TA from control, Actg1-msKO, and Actb-msKO mice at 22-25 months of age. (M) Quantification of mitochondrial length:width ratio. (D-L) Longitudinal sections of TA from control, Actg1-msKO, and Actb-msKO mice at 6 (D-F), 12 (G-I), and 22-25 (J-L) months of age. White arrowheads denote normal SR, white arrows denote dilated SR. (N) Quantification of the percentage of images examined that displayed dilated SR. Scale bars = 1µm.

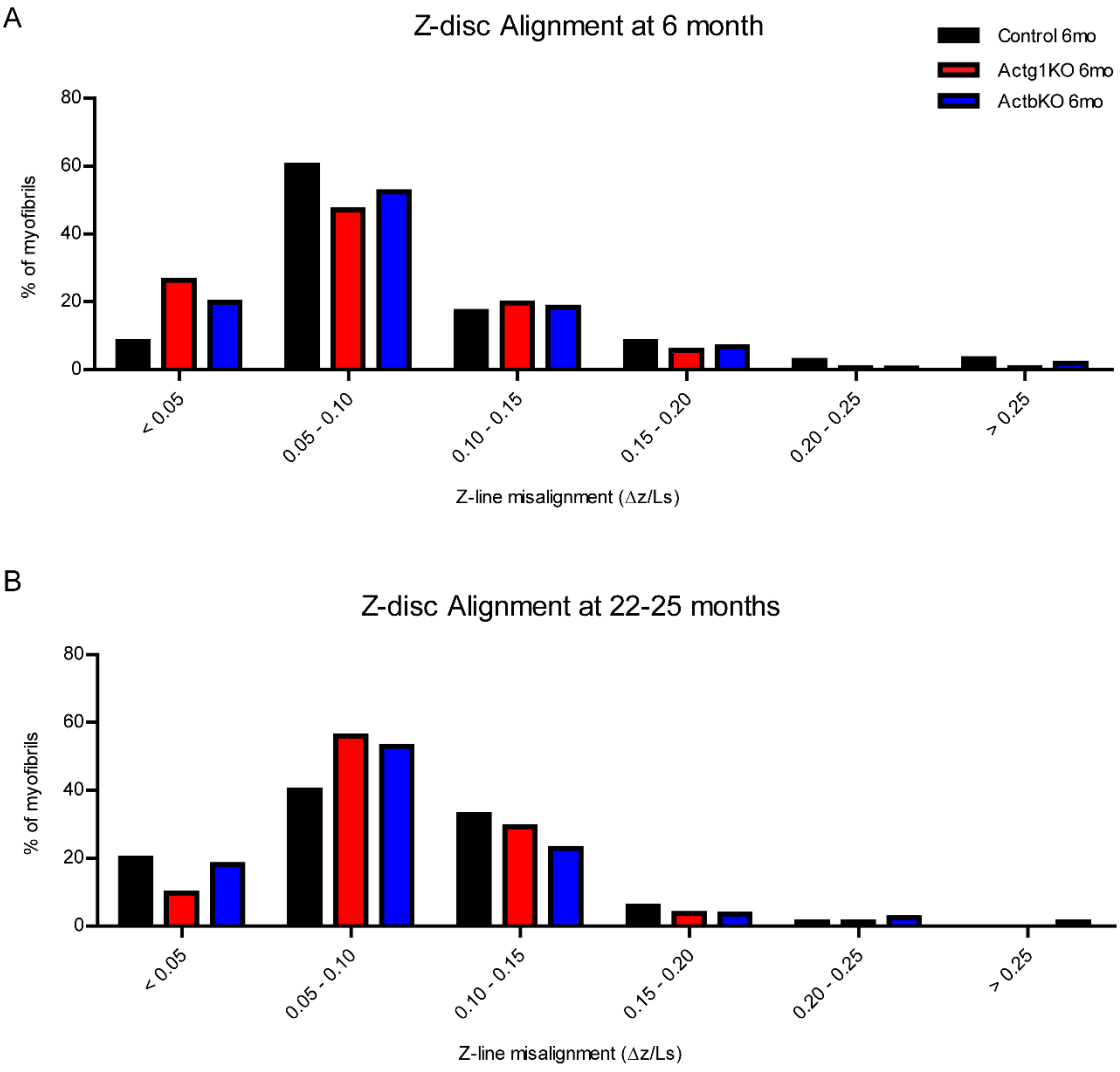

Supplementary Figure 3-1 No shift in Z-disk alignment in Actg1 and Actb KO skeletal muscle.

Changes in Z-disk alignment of adjacent sarcomere pairs at 6 months (A) and 22-25 months (B).

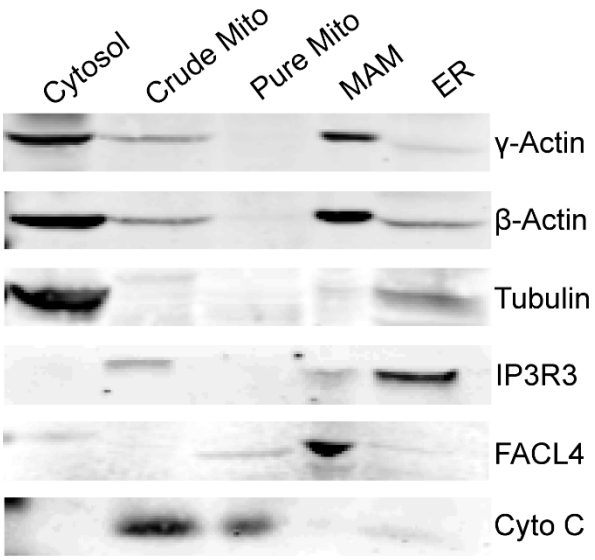

Figure 3-2 Enrichment of γcyto- and βcyto-actin in isolated mitochondrial associated membrane.

Shown are identical western blots loaded with equal amounts of protein from the fractions obtained during the preparation of isolated mitochondrial associated membranes from mouse liver and stained with antibodies to the indicated protein.

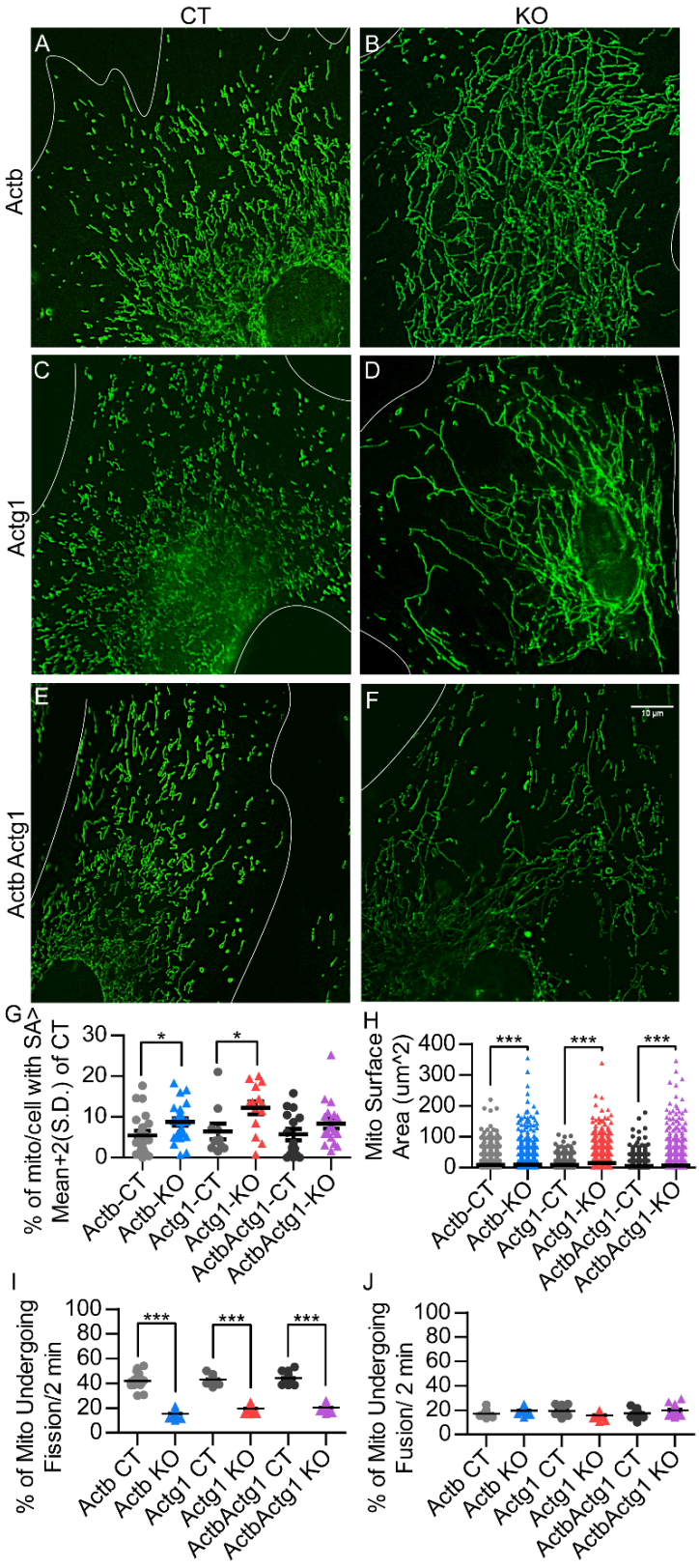
CT
KO
A
B
C
D
E
F
Actb
Actg1
Actb Actg1
10 µm
G
% of mito/cell with SA> Mean+2(S.D.) of CT
Actb-CT
Actb-KO
Actg1-CT
Actg1-KO
ActbActg1-CT
ActbActg1-KO
H
Mito Surface Area (um^2)
I
% of Mito Undergoing Fission/2 min
J
% of Mito Undergoing Fusion/ 2 min

Figure 3-3 Ablation of γcyto- or βcyto-actin results in increased mitochondrial area and decreased fission.

(A-F) Mitochondria appear elongated in Actg1 KO Actb KO, and Actb/Actg1 dKO MEFs compared to control (CT). Scale bar = 10μm. (G) The percentage of mitochondria with surface areas greater than the mean of the control plus 2 standard deviations. (H) Surface area of each mitochondrion per genotype. (I-J) Quantitation of fission and fusion frequencies in CT, Actg1 KO, Actb KO, and Actb/Actg1 dKO MEFs (Done in live cells not shown).

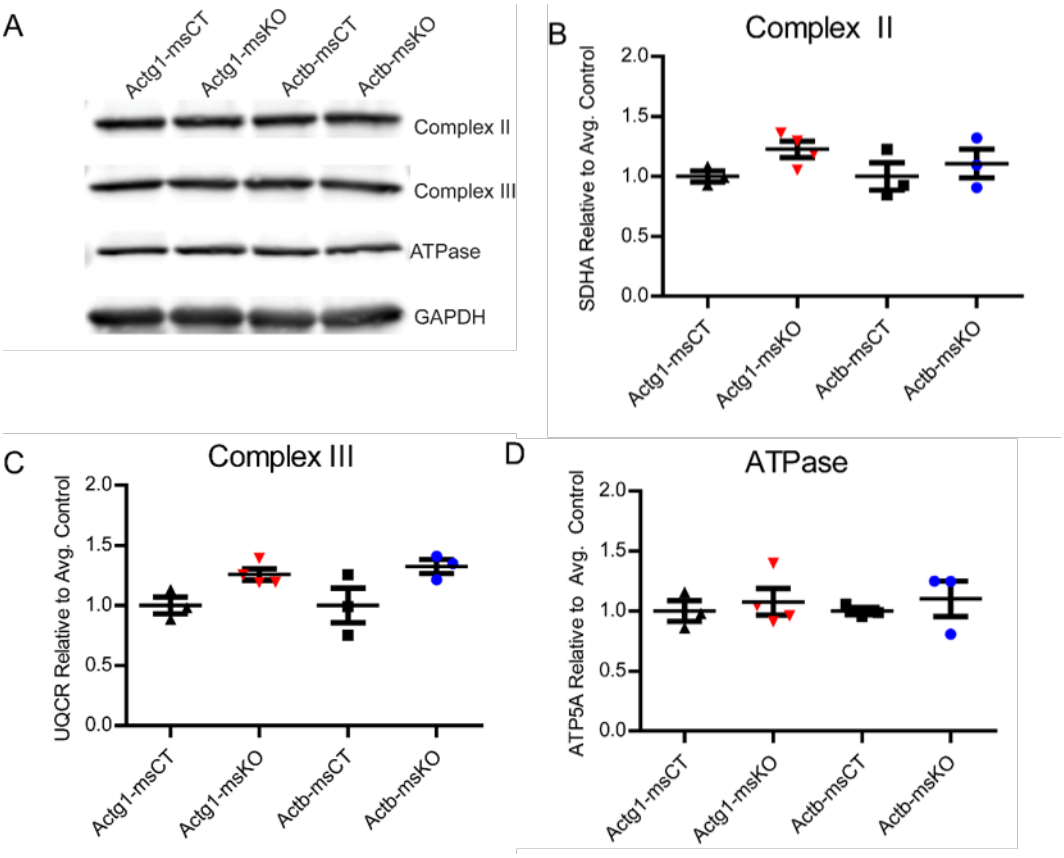

Supplementary Figure 3-2 Normal abundance of electron transport chain complex proteins in Actg1 and Actb KO skeletal muscle.

(A) Representative western blot showing immunoreactivity to proteins from complex II, III, and V. (B) Quantification of SDHA, a complex II protein, immunoreactivity normalized to GAPDH and relative to CT mean. (C) Quantification of UQCR, a complex III protein, immunoreactivity normalized to GAPDH and relative to CT mean. (D) Quantification of ATP5A, a complex V protein, immunoreactivity normalized to GAPDH and relative to CT mean.

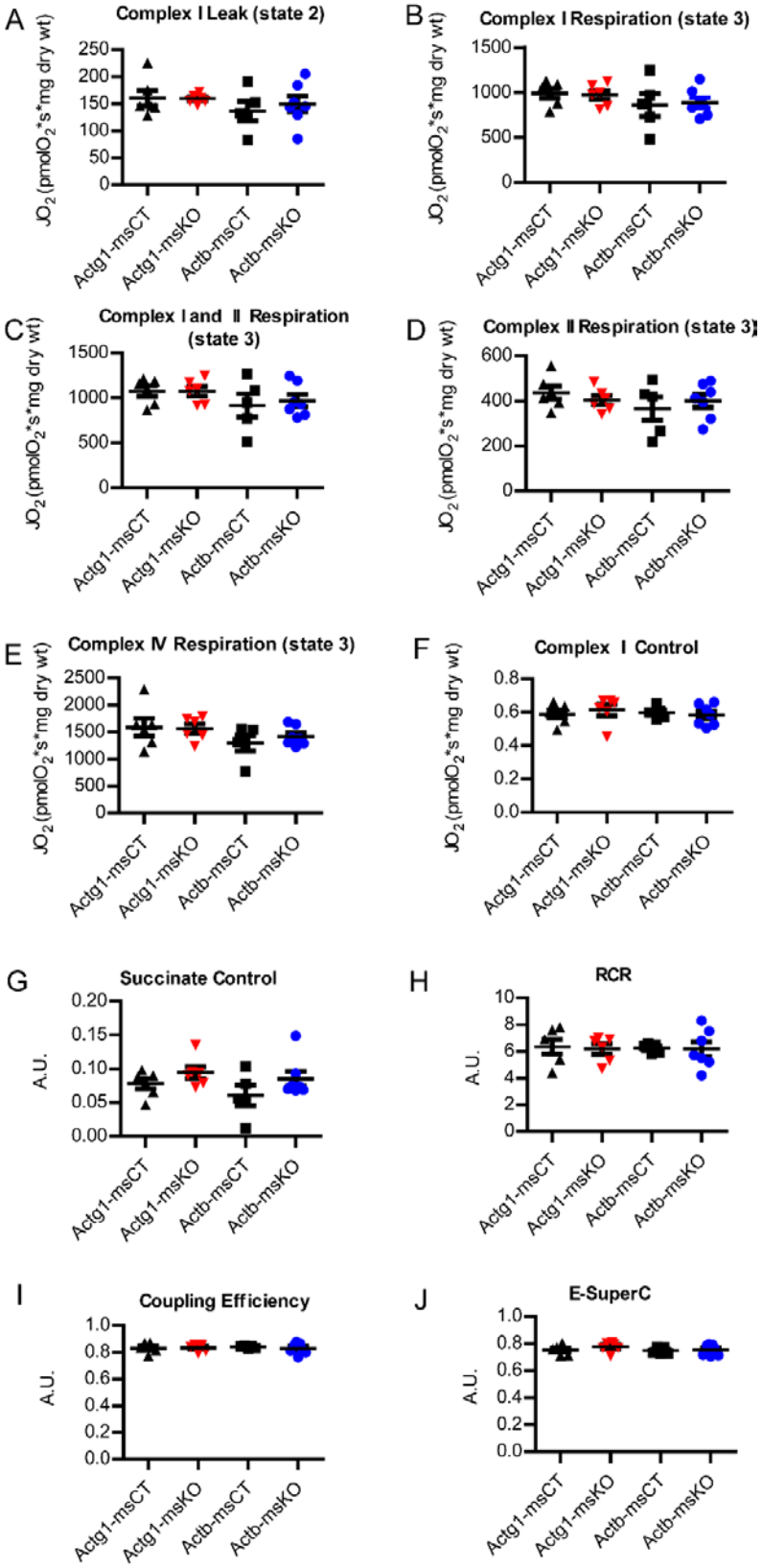
A
Complex I Leak (state 2)
JO_2 (pmolO_2*s*mg dry wt)
250
200
150
100
50
0
Actg1-msCT
Actg1-msKO
Actb-msCT
Actb-msKO
B
Complex I Respiration (state 3)
JO_2 (pmolO_2*s*mg dry wt)
1500
1000
500
0
Actg1-msCT
Actg1-msKO
Actb-msCT
Actb-msKO
C
Complex I and II Respiration (state 3)
JO_2 (pmolO_2*s*mg dry wt)
1500
1000
500
0
Actg1-msCT
Actg1-msKO
Actb-msCT
Actb-msKO
D
Complex II Respiration (state 3)
JO_2 (pmolO_2*s*mg dry wt)
600
400
200
0
Actg1-msCT
Actg1-msKO
Actb-msCT
Actb-msKO
E
Complex IV Respiration (state 3)
JO_2 (pmolO_2*s*mg dry wt)
2500
2000
1500
1000
500
0
Actg1-msCT
Actg1-msKO
Actb-msCT
Actb-msKO
F
Complex I Control
JO_2 (pmolO_2*s*mg dry wt)
0.8
0.6
0.4
0.2
0.0
Actg1-msCT
Actg1-msKO
Actb-msCT
Actb-msKO
G
Succinate Control
A.U.
0.20
0.15
0.10
0.05
0.00
Actg1-msCT
Actg1-msKO
Actb-msCT
Actb-msKO
H
RCR
A.U.
10
8
6
4
2
0
Actg1-msCT
Actg1-msKO
Actb-msCT
Actb-msKO
I
Coupling Efficiency
A.U.
1.0
0.8
0.6
0.4
0.2
0.0
Actg1-msCT
Actg1-msKO
Actb-msCT
Actb-msKO
J
E-SuperC
A.U.
1.0
0.8
0.6
0.4
0.2
0.0
Actg1-msCT
Actg1-msKO
Actb-msCT
Actb-msKO

Figure 3-4 Normal mitochondrial function in Actg1 and Actb KO skeletal muscle.

(A-J) Oxygen consumption parameters measured in isolated gastrocnemius fibers. (A) Complex I leak (CI leak), JO2 was measured in the presence of pyruvate, malate, and glutamate (state 2). (B) Complex I respiration rate (CI), JO2 was measured in the presence of ADP (state 3). (C) Complex I+II respiration rate (CI+II), JO2 was measured in the presence of succinate. (D) Complex II respiration rate (CII), JO2 was measured in the presence of rotenone. (E) Complex IV respiration rate, JO2 was measured in the presence of antimycin A, ascorbic acid, and TMPD. (F) Complex I control is the ratio of (JO2 Complex I+II - JO2 Complex II)/JO2 Complex I+II. (G) Succinate Control (JO2 CI+II-JO2 CI)/JO2 CI+II. (H) RCR is the respiratory control ratio it is the ratio of JO2 CI/JO2 CI leak. (I) Biochemical coupling efficiency is the ratio of (JO2 CI - JO2 CI leak)/JO2 CI. (J) E-supercomplex is the ratio of JO2 CI+II/ (JO2 CI + JO2 CII).

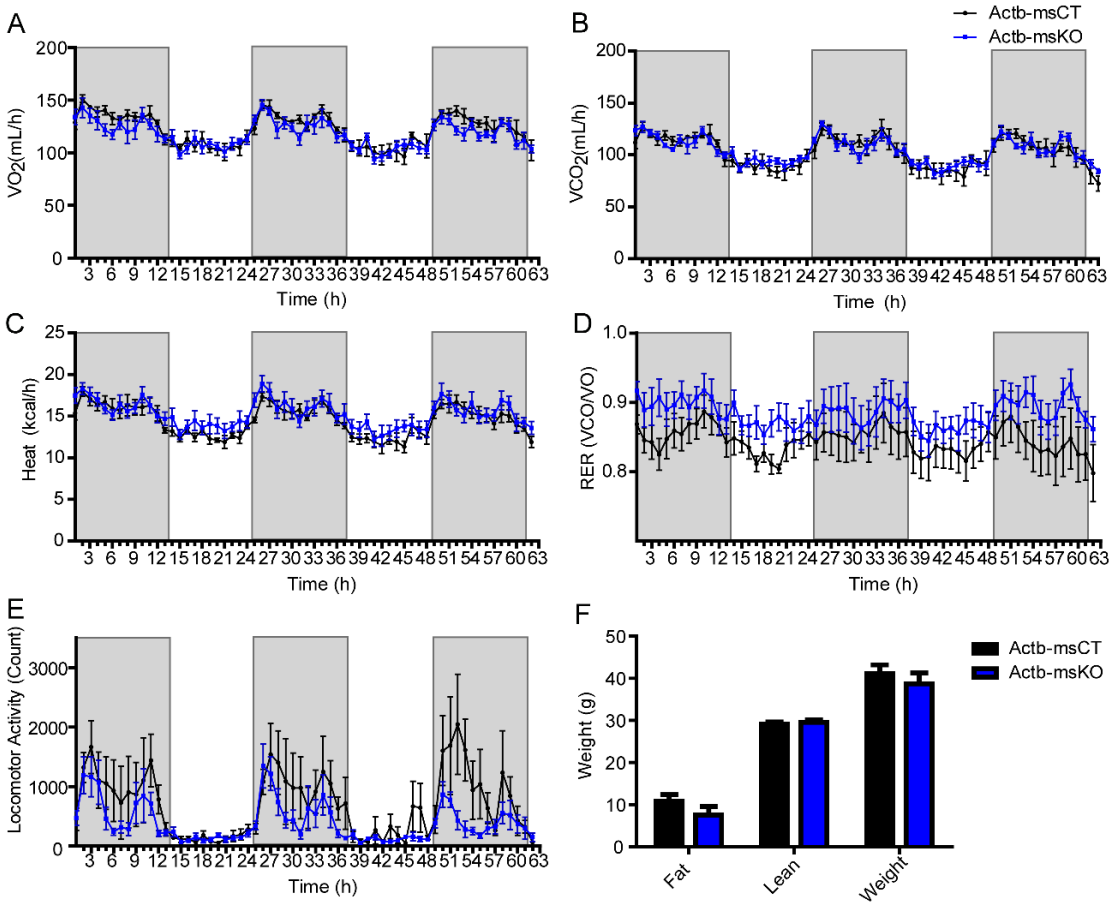

Supplementary Figure 3-3 Normal whole body respiration in 22-25 month old muscle-specific Actb KO mice.

(A-E) Whole body mitochondrial respirometry of 22-25 month old mice. (A) O2 consumption. (B) CO2 consumption. (C) Heat released. (D) Respiratory exchange ratio of O2 to CO2. (E) Ambulation. (F) Body composition of mice used in study. Experiments performed by University of Minnesota Phenotyping Core.

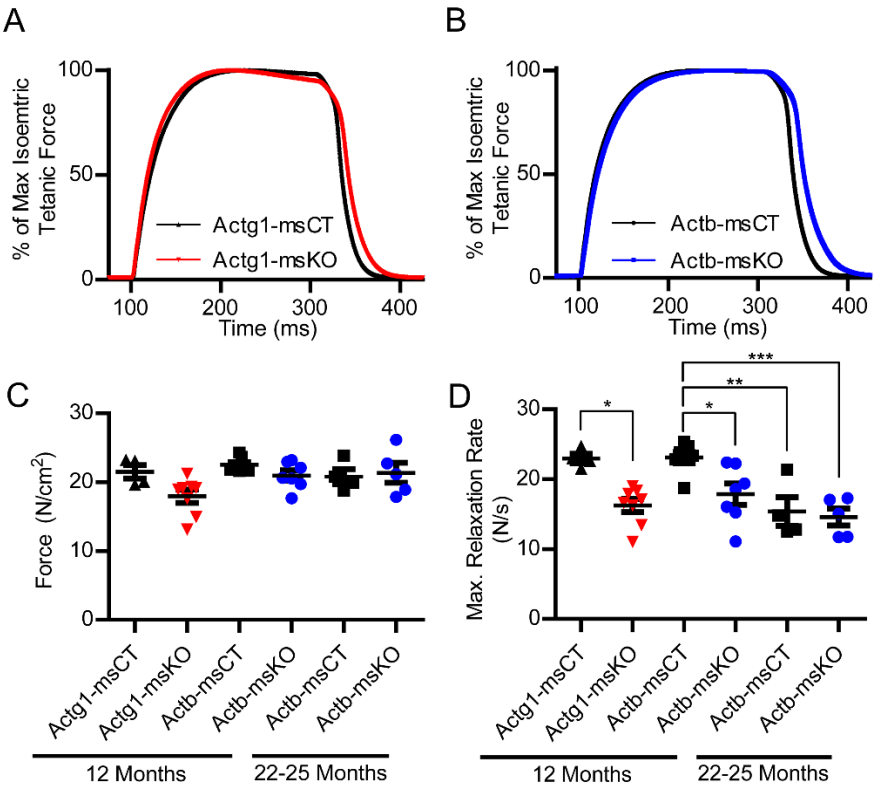

Figure 3-5 Impaired relaxation rates in Actb and Actg1 KO skeletal muscle.

(A-B) Representative isometric contraction force tracings of tetanically-stimulated 12 month old control, Actg1-msKO (A), and Actb-msKO (B) EDL muscles. (C) Peak specific forces generated during maximal isometric tetanic contractions. (D) Maximal rates of relaxation. Experiments performed with the help of Angus Lindsey.

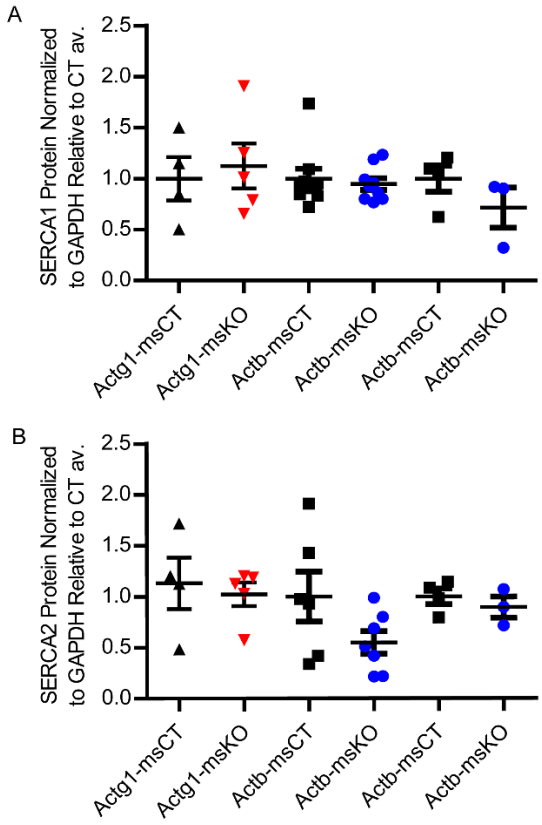

Figure 3-6 Normal SERCA 1 and 2 abundance in Actb and Actg1 KO skeletal muscle.

(A-B) Quantification of SERCA 1 and 2 immunoreactivity normalized to GAPDH relative to WT mean.

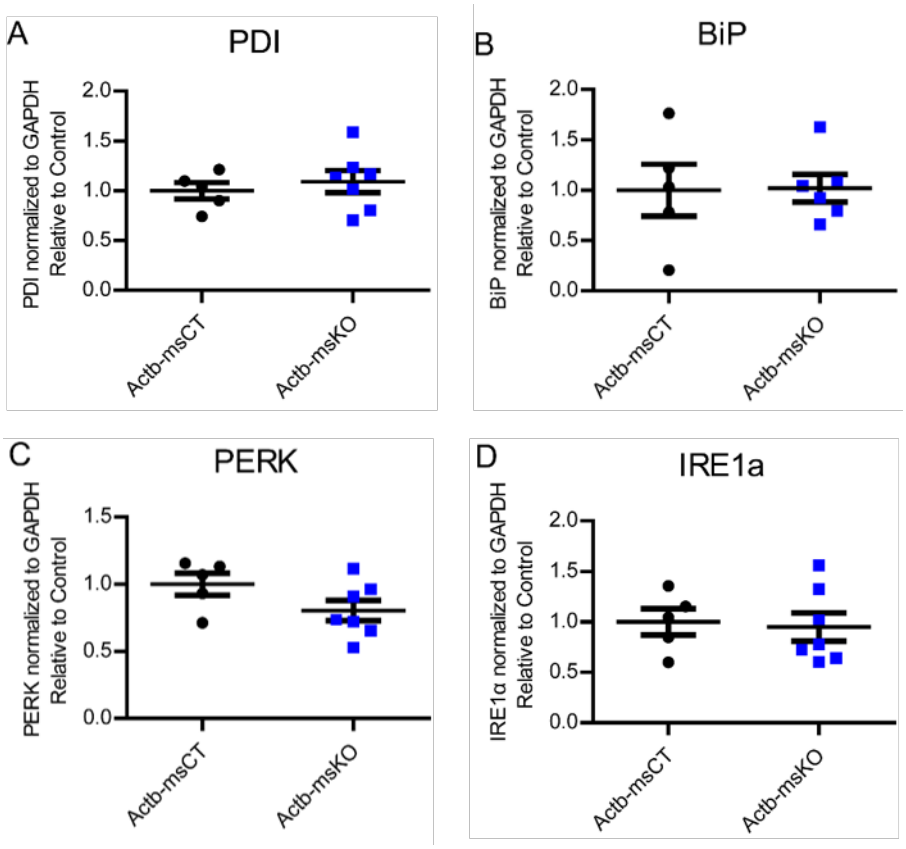

Supplementary Figure 3-4 Endoplasmic reticulum stress response pathway proteins are not upregulated in muscle-specific Actb KO mice at 12 months old.

Western blot showing immunoreactivity to endoplasmic reticulum stress pathway proteins. Quantification of immunoreactivity to PDI (A), BiP (B), PERK (C), and IRE1α (D). All samples were normalized to GAPDH and relative to CT mean.

Table 3-1 Twitch and tetanic isometric contraction measurements in control, Actg1-msKO, and Actb-msKO EDL muscles.

Age	12mo				22+mo	
Genotype	Actg1-msCT	Actg1-msKO	Actb-msCT	Actb-msKO	Actb-msCT	Actb-msKO
Specific Force (N/cm2)	21.5 ±1.0	18.0 ±0.9	22.5 ±0.4	21.0 ±0.7	20.8 ±1.1	21.4 ±1.5
Maximal Contraction Rate (N/s)	17.0 ±1.0	13.7 ±0.5	15.8 ±0.7	14.9 ±0.7	15.1 ±0.6	14.6 ±0.8
Maximal Relaxation Rate (N/s)	23.0 ±0.7	16.2 ±1.0*	23.1 ±0.8	17.9 ±1.5*	15.4 ±2.1**	14.6 ±1.2***
1/2 Relaxation Time (s/kg)	1.2 ±0.2	1.6 ±0.2	1.3 ±0.1	1.3 ±0.10	1.8 ±0.3	1.7 ±0.1
Force Development Time(s/kg)	1.2 ±0.1	1.5 ±0.1	1.5 ±0.2	1.5 ±0.1	1.4 ±0.1	1.6 ±0.1
Fatigue (% of initial maximal tetanic isometric force)	60.8 ±2.3	64.7 ±2.1	60.8 ±2.3	64.7 ±1.8	58.3 ±2.7	64.6 ±2.5
Force Recovery after Fatigue (% of initial maximal tetanic isometric force)	93.0 ±2.1	90.8 ±4.1	93.7 ±1.4	92.5 ±1.8	91.5 ±2.7	95.7 ±2.4
Maximal Contractile force recovery after Fatigue (% of initial maximal contractile force)	87.9 ±2.2	90.7 ±2.4	93.4 ±0.8	91.8 ±2.5	89.9 ±3.4	93.4 ±2.6
Maximal Relaxation Force Recovery after Fatigue (% of initial maximal relaxation force)	91.0±3.9	81.5 ±5.3	90.8 ±2.4	90.3 ±2.8	96.1 ±4.8	95.0 ±2.7

Chapter 4 : Conclusions and Discussion

Conclusions

I: *My work focused on further elucidating of how ablation of γ_{cyto}- or β_{cyto}-actin isoforms in skeletal muscle leads to a mild progressive myopathy in mice. Towards that goal we have demonstrated that:*

- γ_{cyto}- and β_{cyto}-actin are enriched at the mitochondrial associated membrane interface between mitochondria and endoplasmic reticulum.
- Loss of γ_{cyto}- or β_{cyto}-actin led to perturbations in mitochondrial and sarcoplasmic reticulum morphologies in skeletal muscle of aged mice.
- The changes in mitochondria morphology in γ_{cyto}- and β_{cyto}- actin knockout muscle are not linked to detectable functional changes of the mitochondria.
- γ_{cyto}- and β_{cyto}-actin are both required for normal mitochondrial fission.
- The observed sarcoplasmic reticulum morphological changes in γ_{cyto}- and β_{cyto}- actin knockout muscle do correspond to changes in sarcoplasmic reticulum function prior to the manifestation of morphological changes.

II: *My work also aimed to shed light on the redundant and unique functions of γ_{cyto}- or β_{cyto}-actin. Here we have shown that:*

- Phenotypes resulting from loss of either γ_{cyto}- or β_{cyto}-actin had a long lag time, likely due to functional redundancy.
- The similarity of the phenotypes observed in the absence of γ_{cyto}- or β_{cyto}-actin is suggestive that the isoforms have functional cooperativity in many circumstances.

- The decreased ATP content when β_{cyto}-actin, but not γ_{cyto}-actin, is ablated supports the concept that γ_{cyto}- and β_{cyto}-actin have unique functions.

Discussion

I: Ablation of either γ_{cyto}- or β_{cyto}- actin from skeletal muscle results in a mild but progressive myopathy marked by successive rounds of muscle degeneration and regeneration (Prins et al., 2011; Sonnemann et al., 2006). How loss of either γ_{cyto}- or β_{cyto}- actin from skeletal muscle could lead to this mild myopathy was unclear. The primary aim of this thesis is to identify how ablation of either cytoplasmic actin from skeletal muscle could lead to a mild progressive myopathy.

As γ_{cyto}- or β_{cyto}- actin compose such a small percentage of the total actin pool in skeletal muscle it could be difficult to decipher the functional impact they are having. To shed light on how γ_{cyto}- or β_{cyto}- actin ablation in skeletal muscle leads to a mild progressive myopathy, we utilized localization as a guide for where to look. In skeletal muscle, cytoplasmic actin isoforms have been shown to colocalize with two organelles which can readily affect cell viability; mitochondria and the Z-disk containing SR (Craig and Pardo, 1983; Kee et al., 2004; Nakata et al., 2001; Papponen et al., 2009; Rybakova et al., 2000). Here we demonstrated that both γ_{cyto}- and β_{cyto}-actin are enriched in the mitochondria-associated membrane fraction, which is the interface between mitochondria and endoplasmic reticulum. The presence of both γ_{cyto}- and β_{cyto}-actin at the mitochondria-associated membrane interface provided a potential platform through which cytoplasmic actin isoforms could affect SR and mitochondria. Upon investigation of γ_{cyto}- and β_{cyto}- actin knockout skeletal muscle we found that both mitochondria and SR morphology was altered, but only in aged animals. The SR and

mitochondrial morphological changes we observed are qualitatively similar to those seen by other groups who targeted actin associated proteins (Domenighetti et al., 2014; Gokhin and Fowler, 2011; Gokhin et al., 2010; Wang et al., 2013), but develop much later than what was found in the other studies.

For an in-depth examination of the role cytoplasmic actin isoforms had in mitochondrial dynamics, we turned to a more accessible model system: MEFs. The elongated mitochondrial morphologies and decreased rate of fission in knockout MEFs indicated that γ_{cyto}- and β_{cyto}-actin are involved in mitochondrial dynamics. Involvement of cytoplasmic actin isoforms in mitochondrial dynamics is consistent with recent work which revealed a step in mitochondrial fission requiring both actin and the endoplasmic reticulum (Korobova et al., 2013; Manor et al., 2015).

Having further characterized the role of cytoplasmic actin in mitochondrial dynamics and morphology, we wanted to determine if a functional change preceded the morphological perturbations seen in γ_{cyto}- and β_{cyto}-actin knockout skeletal muscle. Mitochondria are central orchestrators of cell viability presenting an attractive target through which cytoplasmic actin isoforms affect skeletal muscle cell viability and led to the observed myopathy. In MEFs we saw that cell growth and ATP content are decreased when β_{cyto}- actin is ablated but no changes in mitochondrial respiratory function were detected, which may be due to the low energy expenditure of primary MEFs. In contrast, skeletal muscle has a high energy demand. To determine if functional changes preceded the morphological

malformations seen in γ_{cyto}- and β_{cyto}-actin knockout skeletal muscle at 22 months, we measured mitochondrial respiratory function in skeletal muscle fiber bundles at 12 months. As shown in Chapter 3, no perturbations in mitochondrial oxygen consumption were observed, which indicated that defects in mitochondrial respiration are not a primary contributor to the progressive myopathy of γ_{cyto}- and β_{cyto}-actin knockout skeletal muscle.

Since SR morphology was also altered when γ_{cyto}- and β_{cyto}-actin were ablated in skeletal muscle, we investigated SR function prior to the manifestation of SR morphological changes. The SR in skeletal muscle is a vital regulator of Ca^{2+}, and subsequently contraction, cell stress, and cell death. Functional alterations in the SR could contribute to the morphological phenotype and the overall myopathy found in the absence of either cytoplasmic actin (Fontes-Oliveira et al., 2013). To determine if any functional changes preceded the morphological malformations, at 12 months we measured skeletal muscle relaxation kinetics, which can be indicative of SR functional changes. Examination of relaxation kinetics found that the maximal relaxation rate was slowed compared to controls in both γ_{cyto}- and β_{cyto}-actin knockout animals. The decreased maximal relaxation rate in 12 month knockout γ_{cyto}- or β_{cyto}-actin muscle is suggestive of SR dysfunction, as relaxation rate is linked to the ability to remove Ca^{2+} from the cytoplasm into the SR. The SR is primarily responsible for Ca^{2+} removal and storage following contraction and altered relaxation rates are associated with SR dysfunction (Westerblad and Lannergren, 1991). Ca^{2+} flow into the SR occurs via

SERCA (Berchtold et al., 2000). Though we observed no alterations in SERCA abundance, it may be functionally deficient. Another mechanism through which Ca^{2+} sequestration into the SR could be effected is Ca^{2+} leak through the ryanodine receptor channel. Therefore, in γ_{cyto}- and β_{cyto}-actin knockout skeletal muscle a phenotype suggestive of abnormal SR function preceded the manifestation of SR morphological changes, supporting the idea that SR dysfunction may have contributed to the mild progressive myopathy.

Interestingly, the decrease in maximal relaxation rate of knockout muscle seen at 12 months was negated by age. By 22-25 months control muscle maximal relaxation rate had dropped to levels comparable to knockout muscle at 12 months, while the 22-25 month knockout muscle had remained steady at the lower rate, indicating that ablation of γ_{cyto}- or β_{cyto}-actin may mimic the stress of aging and lead to a premature aging phenotype in relation to muscle relaxation.

II: The individual contributions by γ_{cyto}- and β_{cyto}- actin to the diverse array of functions attributed to cytoplasmic actin has long been a focus of research. Differing by only 4 amino acids at the N-terminus of the protein, the evolutionary benefit for maintaining both γ_{cyto}- and β_{cyto}- actin isoforms in birds and mammals is not readily apparent. In mice, whole body ablation of γ_{cyto}-actin leads to the expected Mendelian numbers at birth, but two-thirds die within the first 24 hours and an additional two-thirds of the survivors die prematurely (Belyantseva et al., 2009). A more severe phenotype was observed in β_{cyto}-actin hypomorph and knockout animals, which proved embryonic lethal (Bunnell et al., 2011; Shawlot et al., 1998; Shmerling et al., 2005b). The animal models highlight the differing importance γ_{cyto}- and β_{cyto}-actin have *in vivo* which led us to investigate the separate and overlapping functional relevance of γ_{cyto}- and β_{cyto}-actin.

As our studies on cytoplasmic actin isoforms in skeletal muscle shed light on functional implications of γ_{cyto}- and β_{cyto}-actin, they also provided insight into γ_{cyto}- and β_{cyto}-actin redundant and unique functions. Many of the phenotypes we found when γ_{cyto}- and β_{cyto}-actin were ablated were similar in both knockout models including: morphological alterations in mitochondria and SR, mitochondrial fission, and decreased maximal relaxation rate indicative of SR dysfunction. The prolonged lag-time to phenotype manifestation indicated that the cause of these morphological changes was mild and is likely the result of a high degree of γ_{cyto}- and β_{cyto}-actin functional overlap. The presence of an analogous phenotype in both γ_{cyto}- and β_{cyto}-actin knockouts suggested to us that there was incomplete

functional overlap between the two isoforms which resulted in the observed phenotypes. The incomplete functional overlap and the similar nature of the phenotypes implies that under normal circumstances γ_{cyto}- and β_{cyto}-actin work together and that co-functionality is disrupted in both knockout models. Not all phenotypes we saw were comparable in γ_{cyto}- and β_{cyto}-actin knockouts. In MEFs we found that ATP content was decreased in β_{cyto}-actin, but not γ_{cyto}-actin, knockouts. The attribution of a unique phenotype to β_{cyto}-actin knockout MEFs is consistent with the more severe phenotype seen in β_{cyto}-actin whole body knockout mice.

Continuing Study

Further experiments examining the functional necessity of γ_{cyto}- and β_{cyto}-actin at the mitochondria-associated membrane interface may help us to understand how both cytoplasmic actin isoforms are important for mitochondrial fission. Other groups have shown actin to be involved in mitochondrial fission via an endoplasmic reticulum mechanism (Korobova et al., 2013; Manor et al., 2015). The initial step in characterizing the contribution of both γ_{cyto}- and β_{cyto}-actin would be to visualize endoplasmic reticulum. By imaging the endoplasmic reticulum and mitochondria in live knockout MEFs we could measure the number of endoplasmic reticulum/mitochondria contact sites in control and knockout MEFs, which would determine whether either or both cytoplasmic actin isoforms function in site formation. Alternatively, a finding of the same number of sites but fewer fission events would suggest that actin dynamics are hindered and polymerization cannot provide the constrictive force required. The same experimental setup could be extended through the use of drugs that stimulate mitochondrial fission such as FCCP and the endoplasmic reticulum/mitochondria contact sites monitored. Additionally, re-introduction of γ_{cyto}- or β_{cyto}-actin back into the MEFs from which they were ablated could shed further light on the importance of cytoplasmic actin isoforms in mitochondrial fission, however, our primary MEFs do not tolerate exogenous expression well so finding the optimal technique for exogenous expression would be critical. Immortalization would circumvent the toxicity induced

cell death we see in our primary MEFs, however the mitochondrial fission phenotype is not present in immortalized knockout cells. Knowing the specific contribution of γ_{cyto}- and β_{cyto}-actin to mitochondrial fission is relevant to all cell types because of the ubiquitous expression of cytoplasmic actin isoforms.

Since we observed a change in relaxation kinetics characteristic of a decrease in SR function, examination of SR Ca^{2+} transients, especially the activity of SERCA and the ryanodine receptor could lead to further understanding of the mechanism. The caveats to studying Ca^{2+} transients specifically at the SR are: getting a SR specific Ca^{2+} reporter into live skeletal muscle fibers, the mild nature of the phenotype, and having an assay sensitive enough to detect small variations in Ca^{2+} transients in the SR required to produce a reliable outcome. One solution could be to visually examine SR Ca^{2+} in isolated myofibers (Ziman et al., 2010). Isolated myofibers would allow for the introduction of the SR Ca^{2+} probe Fura-2 AM, however, the myofibers cannot be electrically stimulated to contract. None-the-less, valuable information could still be gained with the use of SERCA inhibitors, such as thapsigargin, and activators could be utilized to assess whether the SR is leaking Ca^{2+}. Because organization of mitochondria and the SR are highly stable in adult skeletal muscle the relationship between cytoplasmic actins, mitochondria and the sarco/endoplasmic reticulum may be more accessible to study in MEFs. The first step will be to identify if there is also an endoplasmic reticulum phenotype in MEFs. If a phenotype is identified then γ_{cyto}- and β_{cyto}-actin endoplasmic reticulum interactions could be characterized, initially via the known

endoplasmic reticulum/actin associated proteins tropomodulin 3 and inverted formin 2 (Gokhin and Fowler, 2011; Korobova et al., 2013).

Insight into the general cellular importance of cytoplasmic actins was gained through our studies in primary MEFs, which provided a γ_{cyto}- and β_{cyto}-actin double knockout model. Intriguingly many of the phenotypes associated with ablation of either one of the cytoplasmic actin isoforms in MEFs were not worsened in the double knockouts, as was the case with mitochondrial morphology and fission. The consistency of phenotype in the absence of one or both cytoplasmic actin isoforms indicates that each isoform is required, and lacking one isoform is just as detrimental as lacking both. To more completely understand the functional significance of having two cytoplasmic isoforms an *in vivo* model is needed. Though single γ_{cyto}- or β_{cyto}-actin muscle specific knockouts have provided insight into the function of cytoplasmic actin isoforms, the mild skeletal muscle myopathy observed is likely a result of functional overlap between the two actin isoforms masking the role each isoforms plays in adult tissue. Double γ_{cyto}- and β_{cyto}-actin muscle specific knockouts would shed more light on the functional significance of these isoforms in skeletal muscle, however, attempts to generate these mice have proved unsuccessful thus far. The challenge in generating skeletal muscle γ_{cyto}- and β_{cyto}-actin double knockouts is probably becsue there are multiple populations of muscle progenitor cells and the multinucleate nature of myofibers, both of which result in cellular heterogeneity allowing for compensation when gene knockout is incomplete (Biressi et al., 2007). Successfully driving recombination at four alleles

in skeletal muscle is difficult, as other groups have seen (Haldar et al., 2008). A potential solution for these problems is to use transgenic muscle specific MyoD Cre (Chen et al., 2005). MyoD is expressed early in the muscle cell lineage, allowing for targeting of all progenitor populations (Chen et al., 2001; Faerman and Shani, 1993; Sassoon et al., 1989). Additionally, the transgene for MyoD Cre could be present in high enough copy number to drive recombination in multiple nuclei and subsequent knockout of both γ_{cyto}- and β_{cyto}-actin (Chen et al., 2005).

Here we have extended our current understanding of the functional implications of γ_{cyto}- and β_{cyto}-actin in skeletal muscle and how they might contribute to the mild myopathy observed when either isoforms is absent in skeletal muscle. We showed that γ_{cyto}- and β_{cyto}-actin are involved in mitochondrial fission. In skeletal muscle, we found that mitochondrial and SR morphological phenotypes were preceded by functional changes indicative of decreased SR function. Our work also lead to more questions about the specific functions of cytoplasmic actin isoforms at the mitochondria/SR interface. Definitive understanding of the functional importance of γ_{cyto}- and β_{cyto}-actin requires the generation of a skeletal muscle specific γ_{cyto}- and β_{cyto}-actin double knockout. Ultimately, a double knockout will allow for determination of the role cytoplasmic actin redundancy has in phenotype development.

Bibliography

Almenar-Queralt, A. and Lee, A. (1999). Identification of a novel tropomodulin isoform, skeletal tropomodulin, that caps actin filament pointed ends in fast skeletal muscle. *J. Biol. Chem.* **274**, 28466–28475.

Almuzzaini, B., Sarshad, A. A., Rahmanto, A. S., Hansson, M. L., Von Euler, A., Sangfelt, O., Visa, N., Farrants, A.-K. O. and Percipalle, P. (2016). In b-actin knockouts, epigenetic reprogramming and rDNA transcription inactivation lead to growth and proliferation defects. *FASEB J.* **1**, 2860–73.

Andersson, D. C., Betzenhauser, M. J., Reiken, S., Meli, A. C., Umanskaya, A., Xie, W., Shiomi, T., Zalk, R., Lacampagne, A. and Marks, A. R. (2011). Ryanodine receptor oxidation causes intracellular calcium leak and muscle weakness in aging. *Cell Metab.* **14**, 196–207.

Anesti, V. and Scorrano, L. (2006). The relationship between mitochondrial shape and function and the cytoskeleton. *Biochim. Biophys. Acta - Bioenerg.* **1757**, 692–699.

Ayalon, G., Davis, J. Q., Scotland, P. B. and Bennett, V. (2008). An ankyrin-based mechanism for functional organization of dystrophin and dystroglycan. *Cell* **135**, 1189–200.

Basseri, S. and Austin, R. C. (2012). Endoplasmic reticulum stress and lipid metabolism: Mechanisms and therapeutic potential. *Biochem. Res. Int.* **2012**, 1–13.

Belyantseva, I. a, Perrin, B. J., Sonnemann, K. J., Zhu, M., Stepanyan, R., McGee, J., Frolenkov, G. I., Walsh, E. J., Friderici, K. H., Friedman, T. B., et al. (2009). Gamma-actin is required for cytoskeletal maintenance but not development. *Proc. Natl. Acad. Sci. U. S. A.* **106**, 9703–8.

Berchtold, M. W., Brinkmeier, H., Mu, M., Martin, W., Brinkmeier, H. and Mu, M. (2000). Calcium Ion in Skeletal Muscle : Its Crucial Role for Muscle Function , Plasticity , and Disease. **80**, 1215–1265.

Bergeron, S. E., Zhu, M., Thiem, S. M., Friderici, K. H. and Rubenstein, P. A. (2010). Ion-dependent polymerization differences between mammalian α- and ß-nonmuscle actin isoforms. *J. Biol. Chem.* **285**, 16087–16095.

Biressi, S., Molinaro, M. and Cossu, G. (2007). Cellular heterogeneity during vertebrate skeletal muscle development. *Dev. Biol.* **308**, 281–293.

Blanchet, L., Smeitink, J. A. M., van Emst-de Vries, S. E., Vogels, C., Pellegrini, M., Jonckheere, A. I., Rodenburg, R. J. T., Buydens, L. M. C., Beyrath, J., Willems, P. H. G. M., et al. (2015). Quantifying small molecule phenotypic effects using mitochondrial morpho-functional fingerprinting and machine learning. *Sci. Rep.* **5**, 1–7.

Brito, O. M. De and Scorrano, L. (2008). Mitofusin 2 tethers endoplasmic reticulum to mitochondria. *Nature* **456**, 605–610.

Brown, M. and Hasser, E. M. (1996). Complexity of age-related change in skeletal muscle. *J. Gerontol. A. Biol. Sci. Med. Sci.* **51**, B117-23.

Bunnell, T. M. and Ervasti, J. M. (2010). Delayed embryonic development and impaired cell growth and survival in Actg1 null mice. *Cytoskeleton* **67**, 564–72.

Bunnell, T. M. and Ervasti, J. M. (2011). Structural and functional properties of the actin gene family. *Crit. Rev. Eukaryot. Gene Expr.* **21**, 255–66.

Bunnell, T. M., Burbach, B. J., Shimizu, Y. and Ervasti, J. M. (2011). β-Actin specifically controls cell growth, migration, and the G-actin pool. *Mol. Biol. Cell* **22**, 4047–58.

Burté, F., Carelli, V., Chinnery, P. F. and Yu-Wai-Man, P. (2014). Disturbed mitochondrial dynamics and neurodegenerative disorders. *Nat. Rev. Neurol.* **11**, 11–24.

Carlier, M. F. and Pantaloni, D. (1997). Control of actin dynamics in cell motility. *J. Mol. Biol.* **269**, 459–67.

Chami, M., Oulès, B., Szabadkai, G., Tacine, R., Rizzuto, R. and Paterlini-Bréchot, P. (2008). Role of SERCA1 Truncated Isoform in the Proapoptotic Calcium Transfer from ER to Mitochondria during ER Stress. *Mol. Cell* **32**, 641–651.

Cheever, T. R., Olson, E. A. and Ervasti, J. M. (2011). Axonal Regeneration and Neuronal Function Are Preserved in Motor Neurons Lacking ß-Actin In Vivo. **6**, 1–13.

Cheever, T. R., Li, B. and Ervasti, J. M. (2012). Restricted morphological and behavioral abnormalities following ablation of beta-actin in the brain. *PLoS One* **7**, 1–10.

Chen, H. and Chan, D. C. (2005). Emerging functions of mammalian mitochondrial fusion and fission. *Hum. Mol. Genet.* **14**, R283-9.

Chen, H. and Chan, D. C. (2009). Mitochondrial dynamics-fusion, fission, movement, and mitophagy-in neurodegenerative diseases. *Hum. Mol. Genet.* **18**, 169–176.

Chen, H., Detmer, S. A., Ewald, A. J., Griffin, E. E., Fraser, S. E. and Chan, D. C. (2000). Mitofusins Mfn1 and Mfn2 coordinately regulate mitochondrial fusion and are essential for embryonic embryonic development. *J. Cell Biol.* **160**, 189–200.

Chen, J. C. J., Love, C. M. and Goldhamer, D. J. (2001). Two upstream enhancers collaborate to regulate the spatial patterning and timing of MyoD transcription during mouse development. *Dev. Dyn.* **221**, 274–288.

Chen, J. C. J., Mortimer, J., Marley, J. and Goldhamer, D. J. (2005). MyoD-cre Transgenic Mice : A Model for Conditional Mutagenesis and Lineage Tracing of Skeletal Muscle. **121**, 116–121.

Chen, H., Ren, S., Clish, C., Jain, M., Mootha, V., McCaffery, J. M. and Chan, D. C. (2015). Titration of mitochondrial fusion rescues Mff-deficient cardiomyopathy. *J. Cell Biol.* **211**, 795–805.

Chevet, E., Cameron, P. H., Pelletier, M. F., Thomas, D. Y. and Bergeron, J. J. M. (2001). The endoplasmic reticulum: Integration of protein folding, quality control, signaling and degradation. *Curr. Opin. Struct. Biol.* **11**, 120–124.

Clapham, D. E. (2007). Calcium Signaling. *Cell* **131**, 1047–1058.

Condeelis, J. and Singer, R. H. (2005). How and why does beta-actin mRNA target? *Biol. Cell* **97**, 97–110.

Cordes, K. R., Sheehy, N. T., White, M. P., Berry, E. C., Morton, S. U., Muth, A. N., Lee, T.-H., Miano, J. M., Ivey, K. N. and Srivastava, D. (2009). miR-145 and miR-143 regulate smooth muscle cell fate and plasticity. *Nature* **460**, 1–7.

Craig, S. W. and Pardo, J. V (1983). Gamma actin, spectrin, and intermediate filament proteins colocalize with vinculin at costameres, myofibril-to-sarcolemma attachment sites. *Cell Motil.* **3**, 449–462.

Crawford, K., Flick, R., Close, L., Shelly, D., Paul, R., Bove, K., Kumar, A. and Lessard, J. (2002). Mice lacking skeletal muscle actin show reduced muscle strength and growth deficits and die during the neonatal period. *Mol.Cell Biol.* **22**, 5887–5896.

Csordás, G. and Hajnóczky, G. (2009). SR/ER-mitochondrial local

communication: Calcium and ROS. *Biochim. Biophys. Acta - Bioenerg.* **1787**, 1352–1362.

Davis, J. and Molkentin, J. D. (2013). Myofibroblasts: Trust your heart and let fate decide. *J. Mol. Cell. Cardiol.* **70**, 9–18.

Dayanithi, G., Chen-Kuo-Chang, M., Viero, C., Hamel, C., Muller, A. and Lenaers, G. (2010). Characterization of Ca2+ signalling in postnatal mouse retinal ganglion cells: involvement of OPA1 in Ca2+ clearance. *Ophthalmic Genet.* **31**, 53–65.

De Vos, K. J., Allan, V. J., Grierson, A. J. and Sheetz, M. P. (2005). Mitochondrial function and actin regulate dynamin-related protein 1-dependent mitochondrial fission. *Curr. Biol.* **15**, 678–83.

Distelmaier, F., Valsecchi, F., Forkink, M., van Emst-de Vries, S., Swarts, H. G., Rodenburg, R. J. T., Verwiel, E. T. P., Smeitink, J. a. M., Willems, P. H. G. M. and Koopman, W. J. H. (2012). Trolox-Sensitive Reactive Oxygen Species Regulate Mitochondrial Morphology, Oxidative Phosphorylation and Cytosolic Calcium Handling in Healthy Cells. *Antioxid. Redox Signal.* **17**, 1657–1669.

Domenighetti, A. A., Chu, P. H., Wu, T., Sheikh, F., Gokhin, D. S., Guo, L. T., Cui, Z., Peter, A. K., Christodoulou, D. C., Parfenov, M. G., et al. (2014). Loss of FHL1 induces an age-dependent skeletal muscle myopathy associated with myofibrillar and intermyofibrillar disorganization in mice. *Hum. Mol. Genet.* **23**, 209–225.

Duan, R. and Gallagher, P. J. (2009). Dependence of myoblast fusion on a cortical actin wall and nonmuscle myosin IIA. *Dev. Biol.* **325**, 374–85.

Dugina, V., Zwaenepoel, I., Gabbiani, G., Clément, S. and Chaponnier, C. (2009). Beta and gamma-cytoplasmic actins display distinct distribution and functional diversity. *J. Cell Sci.* **122**, 2980–8.

Ebashi, S. and Endo, M. (1968). Calcium ion and muscle contraction. *Prog. Biophys. Mol. Biol.* **18**, 123–183.

Eisner, V., Csordas, G. and Hajnoczky, G. (2013). Interactions between sarco-endoplasmic reticulum and mitochondria in cardiac and skeletal muscle - pivotal roles in Ca(2)(+) and reactive oxygen species signaling. *J. Cell Sci.* **126**, 2965–2978.

Eisner, V., Lenaers, G. and Hajnóczky, G. (2014). Mitochondrial fusion is frequent in skeletal muscle and supports excitation-contraction coupling. *J. Cell Biol.* **205**, 179–195.

Ermak, G. and Davies, K. J. (2002). Calcium and oxidative stress: from cell signaling to cell death. *Mol Immunol* **38**, 713–721.

Faerman, A. and Shani, M. (1993). The expression of the regulatory myosin light chain 2 gene during mouse embryogenesis. *Development* **118**, 919–29.

Fontes-Oliveira, C. C., Busquets, S., Toledo, M., Penna, F., Paz Aylwin, M., Sirisi, S., Silva, A. P., Orpí, M., García, A., Sette, A., et al. (2013). Mitochondrial and sarcoplasmic reticulum abnormalities in cancer cachexia: altered energetic efficiency? *Biochim. Biophys. Acta* **1830**, 2770–8.

Frid, M. G., Shekhonin, B. V, Koteliansky, V. E. and Glukhova, M. A. (1992). Phenotypic changes of human smooth muscle cells during development: late expression of heavy caldesmon and calponin. *Dev. Biol.* **153**, 185–93.

Frontera, W. R. and Ochala, J. (2015). Skeletal muscle: a brief review of structure and function. *Calcif. Tissue Int.* **96**, 183–195.

Gautier, C. A., Kitada, T. and Shen, J. (2008). Loss of PINK1 causes mitochondrial functional defects and increased sensitivity to oxidative stress. *Proc. Natl. Acad. Sci.* **105**, 11364–11369.

Giaime, E., Yamaguchi, H., Gautier, C. A., Kitada, T. and Shen, J. (2012). Loss of DJ-1 does not affect mitochondrial respiration but increases ROS production and mitochondrial permeability transition pore opening. *PLoS One* **7**, e40501.

Gilady, S. Y., Bui, M., Lynes, E. M., Benson, M. D., Watts, R., Vance, J. E. and Simmen, T. (2010). Ero1α requires oxidizing and normoxic conditions to localize to the mitochondria-associated membrane (MAM). *Cell Stress Chaperones* **15**, 619–629.

Glancy, B., Hartnell, L. M., Malide, D., Yu, Z.-X., Combs, C. A., Connelly, P. S., Subramaniam, S. and Balaban, R. S. (2015). Mitochondrial reticulum for cellular energy distribution in muscle. *Nature* **523**, 617–620.

Gokhin, D. S. and Fowler, V. M. (2011). Cytoplasmic gamma-actin and tropomodulin isoforms link to the sarcoplasmic reticulum in skeletal muscle fibers. *J. Cell Biol.* **194**, 105–20.

Gokhin, D. S., Lewis, R. a, McKeown, C. R., Nowak, R. B., Kim, N. E., Littlefield, R. S., Lieber, R. L. and Fowler, V. M. (2010). Tropomodulin isoforms regulate thin filament pointed-end capping and skeletal muscle physiology. *J. Cell Biol.* **189**, 95–109.

Gordon, K., Clouaire, T., Bao, X. X., Kemp, S. E., Xenophontos, M., De Las

Heras, J. I. and Stancheva, I. (2014). Immortality, but not oncogenic transformation, of primary human cells leads to epigenetic reprogramming of DNA methylation and gene expression. *Nucleic Acids Res.* **42**, 3529–3541.

Gorlach, A., Klappa, P. and Kietzmann, T. (2006). The endoplasmic reticulum: folding, calcium homeostasis, signaling, and redox control. *Antioxid Redox Signal* **8**, 1391–1418.

Grimm, S. (2012). The ER-mitochondria interface: The social network of cell death. *Biochim. Biophys. Acta - Mol. Cell Res.* **1823**, 327–334.

Haldar, M., Karan, G., Tvrdik, P. and Capecchi, M. R. (2008). Two cell lineages, myf5 and myf5-independent, participate in mouse skeletal myogenesis. *Dev. Cell* **14**, 437–445.

Hall, Z. W., Lubit, B. W. and Schwartz, J. H. (1981). Cytoplasmic actin in postsynaptic structures at the neuromuscular junction. *J. Cell Biol.* **90**, 789–92.

Hanft, L. M., Rybakova, I. N., Patel, J. R., Rafael-Fortney, J. a and Ervasti, J. M. (2006). Cytoplasmic gamma-actin contributes to a compensatory remodeling response in dystrophin-deficient muscle. *Proc. Natl. Acad. Sci. U. S. A.* **103**, 5385–90.

Hanft, L. M., Bogan, D. J., Mayer, U., Kaufman, S. J., Kornegay, J. N. and Ervasti, J. M. (2007). Cytoplasmic gamma-actin expression in diverse animal models of muscular dystrophy. *Neuromuscul. Disord.* **17**, 569–74.

Hofmann, W. a, Stojiljkovic, L., Fuchsova, B., Vargas, G. M., Mavrommatis, E., Philimonenko, V., Kysela, K., Goodrich, J. a, Lessard, J. L., Hope, T. J., et al. (2004). Actin is part of pre-initiation complexes and is necessary for transcription by RNA polymerase II. *Nat. Cell Biol.* **6**, 1094–101.

Hu, P., Wu, S. and Hernandez, N. (2004). A role for beta-actin in RNA polymerase III transcription. *Genes Dev.* **18**, 3010–5.

Hudson, R. S., Yi, M., Esposito, D., Watkins, S. K., Hurwitz, A. A., Yfantis, H. G., Lee, D. H., Borin, J. F., Naslund, M. J., Alexander, R. B., et al. (2012). MicroRNA-1 is a candidate tumor suppressor and prognostic marker in human prostate cancer. *Nucleic Acids Res.* **40**, 3689–703.

Hüttelmaier, S., Zenklusen, D., Lederer, M., Dictenberg, J., Lorenz, M., Meng, X., Bassell, G. J., Condeelis, J. and Singer, R. H. (2005). Spatial regulation of beta-actin translation by Src-dependent phosphorylation of ZBP1. *Nature* **438**, 512–5.

Hüttemann, M., Lee, I., Pecinova, A., Pecina, P., Przyklenk, K. and Doan, J. W. (2008). Regulation of oxidative phosphorylation, the mitochondrial membrane potential, and their role in human disease. *J. Bioenerg. Biomembr.* **40**, 445–456.

Jalali, S., Ramanathan, G. K., Parthasarathy, P. T., Aljubran, S., Galam, L., Yunus, A., Garcia, S., Cox, R. R., Lockey, R. F. and Kolliputi, N. (2012). Mir-206 regulates pulmonary artery smooth muscle cell proliferation and differentiation. *PLoS One* **7**, e46808.

Johnson, B. D. and Byerly, L. (1993). A Cytoskeletal Mechanism for Ca 2 + Channel Metabolic Dependence and Inactivation by Intracellular Ca 2 +. **10**, 797–804.

Karakozova, M., Kozak, M., Wong, C. C. L., Bailey, A. O., Yates, J. R., Mogilner, A., Zebroski, H. and Kashina, A. (2006). Arginylation of beta-actin regulates actin cytoskeleton and cell motility. *Science* **313**, 192–6.

Kee, A. J., Schevzov, G., Nair-Shalliker, V., Robinson, C. S., Vrhovski, B., Ghoddusi, M., Qiu, M. R., Lin, J. J.-C., Weinberger, R., Gunning, P. W., et al. (2004). Sorting of a nonmuscle tropomyosin to a novel cytoskeletal compartment in skeletal muscle results in muscular dystrophy. *J. Cell Biol.* **166**, 685–96.

Khaitlina, S. Y. (2001). Functional specificity of actin isoforms. *Int. Rev. Cytol.* **202**, 35–98.

Kislauskis, E. H., Li, Z., Singer, R. H. and Taneja, K. L. (1993). Isoform-specific 3'-untranslated sequences sort alpha-cardiac and beta-cytoplasmic actin messenger RNAs to different cytoplasmic compartments. *J. Cell Biol.* **123**, 165–72.

Kornmann, B., Currie, E., Collins, S. R., Schuldiner, M., Nunnari, J., Weissman, J. S. and Walter, P. (2009). An ER-Mitochondria Tethering Complex Revealed by a Synthetic Biology Screen. *Science (80-.).* **325**, 477–481.

Korobova, F., Ramabhadran, V. and Higgs, H. N. (2013). An actin-dependent step in mitochondrial fission mediated by the ER-associated formin INF2. *Science* **339**, 464–7.

Krisans, S. K. and Coleman, R. A. (2002). Rat liver acyl-CoA synthetase 4 is a peripheral-membrane protein located in two distinct subcellular organelles, peroxisomes, and mitochondrial-associated membrane. *Arch. Biochem. Biophys.* **404**, 263–270.

Kumar, A., Crawford, K., Close, L., Madison, M., Lorenz, J., Doetschman, T., Pawlowski, S., Duffy, J., Neumann, J., Robbins, J., et al. (1997). Rescue of cardiac a-actin-deficient mice by enteric smooth muscle g-actin. *Proc.Natl.Acad.Sci.U.S.A* **94**, 4406–4411.

Kuo, S.-M., Burl, L. R. and Hu, Z. (2012). Cellular phenotype-dependent and -independent effects of vitamin C on the renewal and gene expression of mouse embryonic fibroblasts. *PLoS One* **7**, e32957.

Kushnareva, Y. E., Gerencser, A. A., Bossy, B., Ju, W.-K., White, A. D., Waggoner, J., Ellisman, M. H., Perkins, G. and Bossy-Wetzel, E. (2013). Loss of OPA1 disturbs cellular calcium homeostasis and sensitizes for excitotoxicity. *Cell Death Differ.* **20**, 353–65.

Lark, D. S., Torres, M. J., Lin, C.-T., Ryan, T. E., Anderson, E. J. and Neufer, P. D. (2016). Direct real-time quantification of mitochondrial oxidative phosphorylation efficiency in permeabilized skeletal muscle myofibers. *Am. J. Physiol. - Cell Physiol.* **311**, C239–C245.

Lechuga, S., Baranwal, S., Li, C., Naydenov, N. G., Kuemmerle, J. F., Dugina, V., Chaponnier, C. and Ivanov, A. I. (2014). Loss of γ-cytoplasmic actin triggers myofibroblast transition of human epithelial cells. *Mol. Biol. Cell* **25**, 3133–3146.

Leung, K. M., van Horck, F. P., Lin, A. C., Allison, R., Standart, N. and Holt, C. E. (2006). Asymmetrical beta-actin mRNA translation in growth cones mediates attractive turning to netrin-1. *Nat.Neurosci.* **9**, 1247–1256.

Lewin, T. M., Kim, J., Granger, D. A., Vance, J. E. and Coleman, R. A. (2001). Acyl-CoA Synthetase Isoforms 1 , 4 , and 5 Are Present in Different Subcellular Membranes in Rat Liver and Can Be Inhibited Independently *. *J. Biol. Chem.* **276**, 24674–24679.

Li, G., Mongillo, M., Chin, K. T., Harding, H., Ron, D., Marks, A. R. and Tabas, I. (2009). Role of ERO1-α-mediated stimulation of inositol 1,4,5-triphosphate receptor activity in endoplasmic reticulum stress-induced apoptosis. *J. Cell Biol.* **186**, 783–792.

Liang, S.-H., Zhang, W., McGrath, B. C., Zhang, P. and Cavener, D. R. (2006). PERK (eIF2alpha kinase) is required to activate the stress-activated MAPKs and induce the expression of immediate-early genes upon disruption of ER calcium homoeostasis. *Biochem. J.* **393**, 201–9.

Liu, S., Tetzlaff, M. T., Liu, A., Liegl-Atzwanger, B., Guo, J. and Xu, X. (2012). Loss of microRNA-205 expression is associated with melanoma progression. *Lab. Invest.* **92**, 1084–96.

Lloyd, C. and Gunning, P. (1993). Noncoding regions of the gamma-actin gene influence the impact of the gene on myoblast morphology. *J. Cell Biol.* **121**, 73–82.

Lloyd, C., Schevzov, G. and Gunning, P. (1992). Transfection of nonmuscle beta- and gamma-actin genes into myoblasts elicits different feedback regulatory responses from endogenous actin genes. *J. Cell Biol.* **117**, 775–785.

Ma, Y. and Hendershot, L. M. (2001). The unfolding tale of the unfolded protein response. *Cell* **107**, 827–830.

Manor, U., Bartholomew, S., Golani, G., Christenson, E., Kozlov, M., Higgs, H., Spudich, J. and Lippincott-schwartz, J. (2015). A mitochondria-anchored isoform of the actin-nucleating spire protein regulates mitochondrial division. *Elife* **4**, 1–27.

McHugh, K., Crawford, K. and Lessard, J. (1991). A comprehensive analysis of the developmental and tissue-specific expression of the isoactin multigene family in the rat. *Dev. Biol.* **148**, 442–458.

Miniou, P., Tiziano, D., Frugier, T., Roblot, N., Meur, M. Le and Melki, J. (1999). Gene targeting restricted to mouse striated muscle lineage. *Nucleic Acids Res.* **27**, 10–13.

Miralles, F., Posern, G., Zaromytidou, A. I. and Treisman, R. (2003). Actin dynamics control SRF activity by regulation of its coactivator MAL. *Cell* **113**, 329–342.

Mishra, P. and Chan, D. C. (2016). Metabolic regulation of mitochondrial dynamics. *J. Cell Biol.* **212**, 379–387.

Nakata, T., Nishina, Y. and Yorifuji, H. (2001). Cytoplasmic gamma actin as a Z-disc protein. *Biochem. Biophys. Res. Commun.* **286**, 156–63.

Niwa, M. and Walter, P. (2000). Pausing to decide. *Proc. Natl. Acad. Sci. U. S. A.* **97**, 12396–12397.

Nowak, K. J., Ravenscroft, G., Jackaman, C., Filipovska, A., Davies, S. M., Lim, E. M., Squire, S. E., Potter, A. C., Baker, E., Clément, S., et al. (2009a). Rescue of skeletal muscle alpha-actin-null mice by cardiac (fetal) alpha-actin. *J. Cell Biol.* **185**, 903–15.

Nowak, S. J., Nahirney, P. C., Hadjantonakis, A.-K. and Baylies, M. K. (2009b). Nap1-mediated actin remodeling is essential for mammalian myoblast fusion. *J. Cell Sci.* **122**, 3282–3293.

Odermatt, A., Taschner, P., Khanna, V., Busch, H., Karpati, G., Jablecki, C., Breuning, M. and MacLennan, D. (1996). Mutations in the gene-encoding SERCA1, the fast-twitch skeletal muscle sarcoplasmic reticulum Ca2+ ATPase, are associated with Brody disease. *Nat. Genet.* **14**, 191–4.

Otey, C. A., Kalnoski, M. and Bulinski, J. C. (1988). Immunolocalization of muscle and nonmuscle isoforms of actin in myogenic cells and adult skeletal muscle. *Cell Motil. Cytoskeleton* **9**, 337–348.

Papponen, H., Nissinen, M., Kaisto, T., Myllylä, V. V., Myllylä, R. and Metsikkö, K. (2008). F413C and A531V but not R894X myotonia congenita mutations cause defective endoplasmic reticulum export of the muscle-specific chloride channel CLC-1. *Muscle and Nerve* **37**, 317–325.

Papponen, H., Kaisto, T., Leinonen, S., Kaakinen, M. and Metsikkö, K. (2009). Evidence for gamma-actin as a Z disc component in skeletal myofibers. *Exp. Cell Res.* **315**, 218–25.

Patergnani, S., Suski, J. M., Agnoletto, C., Bononi, A., Bonora, M., De Marchi, E., Giorgi, C., Marchi, S., Missiroli, S., Poletti, F., et al. (2011). Calcium signaling around Mitochondria Associated Membranes (MAMs). *Cell Commun. Signal.* **9**, 19–29.

Patrinostro, X., O'Rourke, A. R., Chamberlain, C. M., Moriarity, B. S., Perrin, B. J. and Ervasti, J. M. (2017). Relative importance of βcyto- and γ cyto-actin in primary mouse embryonic fibroblasts. *Mol. Biol. Cell* **28**, 771–782.

Peckham, M. (2008). Engineering a multi-nucleated myotube, the role of the actin cytoskeleton. *J. Microsc.* **231**, 486–493.

Perrin, B. J. and Ervasti, J. M. (2010). The actin gene family: function follows isoform. *Cytoskeleton (Hoboken).* **67**, 630–4.

Perrin, B. J., Sonnemann, K. J. and Ervasti, J. M. (2010). β-Actin and γ-Actin are each dispensable for auditory hair cell development but required for stereocilia maintenance. *PLoS Genet.* **6**, 1–12.

Perrin, B. J., Strandjord, D. M., Narayanan, P., Henderson, D. M., Johnson, K. R. and Ervasti, J. M. (2013). β-Actin and fascin-2 cooperate to maintain stereocilia length. *J. Neurosci.* **33**, 8114–21.

Perry, C. G. R., Kane, D. A., Lanza, I. R. and Neufer, P. D. (2013). Methods for assessing mitochondrial function in diabetes. *Diabetes* **62**, 1041–1053.

Pletjushkina, O. Y., Lyamzaev, K. G., Popova, E. N., Nepryakhina, O. K., Ivanova, O. Y., Domnina, L. V., Chernyak, B. V. and Skulachev, V. P.

(2006). Effect of oxidative stress on dynamics of mitochondrial reticulum. *Biochim. Biophys. Acta - Bioenerg.* **1757**, 518–524.

Pollard, T. D. and Cooper, J. A. (2009). Actin, a central player in cell shape and movement. *Science* **326**, 1208–12.

Pollard, T. D., Blanchoin, L. and Mullins, R. D. (2000). Molecular Mechanisms Controlling Actin Filament Dynamics in Nonmuscle Cells. *Annu. Rev. Biophys. Biomol. Struct.* **29**, 545–576.

Prins, K. W., Call, J. a, Lowe, D. a and Ervasti, J. M. (2011). Quadriceps myopathy caused by skeletal muscle-specific ablation of β(cyto)-actin. *J. Cell Sci.* **124**, 951–7.

Rakovic, A., Grünewald, A., Kottwitz, J., Brüggemann, N., Pramstaller, P. P., Lohmann, K. and Klein, C. (2011). Mutations in PINK1 and Parkin impair ubiquitination of Mitofusins in human fibroblasts. *PLoS One* **6**, 1–13.

Raturi, A. and Simmen, T. (2013). Biochimica et Biophysica Acta Where the endoplasmic reticulum and the mitochondrion tie the knot : The mitochondria-associated membrane (MAM) ☆.*BBA - Mol. Cell Res.* **1833**, 213–224.

Rizzuto, R., Pinton, P., Carrington, W., Fay, F. S., Fogarty, K. E., Lifshitz, L. M., Tuft, R. A., Pozzan, T., Lawrie, A. M., Rizzuto, R., et al. (1998). Close contacts with the endoplasmic reticulum as determinants of mitochondrial Ca2+ responses. *Science (80-.).* **280**, 1763–6.

Rizzuto, R., Stefani, D. De, Raffaello, A. and Mammucari, C. (2012). Mitochondria as sensors and regulators of calcium signalling. *Nat. Publ. Gr.* **13**, 566–578.

Rosenmund, C. and Westbrook, G. L. (1993). Calcium-induced actin depolymerization reduces NMDA channel activity. *Neuron* **10**, 805–814.

Ross, A. F., Oleynikov, Y., Kislauskis, E. H. and Taneja, K. L. (1997). Characterization of a beta-actin mRNA zipcode-binding protein . *Mol. Cell. Biol.* **17**, 2158–2165.

Rossi, A., Kontarakis, Z., Gerri, C., Nolte, H., Hölper, S., Krüger, M. and Stainier, D. Y. R. (2015). Genetic compensation induced by deleterious mutations but not gene knockdowns. *Nature* **524**, 230–3.

Roveri, a, Coassin, M., Maiorino, M., Zamburlini, A., van Amsterdam, F. T., Ratti, E. and Ursini, F. (1992). Effect of hydrogen peroxide on calcium homeostasis in smooth muscle cells. *Arch. Biochem. Biophys.* **297**, 265–

270.

Rubenstein, P. A. (1990). The functional importance of multiple actin isoforms. *BioEssays* **12**, 309–315.

Rubenstein, P. A. and Wen, K. K. (2014). Insights into the effects of disease-causing mutations in human actins. *Cytoskeleton* **71**, 211–229.

Rusiñol, A. E., Cui, Z., Chen, M. H. and Vance, J. E. (1994). A unique mitochondria-associated membrane fraction from rat liver has a high capacity for lipid synthesis and contains pre-Golgi secretory proteins including nascent lipoproteins. *J. Biol. Chem.* **269**, 27494–27502.

Rybakova, I. N., Patel, J. R. and Ervasti, J. M. (2000). The dystrophin complex forms a mechanically strong link between the sarcolemma and costameric actin. *J. Cell Biol.* **150**, 1209–14.

Sassoon, D., Lyons, G., Wright, W. E., Lin, V., Lassar, A., Weintraub, H. and Buckingham, M. (1989). Expression of two myogenic regulatory factors myogenin and MyoD1 during mouse embryogenesis. *Nature* **341**, 303–307.

Schindelin, J., Arganda-Carreras, I., Frise, E., Kaynig, V., Longair, M., Pietzsch, T., Preibisch, S., Rueden, C., Saalfeld, S., Schmid, B., et al. (2012). Fiji: an open-source platform for biological-image analysis. *Nat. Methods* **9**, 676–682.

Schmidt, L. J., Duncan, K., Yadav, N., Regan, K. M., Verone, A. R., Lohse, C. M., Pop, E. a, Attwood, K., Wilding, G., Mohler, J. L., et al. (2012). RhoA as a mediator of clinically relevant androgen action in prostate cancer cells. *Mol. Endocrinol.* **26**, 716–35.

Schreiber, J., Végh, M. J., Dawitz, J., Kroon, T., Loos, M., Labonté, D., Li, K. W., Van Nierop, P., Van Diepen, M. T., De Zeeuw, C. I., et al. (2015). Ubiquitin ligase TRIM3 controls hippocampal plasticity and learning by regulating synaptic γ-actin levels. *J. Cell Biol.* **211**, 569–586.

Schröder, M. (2008). Endoplasmic reticulum stress responses. *Cell. Mol. Life Sci.* **65**, 862–894.

Schwartz, R. and Rothblum, K. (1981). Gene switching in myogenesis: differential expression of the chicken actin multigene family. *Biochemistry* **20**, 4122–4129.

Shawlot, W., Deng, J. M., Fohn, L. E. and Behringer, R. R. (1998). Restricted beta-galactosidase expression of a hygromycin-lacZ gene targeted to the beta-actin locus and embryonic lethality of beta-actin mutant mice.

Transgenic Res. **7**, 95–103.

Shmerling, D., Danzer, C. P., Mao, X., Boisclair, J., Haffner, M., Lemaistre, M., Schuler, V., Kaeslin, E., Korn, R., Bürki, K., et al. (2005a). Strong and ubiquitous expression of transgenes targeted into the ??-actin locus by Cre/lox cassette replacement. *Genesis* **42**, 229–235.

Shmerling, D., Danzer, C.-P., Mao, X., Boisclair, J., Haffner, M., Lemaistre, M., Schuler, V., Kaeslin, E., Korn, R., Bürki, K., et al. (2005b). Strong and ubiquitous expression of transgenes targeted into the beta-actin locus by Cre/lox cassette replacement. *Genesis* **42**, 229–35.

Shum, M. S. Y., Pasquier, E., Po'uha, S. T., O'Neill, G. M., Chaponnier, C., Gunning, P. W. and Kavallaris, M. (2011). gamma-Actin regulates cell migration and modulates the ROCK signaling pathway. *FASEB J.* **25**, 4423–4433.

Singaravelu, K., Nelson, C., Bakowski, D., De Brito, O. M., Ng, S. W., Di Capite, J., Powell, T., Scorrano, L. and Parekh, A. B. (2011). Mitofusin 2 regulates STIM1 migration from the Ca2+ store to the plasma membrane in cells with depolarized mitochondria. *J. Biol. Chem.* **286**, 12189–12201.

Singhal, P. K., Sassi, S., Lan, L., Au, P., Halvorsen, S. C., Fukumura, D., Jain, R. K. and Seed, B. (2016). Mouse embryonic fibroblasts exhibit extensive developmental and phenotypic diversity. *Proc. Natl. Acad. Sci. U. S. A.* **113**, 122–7.

Small, E. M. (2012). The Actin-MRTF-SRF gene regulatory axis and myofibroblast differentiation. *J. Cardiovasc. Transl. Res.* **5**, 794–804.

Sonnemann, K. J., Fitzsimons, D. P., Patel, J. R., Liu, Y., Schneider, M. F., Moss, R. L. and Ervasti, J. M. (2006). Cytoplasmic gamma-actin is not required for skeletal muscle development but its absence leads to a progressive myopathy. *Dev. Cell* **11**, 387–97.

Spät, A., Szanda, G., Csordás, G. and Hajnóczky, G. (2008). High- and low-calcium-dependent mechanisms of mitochondrial calcium signalling. *Cell Calcium* **44**, 51–63.

Stephenson, D. G., Lamb, G. D. and Stephenson, G. M. M. (1998). Events of the excitation-contraction-relaxation (E-C-R) cycle in fast- and slow-twitch mammalian muscle fibres relevant to muscle fatigue. *Acta Physiol. Scand.* **162**, 229–245.

Szabadkai, G., Bianchi, K., Várnai, P., De Stefani, D., Wieckowski, M. R., Cavagna, D., Nagy, A. I., Balla, T. and Rizzuto, R. (2006). Chaperone-

mediated coupling of endoplasmic reticulum and mitochondrial Ca2+ channels. *J. Cell Biol.* **175**, 901–911.

Tondeleir, D., Lambrechts, A., Müller, M., Jonckheere, V., Doll, T., Vandamme, D., Bakkali, K., Waterschoot, D., Lemaistre, M., Debeir, O., et al. (2012). Cells lacking β-actin are genetically reprogrammed and maintain conditional migratory capacity. *Mol. Cell. Proteomics* **11**, 255–71.

Tschöp, M. H., Speakman, J. R., Arch, J. R. S., Auwerx, J., Brüning, J. C., Chan, L., Eckel, R. H., Farese, R. V, Galgani, J. E., Hambly, C., et al. (2012). A guide to analysis of mouse energy metabolism. *Nat. Methods* **9**, 57–63.

Tupling, a. R., Bombardier, E., Gupta, S. C., Hussain, D., Vigna, C., Bloemberg, D., Quadrilatero, J., Trivieri, M. G., Babu, G. J., Backx, P. H., et al. (2011). Enhanced Ca2+ transport and muscle relaxation in skeletal muscle from sarcolipin-null mice. *Am. J. Physiol. - Cell Physiol.* **301**, C841–C849.

Ueki, N., Sobue, K., Kanda, K., Hada, T. and Higashino, K. (1987). Expression of high and low molecular weight caldesmons during phenotypic modulation of smooth muscle cells. *Proc. Natl. Acad. Sci. U. S. A.* **84**, 9049–9053.

Vasioukhin, V., Bauer, C., Yin, M. and Fuchs, E. (2000). Directed actin polymerization is the driving force for epithelial cell-cell adhesion. *Cell* **100**, 209–219.

Vassilopoulos, S., Gentil, C., Lainé, J., Buclez, P.-O., Franck, A., Ferry, A., Précigout, G., Roth, R., Heuser, J. E., Brodsky, F. M., et al. (2014). Actin scaffolding by clathrin heavy chain is required for skeletal muscle sarcomere organization. *J. Cell Biol.* **205**, 377–93.

Vlahovich, N., Kee, A. J., Van der Poel, C., Kettle, E., Hernandez-Deviez, D., Lucas, C., Lynch, G. S., Parton, R. G., Gunning, P. W. and Hardeman, E. C. (2009). Cytoskeletal tropomyosin Tm5NM1 is required for normal excitation-contraction coupling in skeletal muscle. *Mol. Biol. Cell* **20**, 400–9.

Wade, W. N., Willingham, M. C., Koumenis, C. and Cramer, S. D. (2002). p27Kip1 is essential for the antiproliferative action of 1,25-dihydroxyvitamin D3 in primary, but not immortalized, mouse embryonic fibroblasts. *J. Biol. Chem.* **277**, 37301–37306.

Wallace, D. C. (1999). Mitochondrial Diseases in Man and Mouse. *Science (80-.).* **283**, 1482–1488.

Wang, Y., Mattson, M. P. and Furukawa, K. (2002). Endoplasmic reticulum

calcium release is modulated by actin polymerization. *J Neurochem* **82**, 945–952.

Wang, L., Miao, J., Li, L., Wu, D., Zhang, Y., Peng, Z., Zhang, L., Yuan, Z. and Sun, K. (2013). Identification of an FHL1 protein complex containing gamma-actin and non-muscle myosin IIB by analysis of protein-protein interactions. *PLoS One* **8**, e79551.

Wang, N., Zhang, W., Cui, J., Zhang, H., Chen, X., Li, R., Wu, N., Chen, X., Wen, S., Zhang, J., et al. (2014). The piggyBac transposon-mediated expression of SV40 T antigen efficiently immortalizes mouse embryonic fibroblasts (MEFs). *PLoS One* **9**, e97316.

Westerblad, H. and Lannergren, J. (1991). Slowing of relaxation during fatigue in single mouse muscle fibers . *J. Physiol.* **434**, 323–336.

Westermann, B. (2010). Mitochondrial fusion and fission in cell life and death. *Nat. Publ. Gr.* **11**, 872–884.

Wieckowski, M. R., Giorgi, C., Lebiedzinska, M., Duszynski, J. and Pinton, P. (2009). Isolation of mitochondria-associated membranes and mitochondria from animal tissues and cells. *Nat. Protoc.* **4**, 1582–90.

Willems, P. H. G. M., Rossignol, R., Dieteren, C. E. J., Murphy, M. P. and Koopman, W. J. H. (2015). Redox Homeostasis and Mitochondrial Dynamics. *Cell Metab.* **22**, 207–218.

Yao, J., Sasaki, Y., Wen, Z., Bassell, G. J. and Zheng, J. Q. (2006). An essential role for beta-actin mRNA localization and translation in Ca2+-dependent growth cone guidance. *Nat.Neurosci.* **9**, 1265–1273.

Zhang, F., Saha, S., Shabalina, S. a and Kashina, A. (2010). Differential arginylation of actin isoforms is regulated by coding sequence-dependent degradation. *Science* **329**, 1534–7.

Zhao, K., Wang, W., Rando, O. J., Xue, Y., Swiderek, K., Kuo, A. and Crabtree, G. R. (1998). Rapid and phosphoinositol-dependent binding of the SWI/SNF-like BAF complex to chromatin after T lymphocyte receptor signaling. *Cell* **95**, 625–636.

Ziman, A. P., Ward, C. W., Rodney, G. G., Lederer, W. J. and Bloch, R. J. (2010). Quantitative measurement of Ca2+ in the sarcoplasmic reticulum lumen of mammalian skeletal muscle. *Biophys. J.* **99**, 2705–2714.